



Universidade do Minho
Escola de Ciências

Patrícia Rodrigues Correia

**Zeolite Nanomaterials Aiming Antimicrobial
Activity and Non-Melanoma Skin Cancer
Treatment**

Dissertação de Mestrado

Mestrado em Bioquímica Aplicada

Trabalho efetuado sob a orientação da

Professora Doutora Isabel Correia Neves

Professora Doutora Cristina Almeida-Aguiar

Outubro de 2018

DECLARAÇÃO

Nome: Patrícia Rodrigues Correia

Endereço eletrónico: pg31433@alunos.uminho.pt Telefone: 915468103

Bilhete de Identidade/Cartão do Cidadão: 14589428

Título da dissertação: Zeolite Nanomaterials Aiming Antimicrobial Activity and Non-Melanoma Skin Cancer Treatment

Orientadoras:

Professora Doutora Isabel Correia Neves

Professora Doutora Cristina Almeida-Aguiar

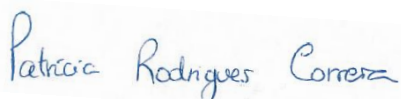
Ano de conclusão: 2018

Mestrado em Bioquímica Aplicada

DE ACORDO COM A LEGISLAÇÃO EM VIGOR, NÃO É PERMITIDA A REPRODUÇÃO DE QUALQUER PARTE DESTA TESE/TRABALHO.

Universidade do Minho, ____/____/____

Assinatura:



ACKNOWLEDGMENTS

After 12 months of dedication to this project, I finish this chapter of my academic course with a sense of satisfaction and accomplishment, with the belief that greater things are yet to come. It has been an intense learning process for me, both at the scientific and personal level and I would like to leave a well-earned word of gratitude to the people who have supported me over this time. First of all, I would like to express my special appreciation to my supervisors, Professor Dr. Isabel Correia Neves, Professor Dr. Cristina Almeida-Aguiar, as well as Professor Dr. Fátima Baltazar and Professor Dr. António Maurício Fonseca for the opportunity I was given of being a part of this project. I must point out their willingness to help me, the constant guidance and feedback while developing this work and the confidence they have always shown in me. They definitely provided me with the tools needed to successfully complete this project.

I would like to acknowledge the help provided by Dr. Sara Granja and Andreia Pereira, who kindly devoted part of their time to teach me everything I needed to know to properly perform the cell viability assays. Thank you for the patience and shared knowledge during my short stay at ICVS.

I am also very grateful to Natália Vilaça for helping me with the drug delivery assays and to Marta Ferreira (my friendly lab neighbour as I like to call her) from the Chemistry Department, who was always readily available to supply me lab material when needed and to help me solve any problem that might arise.

I thank the Centre of Chemistry/Chemistry Department, the Biology Department and the Life and Health Sciences Research Institute (ICVS) for the use of its facilities, equipment and materials to carry out my laboratorial work.

Luckily, I have been surrounded all my life with friends that inspire, motivate and encourage me. They were definitely a key factor for successfully completing this journey. I sincerely thank them for the companionship, for the amazing times we have shared and for making me a happier person. Lastly, to my family, the most important pillar of my life. I thank them for the constant support, incentive, affection and strength they gave me throughout my entire academic course. They had the patience to put up with me when I was in a bad mood or crestfallen but also shared with me moments of happiness, triumph and academic achievements. My success is your success.

To all of you, who have made it possible, my sincere thanks!

ABSTRACT

In the 21st century, nanotechnology has been emerging as a very promising field that is expected to have a revolutionary impact on society, including medicine (commonly known as nanomedicine). Nanoparticles hold tremendous potential as an effective drug delivery system (DDS), as they can be used to improve the uptake of poorly soluble drugs, to target drugs to a specific site and increase drug bioavailability. Among the different existing categories of nanomaterials, zeolites constitute a class of inorganic materials that have been explored in the past few years as promising candidates for this purpose.

The fundamental idea of this work is to direct the use of zeolites as host for the treatment of two interrelated clinical situations: cutaneous lesions resulting from skin cancer development (often exhibiting an ulcerating growth) and possible microbial infections occurring on those injured and susceptible skin areas. NaY zeolite was selected as host for the preparation of the DDS. Silver (in the ionic form, Ag⁺) and 5-Fluorouracil (5-FU), were selected as antimicrobial and antineoplastic agents, respectively, to be introduced into the zeolite structure, combining both pharmacologically active species in the same formulation, thus creating a hybrid DDS designated as (Ag/5-FU)Y. The long-term objective of this project would be to incorporate this DDS into a biocompatible cream/ointment to be used for topic delivery, whose application would be easy and suitable to treat the damaged skin areas.

The obtained results from the characterization analyses demonstrated that both agents were successfully incorporated, without causing relevant changes on the zeolite structure. Moreover, (Ag/5-FU)Y inhibited the growth of all tested bacterial strains, exhibiting lower MIC values than AgY. Regarding the assays on a human skin cancer line (A375), NaY, did not interfere with cell viability, proving its applicability as host for a drug delivery system. Additionally, (Ag/5-FU)Y caused an accentuated decrease in cell viability, that resulted not only from the effect of 5-FU but also from Ag⁺ as well.

RESUMO

No século XXI, a nanotecnologia tem emergido como área muito promissora, da qual se espera que venha a ter um impacto revolucionário na sociedade, incluído no sector da medicina (comumente conhecida por nanomedicina). As nanopartículas apresentam um enorme potencial enquanto sistemas de *drug delivery* (DDS), podendo ser usadas para melhorar a absorção de fármacos pouco solúveis, direcioná-los para locais específicos e aumentar a sua biodisponibilidade. Entre as diferentes categorias de nanomateriais existentes, os zeólitos constituem uma classe de materiais inorgânicos porosos que têm sido explorados nos últimos anos enquanto candidatos promissores para esse propósito.

A ideia fundamental deste trabalho é direcionar a utilização de zeólitos como hospedeiros para o tratamento de duas situações clínicas interrelacionadas: lesões cutâneas resultantes do desenvolvimento do cancro da pele (que muitas vezes demonstra um crescimento ulcerativo) e possíveis infeções microbianas que possam ocorrer nessas zonas feridas e mais suscetíveis da pele. O zeólito NaY foi selecionado como hospedeiro para a preparação do DDS. A prata (na forma iónica, Ag⁺) e o 5-Fluorouracil (5-FU) foram selecionados enquanto agentes antimicrobiano e antineoplásico, respetivamente, para serem introduzidos na estrutura do zeólito, combinando ambas as espécies farmacologicamente ativas na mesma formulação, criando assim um sistema híbrido designado por (Ag/5-FU)Y. O objetivo a longo prazo deste projeto seria incorporar este DDS num creme/pomada para ser usado via tópica, cuja aplicação seria cómoda e adequada ao tratamento de zonas da pele lesadas.

Os resultados das análises de caracterização demonstraram que ambos os agentes foram incorporados com sucesso, não causando alterações relevantes na estrutura do zeólito. Para além disso, (Ag/5-FU)Y inibiu o crescimento de todas as estirpes bacterianas testadas, exibindo valores MIC mais baixos do que Ag⁺. Relativamente aos ensaios de viabilidade numa linha de cancro de pele humana (A375), o zeólito NaY, não interferiu com a viabilidade celular, provando a sua aplicabilidade como hospedeiro num sistema de *drug delivery*. Adicionalmente, (Ag/5-FU)Y causou uma diminuição significativa na viabilidade celular, que resultou, não apenas do efeito do 5-FU mas também da ação de Ag⁺.

INDEX

Acknowledgments	iii
Abstract.....	v
Resumo.....	vii
Index	ix
List of Figures.....	xiii
List of Tables.....	xvii
List of abbreviations and acronyms.....	xix
Chapter 1 - Introduction	1
1.1 Overview.....	3
1.2 Thesis structure.....	5
Chapter 2 – State of the art	7
2.1 Drug Delivery Systems (DDSs).....	9
2.2 Materials used as DDS	10
2.2.1 Porous materials	11
2.2.2 Zeolites	12
2.2.2.1 Faujasite framework structure – Zeolite Y	14
2.3 Microbial infections.....	15
2.3.1 Antimicrobial agents: Silver	16
2.3.1.1 Mechanisms of action	17
2.4 Cancer.....	19
2.4.1. Non-Melanoma Skin Cancer	22
2.4.2.1. 5-FU metabolism.....	26
2.4.2.2 Mechanisms of action	27
Chapter 3 - Experimental procedure	31
3.1. Zeolite host structure and compounds	33
3.2. Preparation of the DDS.....	34
3.2.1. Preparation of AgY by ion exchange method	34

3.2.2. Preparation of Ag(5-FU)Y	35
3.3. <i>In vitro</i> release studies.....	35
3.3.1. 5-Fluorouracil <i>in vitro</i> release – UV/vis spectrophotometry.....	35
3.3.1.1. Instrumentation and experimental conditions	37
3.3.2. Silver <i>in vitro</i> release – Inductively coupled plasma-optical emission spectrometry (ICP-OES)	38
3.3.2.1 Instrumentation and experimental conditions	39
3.4. Characterization techniques	40
3.4.1. X-ray photoelectron spectroscopy (XPS)	40
3.4.1.1. Instrumentation and experimental conditions	41
3.4.2. Thermogravimetric analysis (TGA).....	42
3.4.2.1 Instrumentation and experimental conditions	44
3.4.3. Nitrogen (N ₂) gas adsorption isotherms.....	44
3.4.3.1 Instrumentation and experimental conditions	45
3.4.4. Scanning Electron Microscopy with Energy Dispersive X-ray Spectroscopy (SEM/EDX)	45
3.4.4.1 Instrumentation and experimental conditions	47
3.5. Evaluation of the antimicrobial activity of the DDS	47
3.5.1. Microorganisms used as indicator strains	47
3.5.2. Culture media and growth conditions.....	48
3.5.3. Tested samples	48
3.5.4. Antimicrobial assays.....	49
3.6. Cell viability assays.....	50
3.6.1. Cell culture conditions	50
3.6.2. Cell proliferation assay (Sulforhodamine B).....	51
Chapter 4 - Results and discussion.....	55
4.1. Characterization of samples	57

4.1.1. XPS analysis	57
4.1.2. SEM-EDX analysis.....	60
4.1.3. TGA analysis	63
4.1.4. N ₂ adsorption analysis	65
4.2. <i>In vitro</i> release studies.....	68
4.2.1. 5-Fluorouracil <i>in vitro</i> release from DDS.....	68
4.2.2. Silver <i>in vitro</i> release	70
4.3. Antimicrobial assays	71
4.3.1. Antimicrobial effects of NaY, AgY and (Ag/5-FU)Y	71
4.4. Cell viability assays	76
Chapter 5 - Conclusions and future perspectives.....	81
Chapter 6 - Bibliography	85

LIST OF FIGURES

Figure 1.1. Representative scheme of the main purpose of this work: loading of silver ions and 5-Fluorouracil into the zeolite nanostructure.	5
Figure 2.1. Structure of microporous NaY zeolite and MCM-41 mesoporous silica (Datt <i>et al.</i> 2012).	11
Figure 2.2. A- Chemical structure of a zeolite. In the zeolite structure, each Si (oxidation number +4) atom is bound to 4 oxygen atoms, so the system is electrically neutral, but the presence of Al atom (oxidation number +3) does not allow the balance of the total charge of the framework which generates a negative charge B- Primary building unit of zeolite structure, represented as a 3-D tetrahedron with centrally located Si or Al atoms (adapted from Martins & Cardoso, 2006)	12
Figure 2.3. Architecture of Faujasite zeolite Y, showing the evolution of the structure from the single tetrahedral unit, MO ₄ , until the final 3D channel system (Sivaguru <i>et al.</i> 2006).	15
Figure 2.4. Silver ions mode of action to Gram negative (left) and Gram-positive (right) bacteria. (1) Pore formation; metabolites and ions leakage (represented as plus and minus) (2) Denaturation of structural and cytoplasmic proteins; inactivation of enzymes. (3) Inactivation of respiratory chain enzymes. (4) Increase of intracellular reactive oxygen species (ROS) concentration. (5) Interaction with ribosome subunit. (6) Interaction with nucleic acids (Kędziora <i>et al.</i> 2018).	18
Figure 2.5. The stages of malignant tumour development. a. A cell suffers a mutation that makes it more likely to divide than normal. b. Cell descendants grow and divide too often, a condition called hyperplasia. One of those cells suffers another mutation which increases its propensity to divide. c. Cells start to divide excessively and acquire an abnormal look, a condition called dysplasia. d. As the events of mutation continue, cells become very uncharacteristic in both growth and appearance, leading to the formation of a tumour mass from these cells and, if it stays contained within its tissue of origin, it is called in situ cancer. e. If some cells within that tumour mass suffer additional mutations, they might invade neighbouring tissues and reach the blood or lymphatic system and the escaped cells can migrate to other body sites and establish new tumours (metastases). In that case, the tumour is said to be malignant (Cooper 2000).	20
Figure 2.6. The hallmarks of cancer (Hanahan and Weinberg 2011).	21
Figure 2.7. Schematic representation of normal skin. Basal cell keratinocytes and squamous epithelial keratinocytes (the source cells for BCC and SCC, respectively) are located in the relatively avascular epidermis. Melanocytes are also present and serve as the source cell for melanoma	

development. The basement membrane zone defines the separation between epidermis and dermis, situated underneath the basal cell keratinocytes (Berwick et al. 2006).23

Figure 2.8. Molecular structures of: A) uracil and B) 5-FU (Gester 2014).25

Figure 2.9. Summarized 5-FU anabolism and catabolism (adapted from Miura *et al.* 2010).26

Figure 2.10. Mechanism of thymidylate synthase inhibition by 5-fluorouracil (Longley *et al.* 2003).28

Figure 2.11. 5-Fluorouracil cytotoxic mechanisms following cellular uptake. 5-FU is converted to three main active metabolites: fluorodeoxyuridine monophosphate (FdUMP), fluorodeoxyuridine triphosphate (FdUTP) and fluorouridine triphosphate (FUTP), which cause DNA and RNA damage {Longley *et al.* 2003}.29

Figure 3.1. AgY preparation process. NaY is used as starting material and immersed in an AgNO_3 solution that contains the cation of interest, Ag^+34

Figure 3.2. Basic structure of a spectrophotometer (retrieved from http://jacobsschool.ucsd.edu/cosmos/2016/cluster5/Lego_Spectrophotometer.html)36

Figure 3.3. Schematic diagram of an inductively coupled plasma (ICP) spectrometer (retrieved from <https://www.azom.com>).38

Figure 3.4. Photoemission process that occurs during XPS analysis. An electron from the K-shell is ejected from an atom as a 1s photoelectron after ionization by incident X-rays (Zaidi 2011). 40

Figure 3.5. A) Thermal decomposition curve of a material. T_i indicates the temperature at which starts the mass variation and T_f refers to the temperature at which the process responsible for mass variation ends; B) Representative TGA and DTG curves. The continuous line represents the thermal decomposition that results in mass loss and the dotted line represents the 1st derivative curve, where the peaks indicate the temperatures at which the rate of that decomposition is maximum (Heal, 2002).43

Figure 3.6. Gas adsorption process.44

Figure 3.7. Main components of a scanning electron microscope (Inkson, 2016).46

Figure 3.8. Interaction between the incident electron beam (dotted arrow) and the sample surface. Electrons penetrate the specimen resulting in the emission of secondary, backscattered and Auger electrons, as well as x-rays and light.46

Figure 3.9. Curve of bacterial growth. The graph represents the four-phase pattern of population growth when bacteria are raised in closed culture such as a petri dish or test tube where no

additional nutrients are added, no waste or dead cells are removed and where there is no additional space (Wang <i>et al.</i> 2015).....	50
Figure 3.10. Morphological appearance of A375 cells: A) 40x magnification B) 100x magnification. Images obtained with Olympus IX81 microscope.	50
Figure 3.11. Molecular structure of Sulforhodamine B.	51
Figure 3.12. Neubauer chamber and the respective counting grid (corner squares) used for trypan blue staining and cell counting. Neubauer (Marienfiel, Germany) Tiefe 0,100 mm; 0, 0025 mm ² . The number of viable cells/mL was calculated by taking the average cell count from the corner squares, multiplying that averaged value by 10 ⁴ and then by 2 (dilution factor) to correct for the 1:2 dilution from the Trypan Blue addition.....	52
Figure 4.1. XPS spectra (0-1200 eV) of NaY, AgY and (Ag/5-FU)Y.	57
Figure 4.2. High resolution spectra of Ag 3d region for NaY, AgY and (Ag/5-FU)Y.	58
Figure 4.3. Peak deconvolution of: a) high resolution spectrum of Ag 3d region of AgY and b) high resolution spectrum of Ag 3d region of Ag(5-FU)Y.	59
Figure 4.4. High resolution spectra of F 1s region for AgY and (Ag/5-FU)Y.	60
Figure 4.5. Scanning electron microscopy images of zeolites (with different magnifications): a) NaY (5000x magnification), b) AgY (5000x magnification) and c) (Ag/5-FU)Y (5000x magnification and 15000x magnification).	61
Figure 4.6. EDX spectrum of AgY; A) and B) correspond to the analysis of different spots within the same sample.	62
Figure 4.7. EDX spectrum of Ag(5-FU)Y; A) and B) correspond to the analysis of different spots within the same sample.	63
Figure 4.8. Thermogravimetric thermograms of NaY, AgY and (Ag/5-FU)Y samples. Samples were heated between 50 and 700 °C at 10 °C/min. The (Ag/5-FU)Y thermogram is shown in more detail in the below image.	64
Figure 4.9. Nitrogen adsorption-desorption isotherms of AgY and DDS (Ag/5-FU)Y. Dotted line represents the desorption process and the solid line represents the adsorption process.	66
Figure 4.10. The IUPAC classification of adsorption isotherms (Yang <i>et al.</i> 2017).	67
Figure 4.11. Scanning electron microscopy image of the DDS (Ag/5-FU)Y (5000x magnification). The yellow dashed square points out a zone with an amorphous appearance which corresponds to the 5-FU dispersed on the sample's surface.	68

Figure 4.12. UV/vis absorption spectra of the withdrawn aliquots (each one represented in a different colour).....	69
Figure 4.13. Release profiles of 5-FU from the hybrid zeolite system, (Ag/5-FU)Y. Measurements were conducted in simulated physiological conditions, using a phosphate buffer solution (PBS) at pH = 7.4 and 37 °C.	69
Figure 4.14. Molecular dimensions of 5-FU (Al-Thawabeia and Hodali 2015).....	70
Figure 4.15. Release profile of silver ions determined by ICP-OES. Measurements were conducted in simulated physiological conditions, using a phosphate buffer solution (PBS) at pH = 7.4 and 37 °C.....	71
Figure. 4.16. Photographs of the agar plates; Antimicrobial activity assay in the presence of the parent zeolite, NaY 1.0 mg/mL (B) as compared to the control (A), where bacteria were cultured in the absence of zeolite material. This concentration was selected merely as representative. Bacterial growth was not affected by the presence of the zeolite (regardless of the concentration tested: 0.2, 0.5, 1.0 and 2.0 mg/mL) as we can see when comparing with the control.....	72
Figure 4.17. Antimicrobial activity assays against the bacteria indicator strains in the presence of NaY, AgY and (Ag/5-FU)Y. In the presence of both AgY and (Ag/5-FU)Y bacterial growth was successfully inhibited, with more pronounced effects in the case of (Ag/5-FU)Y (lower MIC values).	73
Figure 4.18. Antimicrobial activity assay in the absence (A) and in the presence of an aqueous 5-FU solution (B).	75
Figure 4.19. Cell viability of A375 cells measured by SRB assay after cell incubation with increasing concentrations of NaY throughout 72h. The resulting percentages (calculated as the mean percentage \pm SD of viability) were calculated in relation to the control, meaning that cells cultured in the presence of 0 mg/mL of NaY were considered as 100% of viability.	77
Figure 4.20. Effect of NaY (blue line), Na(5-FU)Y (purple line), AgY (green line) and the hybrid DDS Ag(5-FU)Y (red line) on A375 skin cancer cell viability. Cells were incubated in the presence of the prepared materials for 72 h. Presented values are means \pm SD of three independent experiments, each of them performed in triplicate.	78
Figure 4.21. Fluorescence microscopy images (1000x magnification) showing the cellular localization of NaY zeolite marked with Rhodamine B in RKO cell line (red) (Vilaça <i>et al.</i> 2013). 79	

LIST OF TABLES

Table 3.1. Characteristics of the zeolite NaY.	33
Table 3.2. Characteristics of the compounds to be incorporated into the host.....	33
Table 3.3. Characteristics of the tested bacterial strains.	48
Table 3.4. Formulation of LBA medium per liter of H ₂ O.....	48
Table 3.5. Cell culture medium composition.	51
Table 4.1. Surface composition of each sample. Results are presented in atomic percentage. ...	58
Table 4.2. Binding energies (BE) obtained from the XPS spectrum in the O 1s, Na 1s, F 1s, Al 2s, Si 2p and Ag 3d region of each sample.	60
Tabela 4.3. Loading of 5-FU into zeolite structures.....	65
Table 4.4. Structural properties of the zeolites calculated from the N ₂ gas adsorption isotherms.	67
Table 4.5. MIC values of NaY, AgY and (Ag/5-FU)Y against each of the sensitive indicator strains tested.	73

LIST OF ABBREVIATIONS AND ACRONYMS

5-FdUDP	5-fluorodeoxyuridine diphosphate
5-FdUMP	5-Fluoro-2'-deoxyuridine 5'-monophosphate
5-FdUTP	5-Fluoro-2'-deoxyuridine 5'-diphosphate
5-FU	5-fluoro-1H-pyrimidine-2,4-dione (5-fluorouracil)
5-FUH ₂	5, 6-dihydro-5-fluorouracil
5-FUMP	5-Fluorouridine monophosphate
5-FUTP	5-fluorouridine triphosphate
AK	Actinic Keratosis
ATP	Adenosine triphosphate
BCC	Basal Cell Carcinoma
BE	Binding Energy
DDS	Drug Delivery System
DMEM	Dulbecco's Modified Eagle's Medium
DNA	Deoxyribonucleic acid
DPD	Dihydropyrimidine dehydrogenase
DTG	Differential Thermogravimetric
FAU	Faujasite zeolite framework type
FBAL	Fluoro-beta-alanine
FBS	Fetal bovine serum
FUPA	Fetal bovine serum
ICP-OES	Inductively coupled plasma-optical emission spectrometry
IUPAC	International Union of Pure and Applied Chemistry
IZA	International Zeolite Association
FCC	Fluid Catalytic Cracking
LB	Lysogeny Broth
MIC	Minimum inhibitory concentration
MRSA	Methicillin-resistant <i>Staphylococcus aureus</i>
NMSC	Non-Melanoma Skin Cancer
PBS	Phosphate-Buffered Saline

SBU	Secondary Building Unit
SCC	Squamous Cell Carcinoma
SEM-EDS	Scanning Electron Microscopy coupled with Energy Dispersive Spectroscopy
SRB	Sulforhodamine B
TCA	Trichloroacetic Acid
TGA	Thermogravimetric analysis
TS	Thymidylate synthase
UV/Vis	Ultraviolet/Visible

CHAPTER 1



INTRODUCTION

1.1 Overview

The original ideas and concepts behind nanotechnology were first introduced in 1959 at the annual meeting of the American Physical Society, when the theoretical physicist Richard Feynman delivered his famous lecture entitled *“There’s plenty of room at the bottom”*. He suggested the idea of creating very small devices at the atomic scale by manipulating and arranging individual atoms and molecules, introducing the conceptual fundamentals for the field later called nanotechnology (Khan *et al.* 2017). The term itself was defined several years later, in a 1974 paper, by Tokyo Science University professor Norio Taniguchi (Freitas 2005).

Nanotechnology (“nano” comes from the Greek term “nanos”, meaning “dwarf”) can be defined as the science, engineering and technology involved in the production, characterization, and application of materials and systems with extremely small dimensions, at the nanometre scale length (1-100 nm), by manipulating individual atoms, molecules or compounds (Rajendran *et al.* 2013; Silva 2004). Structuring matter at such a reduced size, confers certain significantly improved properties to these materials, distinguishing them from their bulk counterparts, such as chemical reactivity, magnetism, optical effects, a large surface area relative to size, energy absorption, and biological mobility (Wennersten *et al.* 2008). The emerging world of nanotechnology is regarded as one of the most relevant and revolutionary research endeavours of the 21st century, having an impact on numerous industries, including medicine. The convergence of nanotechnology and medicine has led to the emergence of the field of nanomedicine, defined as the application of nanotechnology in monitoring, diagnosing, preventing, repairing or curing diseases and damaged tissues in biological systems (Gupta 2011; Rajendran *et al.* 2013). Treating or repairing tissues and organs within individually targeted cells, is an approach fundamentally distinct from conventional medicine. The use of nanomaterials in medicine has significantly changed the landscape of pharmaceutical and biotechnology industries, offering new and exciting applications and techniques, some of them (only imagined a few years ago) are making notable progress on the way to becoming realities, while others have already been approved for clinical use (Zhu *et al.* 2014). These applications include nano scale particles used as tags and labels biomarkers for the diagnosis of diseases, magnetic resonance imaging contrast enhancement, bio-detection of pathogens, detection of protein, tissue engineering and one of the most promising and advanced, drug delivery (Murthy 2007). Over the years, drug delivery methods have progressed and evolved considerably to improve patient compliance, drug bioavailability, safety and therapeutic effects

(Sayed *et al.* 2017). In the oncology field for example, which has gone through an accentuated improvement in terms of treatment approaches via nanomedicine strategies, conventional therapeutic strategies have the drawback of distributing therapeutic agents non-specifically in the body, while nanoparticles allow site specific drug delivery, meaning they can deliver therapeutic agents to the restricted diseased body areas that require treatment, resulting in increased local drug concentration and minimizing the possible side-effects in healthy neighbour cells and tissues (Khodabandehloo *et al.* 2016). Furthermore, this highly selective approach allows reduction of drug consumption by delivering an accurate therapeutic dose and reduction of treatment expenses, resulting in cost-effective patient's treatment (Wilczewska *et al.* 2012).

Although the commonly accepted definition refers to nanoparticles as having dimensions lower than 100 nm, not all particles used for medical purposes fulfil this requirement, which does not necessarily affect their functionality in medical applications, so this size limitation is said to be artificial and misleading by some experts. In the case of drug delivery, relatively large nanoparticles might be required to load the necessary amount of drug onto the particles, so, nano systems up to 1000 nm should be considered (Pavlovic *et al.* 2013). The fact that these nanoparticles exhibit a high surface to mass ratio and the ability to bind, adsorb and carry other compounds, is what makes them very attractive for medical purposes (De Jong and Borm 2008).

Several distinct types of nano systems have been explored as promising and viable options for drug delivery such as liposomes, dendrimers, carbon nanotubes, micelles, metallic nanoparticles, mesoporous materials and microporous materials such as zeolites (Saini *et al.* 2010). Zeolites consist on inorganic crystalline aluminosilicates with an ordered and regular system of channels and pores, a large surface area and accessible pore volume which makes them great nanostructures for hosting therapeutic drug molecules (Rimoli *et al.* 2007; Vilaça *et al.* 2013). Additionally, the existing cations within the framework of the zeolite can be easily exchanged by other cations, meaning they can entrap metal ions such as silver or zinc, working as antimicrobial agents (Ferreira *et al.* 2012).

Considering this, the aim of the current project was to load zeolite nanostructures with silver ions, known as an efficient antimicrobial agent, and 5-Fluorouracil, a widely used antineoplastic drug, creating what we can somehow consider as a hybrid zeolite nanomaterial (Ag/5-FU)Y for microbial infections and non-melanoma skin cancer treatment respectively (Figure 1.1). Nevertheless, to achieve this goal, several steps had to be performed, namely: 1) preparation and characterization of the drug delivery systems by loading silver and 5-FU; 2) *in vitro* evaluation of the release behavior

of both agents; 3) *in vitro* assessment of the antimicrobial potential of the DDS using different microorganisms as indicator strains and 4) *in vitro* assessment of the cytotoxicity of the DDS using a human skin cancer cell line.

Ideally, these drug delivery systems prepared for skin applications would be further incorporated into a biocompatible cream to be used for topical delivery, combining the beneficial effects of the antimicrobial and anticancer activities in the same formulation.

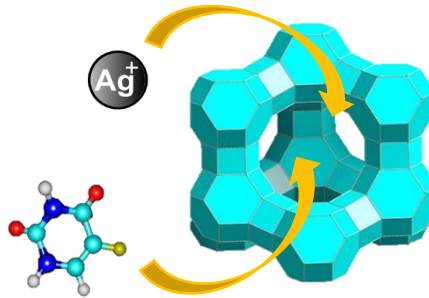


Figure 1.1. Representative scheme of the main purpose of this work: loading of silver ions and 5-Fluorouracil into the zeolite nanostructure.

1.2 Thesis structure

The work developed within the scope of this master thesis will be presented and described in detail throughout six distinct chapters, according to the following outline:

Chapter 1 – Introduction

- Contextualization and importance of the core subject.
- Overview of the main topics related to the thesis project.
- Purpose of this study.

Chapter 2 – State of the art

- Literature review and description of all the theoretical concepts required for a clear comprehension of the developed work.

Chapter 3 – Experimental procedure

- Materials and procedures required for the preparation of drug delivery systems (DDSs) as well as the analytical techniques used for their characterization.

- *In vitro* release studies to evaluate the release behaviour of silver and 5-FU from the DDS.

- *In vitro* evaluation of the antimicrobial potential of the DDS.

- *In vitro* assessment of the DDS cytotoxic effects on a human skin cancer cell line.

Chapter 4 – Results and discussion

- Presentation, interpretation and discussion of the obtained results from the experimental work.

Chapter 5 – Final considerations and future perspectives

- General review and reflective analysis of the results and relevant findings obtained with this study.

- Potential applications of the findings.

- Future follow up research and possible new projects based on the results of the current work.

Chapter 6 – Bibliography

- Complete list of all cited resources used in the thesis writing.

CHAPTER 2



STATE OF THE ART

As mentioned before, the purpose of this work was to develop drug delivery systems (DDSs) based on zeolite nanostructures as host to incorporate silver ions and the antineoplastic agent 5-Fluorouracil (5-FU) for microbial infections and non-melanoma skin cancer treatment, respectively. Therefore, in this chapter all the theoretical concepts required for a solid comprehension of the project will be explained based on the information available in the literature. Drug delivery systems and their applications will be broadly described, more specifically the inorganic systems that we used in this project, the microporous zeolite nanoparticles. The general concepts of zeolites and their applications will be presented, with more emphasis on the faujasite zeolite type (the specific structure of zeolite we selected as host for the drug delivery system). Moreover, the characteristics and mechanisms of action of both therapeutic agents, silver and 5-Fluorouracil, will be extensively approached.

2.1 Drug Delivery Systems (DDSs)

Over the past few decades, the use of drug delivery has suffered substantial advances and even greater modifications are predictable in the near future. DDSs have already had a great influence on medical technology and they constitute one of the most rapidly growing sectors of the pharmaceuticals market. Conventional application of drugs has several drawbacks, such as limited efficiency, reduced biodistribution and lack of sensitivity. Since the development of new therapeutic compounds represents an extremely expensive and time-consuming procedure, the science community has been persistently trying to improve the performance of many existing drugs enabling their application in innovative therapies by developing suitable drug delivery systems (DDSs) capable of treating human diseases in a more efficient way (Wilczewska *et al.* 2012; Tiwari, *et al.* 2012).

From a technical perspective, a DDS can be defined as a formulation, system or device with the ability to introduce and transport safely a certain therapeutic agent within the body to achieve the desired therapeutic effects, controlling its distribution in space and time (Jain 2008; Liu *et al.* 2016). In other words, ideally, a DDS should be able to control both the delivery of a certain drug to a specific organ or location (i.e. targeting) as well as its rate of release. Thus, a DDS is able to increase the overall therapeutic efficacy: targeting allows the drug molecule to selectively accumulate in the diseased area, minimizing or avoiding undesirable side effects, particularly when

dealing with therapeutic agents that are supposed to kill cancer cells but are cytotoxic to the neighbouring healthy cells and tissues as well; on the other hand, controlling the rate of drug release allows the maintenance of its concentration in the body within the ideal therapeutic range and below the toxicity threshold (Barbé *et al.* 2004; Rizvi and Saleh 2018). Additionally, DDSs protect the drug from rapid degradation or clearance and since they increase the drug concentration in target tissues and lower doses of drugs are needed (Wilczewska *et al.* 2012).

Current research on DDSs has been mostly focused on nanotechnology and over recent decades there has been a huge growth in the number of scientific publications presenting relevant results that clearly demonstrate the great potential of nanoparticles as DDSs and why they are expected to change the future scenario of the pharmaceutical industry (Fornaguera and Garcia-Celma 2017). Generally, nanoparticles can incorporate drug molecules or biomolecules (such as polypeptides, proteins and genes) into their structure, with the therapeutic agent generally being dissolved, entrapped, adsorbed, attached and/or encapsulated into a nano-matrix (Liu *et al.* 2016; Singh and Lillard 2009). Modification of certain characteristics of nanoparticles such as size and surface (e.g. coating with specific ligands, change the surface charge and reactivity) allows the optimization of bioavailability, decreases clearance, enhances stability and targets the drug to the desired tissues in the body (Rizvi and Saleh 2018).

One of the great advantages of using nanoparticles for drug delivery is their reduced size, as they can extravasate the endothelium (reaching the site of inflammation), the epithelium (e.g., liver and intestinal tract), penetrate through tumour masses and microcapillaries. In general, the nanosize of these particles allows an effective uptake by a variety of cell types and a selective accumulation of the compound of interest at specific target sites (Singh and Lillard 2009).

The essential objectives concerning the use of nanoparticles to entrap drugs are either improved delivery to, or uptake by target cells and/or a decrease in the toxicity of the free drug to non-target organs. Both situations will promote an increase of therapeutic index (De Jong and Borm 2008).

2.2 Materials used as DDS

A broad range of natural and synthetic materials has been described in the literature and explored as DDS, including liposomes, micelles, dendrimers, hydrogels, carbon nanotubes, emulsions, quantum dots and polymeric systems, exhibiting great potential in controlled and targeted drug

delivery. Among these systems, porous materials are emerging as an innovative category of host/guest systems (Khan *et al.* 2017; Sayed *et al.* 2017).

2.2.1 Porous materials

The International Union of Pure and Applied Chemistry (IUPAC) classifies inorganic porous materials according to their pore size boundary into three categories: macroporous (pore size > 50 nm), mesoporous (pore diameter 2–50 nm), and microporous (pore diameter < 2 nm). Porous nanomaterials, such as mesoporous silica and microporous zeolites (Figure 2.1) are emerging as materials for biomedical applications, specially focused on the development of DDSs because they present certain advantageous properties that make them attractive for this purpose, namely biocompatibility, low toxicity, well-organized stable architecture with uniform pore size, high surface to volume ratio, large inner surface area, allowing the adsorption of a wide variety of drugs and molecules of interest, and the ability to control the properties through surface functionalization (Ahuja and Pathak 2009; Allothman 2012; Arruebo 2011).

Mesoporous silica materials exhibit a larger pore size compared to zeolites, meaning they can host a wider range of compounds and that is the reason why they have been more extensively explored for applications in drug delivery and imaging (Nagarajan, 2012; Wang 2009). However, zeolites share many of the advantageous characteristics displayed by mesoporous silica materials and the fact that they have a reduced pore size is particularly interesting for applications involving small pharmacological molecules and imaging agents. The unique structural features possessed by microporous material like zeolites, such as the size of the pore window, the accessible void space, the dimensionality of the channel system, and the numbers and sites of cations are the reason of their applicability in several processes, namely, ion-exchange, separation, catalysis and their role as host in nanocomposite materials (Datt *et al.* 2012).

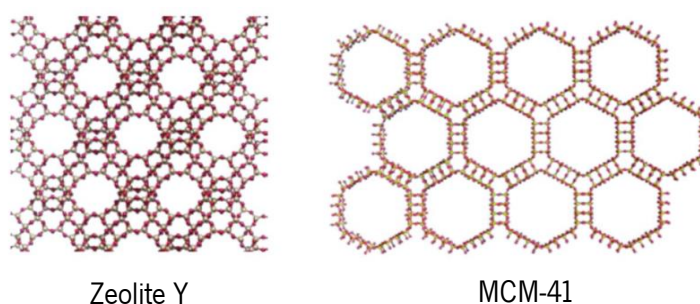


Figure 2.1. Structure of microporous NaY zeolite and MCM-41 mesoporous silica (Datt *et al.* 2012).

2.2.2 Zeolites

Zeolites constitute the most important family within microporous materials. The term “zeolite” was introduced in 1756, by the Swedish mineralogist, Axel Crönsted, referring to certain silicate minerals, in allusion to their behavior of heating in a borax bead (Greek *zeo* = boil; *lithos* = stone). However, the first zeolite structure to be solved (crystal structure determination done by Taylor on Analcime) was only in 1930, nearly two centuries later. It represented a landmark in zeolite mineralogy, since it meant the discovery of $(\text{Si}/\text{Al})\text{O}_4$ tetrahedral as the framework arrangement on the basis of zeolite’s new definition (Shaha *et al.* 2016). Nowadays, the concept behind these solid inorganic materials is well established and consensually defined: zeolites consist of microporous crystalline aluminosilicates and the Si, Al and O atoms are arranged in a 3-Dimensional structure (Rhodes 2010). They possess primary structures composed of MO_n polyhedral (where M is either Si or Al), more specifically tetrahedral units, $[\text{AlO}_4]^-$ and $[\text{SiO}_4]$ (Figure 2.2), which are linked to each other through bridging oxygen ions (Dong *et al.* 2014), forming the secondary building units (commonly referred as SBUs) that basically correspond to the geometric arrangements of the multiple connected tetrahedral and may be simple polyhedrals, such as cubes or hexagonal prisms. Consequently, these SBUs are assembled, generating the ultimate framework structure of the zeolite, with a uniform distribution of molecular-sized pores and cavities (Tzia *et al.* 2012). The final structure of the zeolite is dependent on the geometric shape adopted by the SBUs and the way these repeating units combine with each other, giving rise to different groups of zeolites.

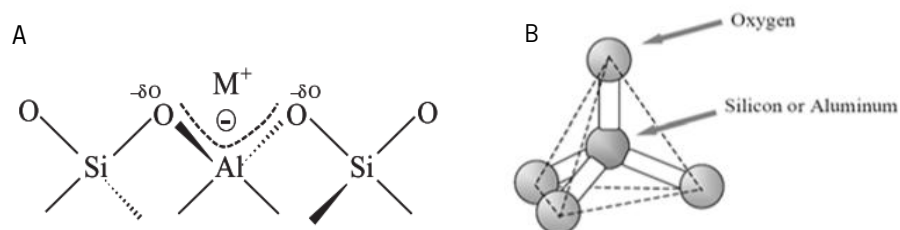


Figure 2.2. A- Chemical structure of a zeolite. In the zeolite structure, each Si (oxidation number +4) atom is bound to 4 oxygen atoms, so the system is electrically neutral, but the presence of Al atom (oxidation number +3) does not allow the balance of the total charge of the framework which generates a negative charge B- Primary building unit of zeolite structure, represented as a 3-D tetrahedron with centrally located Si or Al atoms (adapted from Martins & Cardoso, 2006)

Zeolites with an open structure framework contain several channels and pores of discrete size (range 0.03-2.00 nm) (Shaha *et al.* 2016), occupied by cations (for instance, Na⁺, K⁺, Ca²⁺, Mg²⁺ or NH₄⁺) and water molecules. These cations, that reside in the interstices of the framework, balance the net negative charge of the zeolite lattice, maintaining the electroneutrality of the structure and thanks to their mobility (since they are not bound covalently) they can be reversibly exchanged for other ions with the same charge when aqueous solutions of the ion are passed through those channels and voids of the zeolite (Dong *et al.* 2014; Tzia *et al.*, 2012). The water molecules within the cavities are loosely bound and are easily removed from the framework upon heating, resulting in a high surface area and accessible pore volume (Shameli *et al.* 2011; Vilaça *et al.* 2013).

More than 70 new, different framework structures of zeolites are known. They present pore sizes that range from 0.3 to 1.0 nm and pore volumes from about 0.10 to 0.35 cm³ /g. When considering the zeolite lattice, it should be regarded as slightly flexible, since the size and shape of the framework and pore can vary depending on temperature variations and guest species. Some of the most relevant zeolite types, most of them used for commercial applications, include the minerals zeolite mordenite, chabazite, erionite and clinoptilolite, the synthetic zeolite A, X, Y, L, ZSM - 5, β and MCM-22 and the zeolites F and W (Tzia *et al.* 2012).

Since the time of its discovery back in the 20th century until the contemporary days, the number of areas utilizing zeolites has grown tremendously. To put the potential of zeolites briefly into perspective, we can use several examples of how these materials have been successfully applied in a wide range of industrial sectors: as detergent water softeners (such as zeolite A) replacing environmentally hash phosphates (Marcus *et al.* 1999); as adsorbents (one of the major properties of zeolite) for wastewater treatment, removing organic and inorganic pollutants that disturb the natural balance of the environment (Shaha *et al.* 2016); as catalysts in industrial processes, such as oil refining where the use of zeolites has been considered one of the major accomplishments in the chemistry of the 20th century - ZSM-5 for example was commercialized as an octane enhancement additive in fluid catalytic cracking (known as FCC process that consists of several molecular transformations such as C-C bond breaking in long chain linear alkanes and isomerization of linear into branched alkanes, during which vacuum gasoil converts into gasoline) (Tzia *et al.* 2012) (Soni 2014); as a food additive in processing industries, such as the natural zeolite Clinoptilolite used as additive to feed cows, pigs and horses that absorbs toxins in the food created by molds and microscopic parasites and consequently enhances food absorption by these animals (Tzia *et al.* 2012).

More recently, in addition to the industrial sector and due to their biological properties and stability in biological environments, the application of zeolites has been considered in the biomedical field: for processes in magnetic resonance imaging (Norek *et al.* 2007), in wound treatment (Galownia *et al.* 2006), as drug delivery systems (Amorim *et al.* 2012; Martinho *et al.* 2015; Vilaça *et al.* 2017) and as antimicrobial nanocarriers (Ferreira *et al.* 2016).

2.2.2.1 Faujasite framework structure – Zeolite Y

Zeolite Y is a type of zeolite that belongs to the faujasite family, commonly referred as FAU, the three-letter code assigned by the structure commission of the International Zeolite Association (IZA). Among the zeolites used on an industrial scale, synthetic zeolite Y is one of the most widely employed materials and two of its major applications involve fluid catalytic cracking (FCC), to convert fractions of petroleum crude to more valuable products such as gasoline and diesel, and as adsorbent (Karami *et al.* 2009; Li *et al.* 2015).

Each structural unit of the zeolite Y is typically based on 8 sodalite cages that are linked by oxygen bridges between the hexagonal prisms. While these sodalite cages are too small to accommodate organic molecules, they arrange to form a 3D network of larger void spaces, known as supercages, with a diameter of 1.18 nm. The supercages share a 12-membered ring with an open diameter of 0.74 nm (which corresponds to the pore of the zeolite) and an organic guest molecule can diffuse into the supercage through the channels and cages by way of the 12-membered-ring windows (Amorim *et al.* 2012; Sivaguru *et al.* 2006). Charge-compensating metal ions can occupy three distinct positions within the zeolite structure, I, II and III. The progression from a single tetrahedral primary structure all the way to the final framework structure of zeolite Y, from the faujasite class of zeolites, is exhibited in Figure 2.3. Recent studies have explored the potential of zeolite Y as a material with antimicrobial properties and also as a suitable drug delivery system (DDS) for anticancer drugs, revealing in both cases promising results (Amorim *et al.* 2012; Ferreira *et al.* 2012; Ferreira *et al.* 2016; Martinho *et al.* 2015; Shamelí *et al.* 2011; Vilaça *et al.* 2013). These two applications, antimicrobial activity and anticancer drug encapsulation and delivery, will be further extensively approached since they are on the basis of this project.

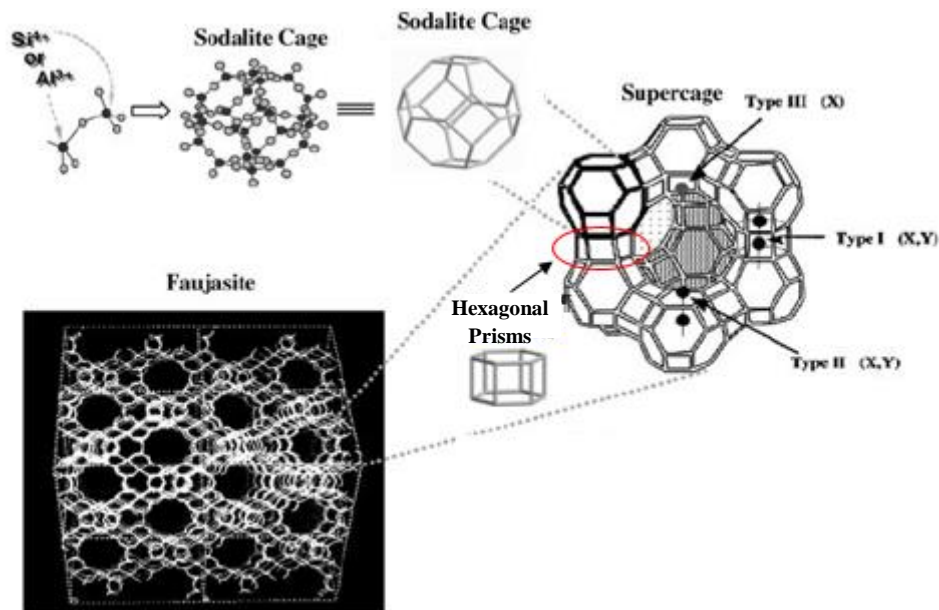


Figure 2.3. Architecture of Faujasite zeolite Y, showing the evolution of the structure from the single tetrahedral unit, MO_4 , until the final 3D channel system (Sivaguru *et al.* 2006).

2.3 Microbial infections

It is known that several microorganisms have a relevant and indispensable role in our surrounding ecosystem as well within our body, which can be itself considered as an ecosystem (microorganisms can inhabit various human body sites such as the skin, nose, mouth and digestive gut), being crucial in maintaining human health. In fact, the human microbiome constitutes an essential component of the host's immunity and many of those microbes are responsible for resistance to colonization by exogenous pathogenic microorganisms (Young 2017).

However, sometimes potential pathogenic agents come in close contact with the host and trigger opportunistic infections in immune-compromised hosts, which can further develop into human diseases (although the limits between infection and disease are not always clear), some of them mild and hardly noticeable, but others can be serious and life-threatening. The agents capable of causing infection (defined as the invasion and development of a certain pathogenic microorganism within a human or animal body, which then multiplies in close association with the host's tissues) fall into five distinct groups: viruses, bacteria, fungi, protozoa, and helminths (these last two usually grouped together as parasites) (Barreto *et al.* 2006; Morgan 1992). Most of this type of diseases are caused by bacteria and viruses. In the specific case of bacteria, there is a multitude of different

human infectious diseases caused by this type of microorganisms (such as pneumonia, tuberculosis, diphtheria, typhoid fever, cholera and syphilis), whose symptoms may range from mild to serious, and some can be fulminating and deadly. The therapeutic answer to these infectious diseases came in the 1940s, when antibiotics were first prescribed to treat humans, marking the beginning of the 'Golden Age' of antibiotics, which revolutionized the treatment of infectious diseases worldwide by successfully saving millions of lives. Unfortunately, over the years, the growing development of resistance to antibiotics began to raise medical concern and it currently represents a serious worldwide public health problem. This antibiotic resistance crisis is the result of the overuse and misuse of these medications, along with a lack of new drug development by the pharmaceutical industry caused by the reduced economic support and complex regulatory requirements (Gould 2016; Ventola 2015).

The World Health Organization has inclusively released, in February 2017, a list of 12 priority pathogens that currently represent a major threat to public health due to their resistance to antibiotics, ranking them in three priority levels (critical, high and medium) (World Health Organization, 2017). This situation demands the improvement and creation of new and cost-effective treatment options and alternative antimicrobial solutions while minimizing the negative impacts on human and animal health and on the environment.

2.3.1 Antimicrobial agents: Silver

The development of materials with antimicrobial properties has been of great interest in academic and technological fields due to its broad range of applications, including water purification systems, medical devices, food packaging and storage, clothing and toiletries (Dong *et al.* 2014). Several works have shown that antimicrobial inorganic materials offer some relevant advantages over conventionally used organic agents, namely chemical stability and thermal resistance, safety to the user and long-lasting action period. Among the existing inorganic antimicrobial agents, silver containing nanomaterials have been receiving renewed interest from the pharmaceutical companies due to the formerly mentioned situation of outbreak of infectious diseases along with the increasing number of resistant bacterial strains to most antibiotics.

Silver has a long history of use in human healthcare and medicine. In ancient times, silver coins were dropped into water serving as a disinfectant. In the 1800s it started to be used as an antiseptic for post-surgical infections, wound therapy and medical devices and was inclusively extensively

used to treat wounded soldiers in World War I. Nowadays, it is routinely used to control microbial growth in a variety of applications, including treatment of burn wounds, dental materials, water treatment, textile fabrics, food packaging and catheters (Kim *et al.* 2007; Rai *et al.* 2009). Silver, when compared with other metals, exhibits higher toxicity to microorganisms while presenting lower toxicity to mammalian cells and has a wide spectrum of antimicrobial properties, which contributed for becoming one of the most intensively studied systems (Chen *et al.* 2011; Salim *et al.* 2016). To exert its antimicrobial properties, silver must be in its ionized form (Ag^+), which is highly reactive and known as the bioactive form of silver, effective against a broad range of microorganisms (Rai *et al.* 2009). On the other hand, silver in its non-ionized form is inert and does not react with human tissue or kill microorganisms (Guggenbichler *et al.* 1999). So, every silver containing compounds that exhibit antimicrobial properties are in one way or another sources of silver ions (Ag^+).

2.3.1.1 Mechanisms of action

Even though the precise mechanisms of antimicrobial activity of silver ions is not completely understood, several studies have reported the structural and morphological changes they induce on bacteria, which provided several mechanistic insights about Ag^+ mode of action (Feng *et al.* 2000; Liao *et al.* 2003). In fact, the inhibitory effect of silver on bacterial growth is probably the sum of distinct mechanisms of action. Ag^+ can bind to thiol groups (essential for either protein stability and/or activity) of structural and functional proteins, such as cytoplasmic structural proteins and enzymes, causing their deactivation (some thiol groups can be part of the catalytic mechanism of certain enzymes or induce conformational changes that allow the binding of the substrates). Silver can also form stable S-Ag bonds with thiol-containing compounds in the cell membrane that are involved in the transmembrane energy generation (metabolic enzymes of the respiratory chain such as cytochrome b), inactivating them. Inhibition of these proteins causes an increase in the level of intracellular oxygen species (eventually culminating in a state of oxidative stress), which are toxic to the cell as they cause damage to proteins, DNA, RNA and lipids. The ability of Ag^+ to associate with the cell wall, cell membrane and cell envelope of microorganisms is also reported to be one of the mechanisms involved in cell death. Its positive charge allows electrostatic attraction with the negative charges of the bacterial cell membrane, compromising its integrity and causing rupture. Dibrov *et al.* showed that low concentrations of Ag^+ induced a massive proton leakage through the bacterial membrane, resulting in complete deenergization and,

ultimately, cell death. Furthermore, it is suggested that silver ions bind to the protein S2 of the 30S ribosomal subunit, causing the denaturation of the ribosome native structure and consequent deactivation of the ribosome complex, which ultimately results in the inhibition of protein biosynthesis. In addition, it was suggested that Ag^+ can bind to microbial DNA, forming bonds with pyrimidine bases and consequently disrupting the hydrogen bonding between the two anti-parallel strands and denaturing the DNA molecule which ultimately results in loss of replication ability. Interestingly, Feng *et al.* demonstrated that bacterial DNA molecules became condensed after being treated with AgNO_3 (probably as a protective mechanism against the denaturing effects of silver ions), which interferes with their replicability capacity since DNA molecules must be in a relaxed state so that replication can be effectively conducted. These proposed mechanisms are schematized in Figure 2.4. (Cao 2017; Dibrov *et al.* 2002; Emamifar, 2011; Feng *et al.* 2000; Kędziora *et al.* 2018; Percival *et al.* 2005; Salim *et al.* 2016; Wang *et al.* 2017;).

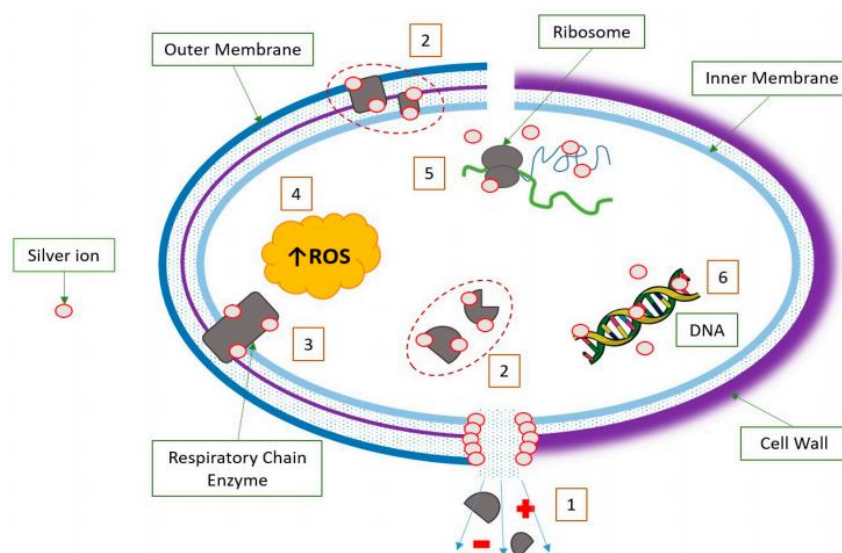


Figure 2.4. Silver ions mode of action to Gram negative (left) and Gram-positive (right) bacteria. (1) Pore formation; metabolites and ions leakage (represented as plus and minus) (2) Denaturation of structural and cytoplasmic proteins; inactivation of enzymes. (3) Inactivation of respiratory chain enzymes. (4) Increase of intracellular reactive oxygen species (ROS) concentration. (5) Interaction with ribosome subunit. (6) Interaction with nucleic acids (Kędziora *et al.* 2018).

Silver can be easily incorporated in a carrier support material such as zeolites, which are considered promising inorganic nanomaterials, capable of hosting metal ions such as silver, copper and zinc and regulate their release, achieving a greater significance relatively to conventional antimicrobial agents. In fact, industry uses several materials coated with silver zeolites to apply

antimicrobial properties to their products. In Japan, for instance, ceramics coated with silver zeolite are of interest for manufacturers (Matsumura *et al.* 2003). The potential applications of synthetic zeolites as antibacterial agents by incorporation of silver ions have been extensively reported (Kwakye-Awuah *et al.* 2007; Milenkovic *et al.* 2017; Rieger *et al.* 2016) and, among the different types of zeolites that can be used as hosts, faujasite (FAU) zeolite is one of the structures extensively explored. Ferreira *et al.* evaluated the antimicrobial activity of both zeolites from the faujasite family, NaY and NaX, loaded with silver ions (AgY and AgX respectively) and the results showed that they successfully inhibited the bacteria and yeast strains tested (Ferreira *et al.* 2012), with AgY showing a more pronounced antimicrobial activity. As mentioned before, NaY zeolites will be used in the present study as a starting material, load with silver ions and then evaluate its antimicrobial activity against selected bacterial strains.

2.4 Cancer

Cancer is a major public health problem worldwide, globally the second leading cause of death (next to cardiovascular diseases) and the deadliest disease in developed countries. In 2016, it was estimated that 42 million people across the world suffered from any of the forms of cancer and approximately 8.9 million people have died from it (Roser and Ritchie 2018). Cancer can be defined as a group of diseases characterized by uncontrolled cell growth and the invasion and spread of those abnormal cells from the site of origin (the primary site) to other sites in the body (Bertram 2000). Unlike normal cells in our body, which are continuously subjected to regulatory signals that dictate whether they should divide, differentiate into another cell or die, cancer cells acquire a degree of autonomy and stop responding to those signals, which causes them to grow and proliferate wildly (Jiang *et al.* 2015; Busch 1974). At the cellular level, the first step of the process of cancer development is tumour initiation, which results from a single mutated cell that starts to proliferate in an abnormal way, leading to the outgrowth of a population of clonally derived tumour cells. Subsequent rounds of mutation occur within those cells and, as a result, some of them acquire properties such as increased growth rate or increased survival and invasion potential which in turn confers them a selective advantage for further expansion (Pardee *et al.* 2008).

Clonal selection continues throughout tumour mass formation, until eventually its growth and expansion are enough to break through the basal membrane barrier of the original tissue site and

spread to other parts of the body. When approaching the concepts of tumour formation and cancer development it is important to establish a clear distinction between a benign tumour and a malignant tumour. A benign tumour remains confined to its original location and does not invade the surrounding tissue or spreads throughout the body and generally it can be removed surgically. On the other hand, a malignant tumour constitutes a more dangerous situation, since it does not remain confined and can invade the surrounding tissue and spread throughout the body, using the circulatory or lymphatic system (a process known as metastasis) and only these cases can be correctly referred to as cancers (Gwatkin 1993; Uzman 2006) (Figure 2.5).

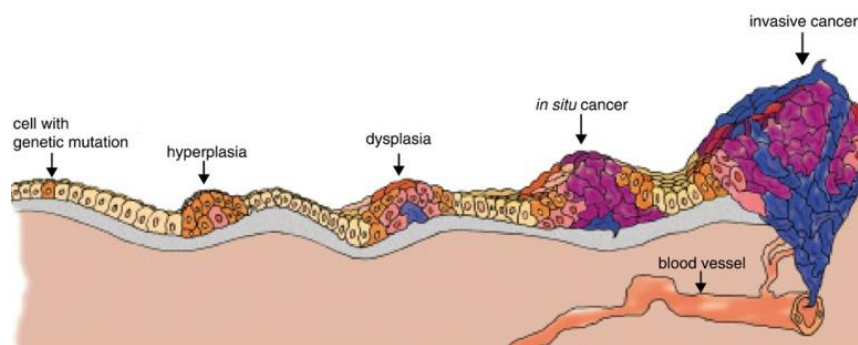


Figure 2.5. The stages of malignant tumour development. **a.** A cell suffers a mutation that makes it more likely to divide than normal. **b.** Cell descendants grow and divide too often, a condition called hyperplasia. One of those cells suffers another mutation which increases its propensity to divide. **c.** Cells start to divide excessively and acquire an abnormal look, a condition called dysplasia. **d.** As the events of mutation continue, cells become very uncharacteristic in both growth and appearance, leading to the formation of a tumour mass from these cells and, if it stays contained within its tissue of origin, it is called in situ cancer. **e.** If some cells within that tumour mass suffer additional mutations, they might invade neighbouring tissues and reach the blood or lymphatic system and the escaped cells can migrate to other body sites and establish new tumours (metastases). In that case, the tumour is said to be malignant (Cooper 2000).

Like all genetic disorders, cancer results from genetic (or epigenetic) alterations in the somatic cells. Tumour cells contain several alterations ranging from single base pair mutations (point mutations) to large chromosomal aberrations (deletions and translocations). These multiple abnormalities accumulate over time in a multi-step process that underlies carcinogenesis, which explains the increased incidence of cancer with age and why the disease has become more prevalent over the years as human lifespan has increased (Gwatkin 1993; Jandrig 2011). Basically, the more time we live the more time our cells are prone to cumulative DNA mutations which may eventually result in a detectable cancer. Initiation and progression of cancer depends on both

external agents: physical carcinogens such as ultraviolet and ionizing radiation; chemical carcinogens such as components of tobacco and vinyl chloride; biological carcinogens such as certain viruses, bacteria or parasites and factors within the cell (inherited mutations, hormones, immune conditions and mutations that can occur as result of metabolism) (Basu 2018). Despite the tremendous efforts over the years from the scientific and medical communities, cancer treatment remains difficult because of the enormous complexity of the disease at the cellular and molecular levels. Each cell behaves autonomously and is influenced by external signals from surrounding cells in the tissue or microenvironment. There are more than 100 distinct types of cancer which can present distinctive behaviours and respond very differently to treatment. Even though the underlying cellular and molecular mechanisms differ from case to case, there are certain common changes that normal cells suffer as they develop gradually to a neoplastic state, in a multistep process that allows them to become tumorigenic and ultimately malignant (Pérez-Losada *et al.* 2011; Uzman 2006). In 2000, scientists Hanahan and Weinberg suggested that the wide range of cancer cell genotypes is a manifestation of six crucial modifications in cell physiology, known as hallmarks of cancer (Hanahan and Weinberg 2000) (Figure 2.6), that together promote tumour growth and metastatic dissemination and are common in most and perhaps all types of human tumours, namely: self-sufficiency in growth signals, insensitivity to anti-growth signals, evasion to programmed cell death (apoptosis), limitless replicative potential, sustained angiogenesis, and tissue invasion and metastasis. Years later, two emerging hallmarks were added: reprogramming energy metabolism and evading immune response, and subjacent to these hallmarks: genome instability and mutation, and tumour-promoting inflammation (Fouad and Aanei 2017; Hanahan and Weinberg 2011).

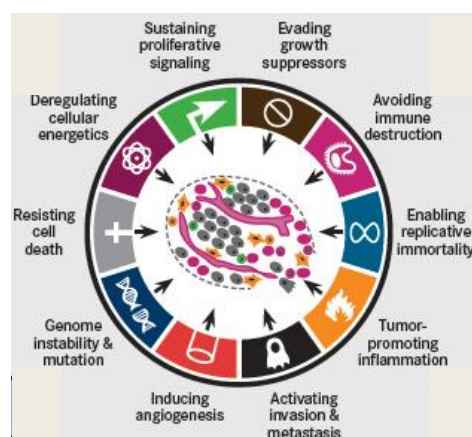


Figure 2.6. The hallmarks of cancer (Hanahan and Weinberg 2011).

Depending on tissue origin and cell type we can have different tumour classifications. Approximately 85-90% of human cancers occur in epithelial cells and are classified as carcinomas. Cancers derived from mesoderm cells (supportive and connective tissues such as bone, muscle, fat or cartilage) are called sarcomas and are rare in humans. Leukemias and lymphomas are both known as 'liquid tumours' or 'blood cancers'. The first is common in children and has its origin in an uncontrolled proliferation of hematopoietic stem cells in the bone marrow. The second arises from immune system cells (lymphocytes T and B) (Gwatkin 1993).

2.4.1. Non-Melanoma Skin Cancer

Non-melanoma skin cancer (NMSC) is the most common malignancy among Caucasians. Although the most relevant risk factor for NMSC occurrence is skin exposure to UV radiation (which initiates approximately 90% of NMSCs), other variants such as Fitzpatrick skin types I and II, genetic susceptibility, immunosuppression, previous manifestation of the disease, age and male sex constitute risk factors. Basal cell carcinoma (BCC) and squamous cell carcinoma (SCC) are the two most common subtypes of NMSC (Figure 2.7), accounting respectively for 70% and 25% of total cases and result from the malignant transformation of epidermal keratinocytes and suppression of the cutaneous inflammatory response (Didona *et al.* 2018; Griffin *et al.* 2016; Lomas *et al.* 2012). BCC and SCC share many similarities, typically both have a good prognosis, rarely spread to other parts of the body and have a low mortality rate, but neglected NMSCs can grow invasively and may metastasize, so detecting them at their initial stages is extremely important to allow a timely treatment and consequently improved prognosis.

BCC occurs mainly on sun-exposed sites, with 80% appearing on the head and neck. Superficial BCCs appear as gradually enlarging erythematous plaques, resembling psoriasis, Bowen's disease or discoid eczema. Despite of the capability of local invasion and destruction of surrounding tissues, BCC shows a low degree of malignancy and limited potential for metastasis. It is the least aggressive form of NMSC, contributing minimally to its mortality rate. On the other hand, SCC exhibits a variable metastatic rate of 0.1–9.9% and accounts for about 75% of deaths due to NMSC. It is characterized by atypical proliferation of invasive squamous cells, which can metastasize, usually appearing in the form of ulcers or indurated keratinising lesions on sun-exposed sites. Moreover, it has a considerable potential for recurrence, which depends on several factors such as the tumour size, the patient's immune system, the depth of the lesion and anatomic localization.

SCC may develop from pre-malignant lesions, such as actinic keratoses (AK, extremely common precancerous lesions in humans, consisting on evolving cutaneous neoplasms of atypical keratinocytes). In fact, an AK lesion is a signal of UV-damaged skin and approximately 1–10% of those cases progress to invasive SCC (Didona *et al.* 2018; Griffin *et al.* 2016).

Although the great majority of NMSCs are relatively non-lethal and treatable, they represent a significant economic burden to health services and an increasing global healthcare problem due to its growing incidence (over the past 20 years, the prevalence of BCC and SCC has increased by 35% and 133%, respectively) and can cause substantial morbidity especially because NMSCs occur on visible areas such as the head, neck and face (Lomas *et al.* 2012).

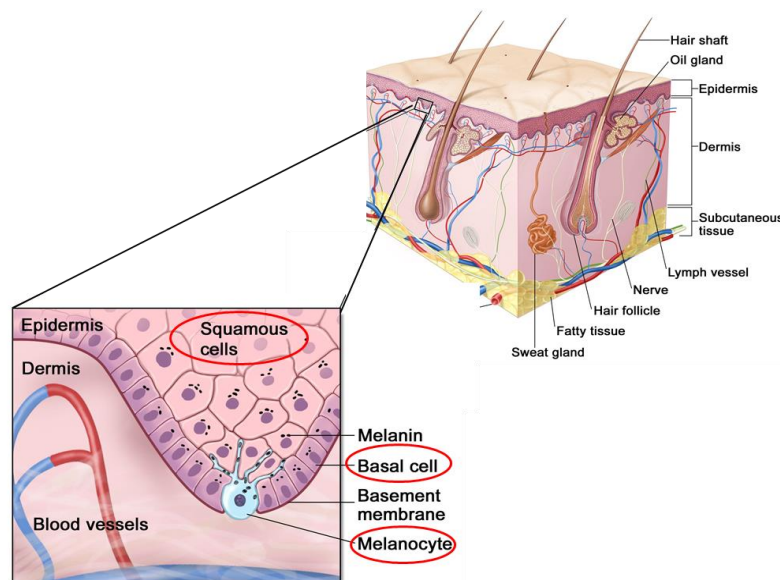


Figure 2.7. Schematic representation of normal skin. Basal cell keratinocytes and squamous epithelial keratinocytes (the source cells for BCC and SCC, respectively) are located in the relatively avascular epidermis. Melanocytes are also present and serve as the source cell for melanoma development. The basement membrane zone defines the separation between epidermis and dermis, situated underneath the basal cell keratinocytes (Berwick *et al.* 2006).

The choice of treatment will depend on several factors, including the type of tumour, how big and aggressive it is, the patient's preference and cosmetics aspects. Surgery, which aims to completely excise the tumour area and some of the tissue around it to ensure that no cancer cells are left behind, has been the first treatment option (the 'gold standard' of the treatment), but there are some alternative methods that can be broadly categorised as physical destruction (radiotherapy), immunomodulation (imiquimod, an immune response modifier that stimulates the innate- and cell-

mediated immune responses) and chemical destruction (such as fluorouracil cream and photodynamic therapy) (Griffin *et al.* 2016). In fact, when considering treatment options for skin cancer, most of the patients give a lot of importance on avoiding scars as much as possible, so the concept of nonsurgical NMSC treatment is appealing for both patients and physicians. Over the last two decades, non-invasive and painless topical medications in the form of creams have been developed to effectively treat the affected area, and since the skin is an easily accessible administration site, this makes the topical via a very attractive one (Engesland *et al.* 2015). One of the drugs considered for this purpose and that has been in use for about 50 years is 5-Fluorouracil (5-FU), being one of the most effective chemotherapeutic agents in the treatment of several cancers such as stomach, breast, head and neck cancers (Cameron *et al.* 1994; Vokes *et al.* 1998). It decreases cell proliferation and induces cellular death, principally in cells that exhibit high mitotic rates, through inhibition of thymidylate synthetase and consequently interfering with DNA synthesis. Topical application of 5-FU as a chemotherapeutic agent for NMSC has been effective for the treatment of superficial BCC (sBCC), *in-situ* SCC (often called Bowen's disease) and mainly for precancerous conditions such as actinic keratosis (Bahner and Bordeaux 2013; van Ruth *et al.* 2006). In addition, it is useful for delineating tumour margins before a definitive surgical procedure. Since it lacks capacity of penetration through the dermis, the drug is generally not recommended for invasive BCCs and SCCs. Previous works have reported the efficacy of topical 5-FU ointment for NMSC treatment and most of the patients that used it, rated their cosmetic results as very positive (Amini *et al.* 2010; Samarasinghe *et al.* 2012). To target tumour cells within the skin and minimize possible systemic and topical adverse effects, the drug must penetrate the skin layers, exerting its effects within the epidermis and dermis. Nanocarriers constitute a drug delivery system that has been extensively explored to transport anti-cancer drugs such as 5-Fluorouracil. Among those nanocarriers, zeolite nanomaterials have been explored as suitable hosts for the encapsulation of drug molecules, mainly due to their suitable structural properties and stability in biological environment. In fact, in the literature it is commonly reported the use of zeolites to accommodate drug molecules inside and release them in a controlled manner, drugs such as 5-FU, ibuprofen and sulfonamide antibiotics. In a recent study, 5-FU was successfully loaded into the NaY zeolite framework and the drug delivery system was able to increase the efficiency of the anticancer drug on HCT-15 and RKO human colon carcinoma cell lines tested, highlighting the idea of the drug-loaded zeolite as a promising system (Paradee *et al.* 2016; Spanakis *et al.* 2014; Vilaça *et al.* 2013).

2.4.2 Antineoplastic drugs: 5-Fluorouracil

5-fluoro-1H,3H-pyrimidine-2,4-dione ($C_4H_3FN_2O_2$), commonly known as 5-fluorouracil is an antimetabolite drug that interferes with both DNA and RNA synthesis, driving cell death (Avenidaño and Menendez 2015). This heterocyclic aromatic organic compound (molecular weight of 130,08 g/mol) has a very similar structure to that of uracil (Zhang *et al.* 2008). In fact, these two analogues only differ at the C-5 position, where 5-FU has a fluorine atom and uracil contains a hydrogen (Gester *et al.* 2014) (Figure 2.8). Pioneer results evidencing the potential use of 5-FU as an anticancer agent were obtained by Rutman *et al.* in 1954. They observed that, in rat hepatomas, exogenous radioactive-labelled uracil pyrimidine was preferentially used for nucleic acid biosynthesis compared to the normal hepatic tissues, evidencing that uracil was needed for sustaining this process, essential for tumour growth (Rutman *et al.* 1954). This experiment highlighted that uracil metabolism could be an effective target to trigger tumour cell death, which led to the idea of synthesizing an uracil analogue that could interfere with nucleic acid synthesis and slow the process of tumour growth. In 1957, Charles Heidelberger synthesized 5-FU for the first time and unravelled its anticancer activity (Heidelberger *et al.* 1957). Since then, it has been widely prescribed as chemotherapeutic agent, either alone or in combination with other drugs and plays an important role in the clinical treatment of solid tumours such as breast, head, neck, aerodigestive tract and especially colorectal cancers (Noordhuis *et al.* 2004). Administered as a cream, it is also useful for the treatment of some skin cancers (Sharquie and Noaimi 2012; van Ruth *et al.* 2006). Essentially, antimetabolite drugs such as 5-FU act by either preventing vital biosynthetic processes or by incorporation into DNA and RNA molecules, inhibiting their normal function. Interestingly, 5-FU does both (Longley *et al.* 2003).

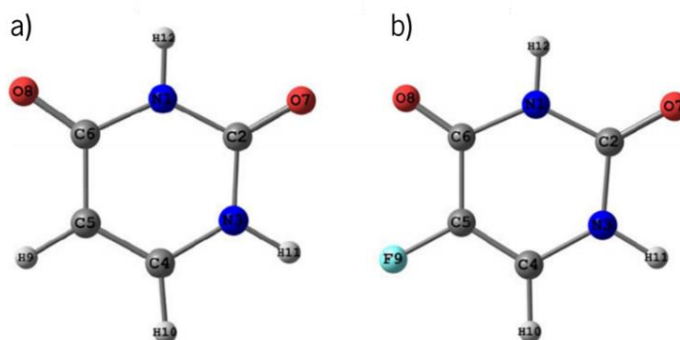


Figure 2.8. Molecular structures of: A) uracil and B) 5-FU (Gester 2014).

2.4.2.1. 5-FU metabolism

After being administered, the drug is subjected to one of two possible metabolic pathways: 80 to 85% of the initial dose is degraded through catabolic reactions that culminate in the conversion of 5-FU to inactive metabolites by the action of dihydropyrimidine dehydrogenase (DPD), mainly present in the liver and consequently eliminated via urinary excretion (Avendaño and Menendez 2015). Only 1 to 3 % of the drug goes through anabolic reactions, where 5-FU is converted to active metabolites, responsible for the cytotoxic effect on tumour cells and normal tissues (Miura *et al.* 2010; Focaccetti *et al.* 2015). The availability of 5-FU for anabolism is regulated primarily by the extent of its catabolism, highlighting the influence of the balance between these two metabolic fates on the biological effects of the drug. Non-metabolized 5-FU is basically harmless to mammalian host and tumour cells (Diasio and Harris 1989). The essential steps of 5-FU metabolism are exhibited in Figure 2.9.

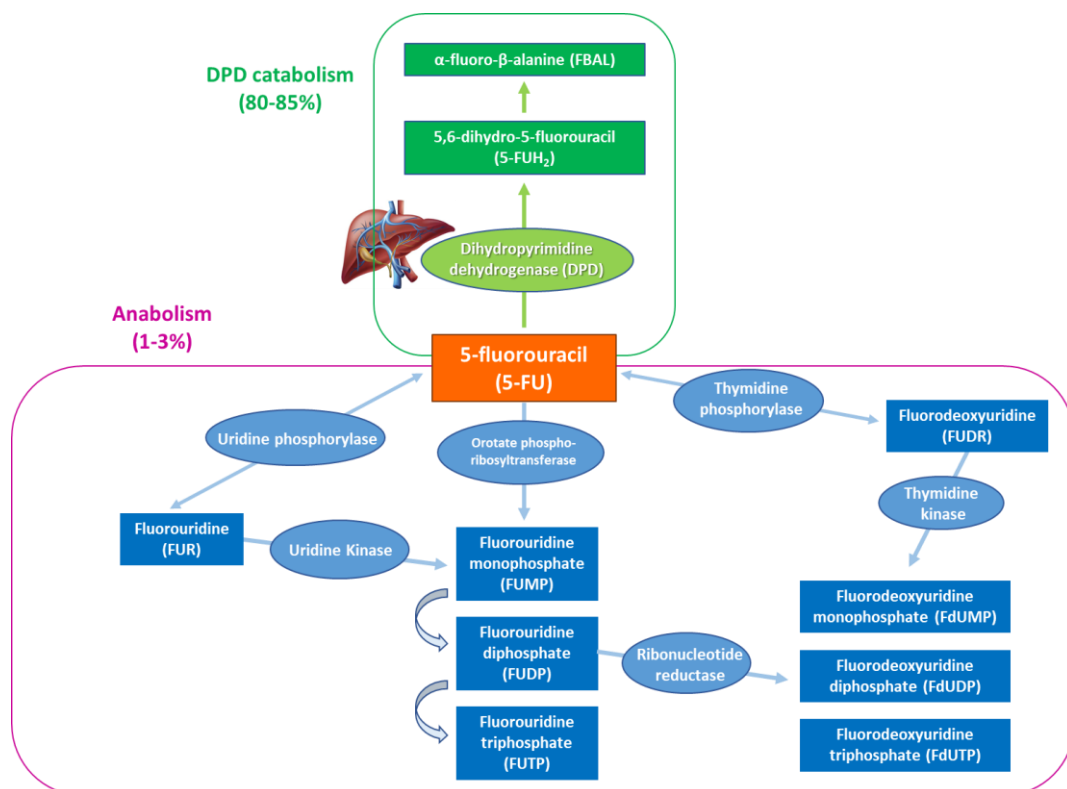


Figure 2.9. Summarized 5-FU anabolism and catabolism (adapted from Miura *et al.* 2010).

5-FU catabolism

The first catabolic step of 5-FU consists on the reduction of the double bond in the pyrimidine ring, catalysed by the enzyme DPD, resulting in the formation of dihydro-5-fluorouracil (5-FUH₂). This reaction is the rate-limiting step since it determines the amount of 5-FU that remains available for the anabolic pathway. The product of DPD, 5-FUH₂, is unstable and is further broken down to a transient intracellular catabolite, α -fluoro- β -ureidopropionic acid (FUPA), which is finally converted to α -fluoro- β -alanine (FBAL), the major urinary catabolite of the process (Diasio 2002; Miura *et al.* 2010).

5-FU anabolism

The cellular uptake and the anabolic pathways of 5-fluorouracil are essentially the same pathways used by pyrimidine uracil (Parker and Stivers 2011). 5-FU rapidly enters the cell through the transport mechanism of simple diffusion, where it is enzymatically converted to three main active metabolites: fluorodeoxyuridine monophosphate (FdUMP), fluorodeoxyuridine triphosphate (FdUTP) and fluorouridine triphosphate (FUTP) (Schilsky 1998). These metabolites interfere with both DNA and RNA synthesis and the action of the enzyme thymidylate synthase (TS), leading to severe cell damage and eventually cell death (Miura *et al.* 2010). Cytotoxic effects will be further described in the next section.

2.4.2.2 Mechanisms of action

Thymidylate synthase inhibition

Several studies have indicated that the anticancer effects exhibited by 5-FU are mainly caused by inhibition of thymidylate synthase (TS), a key enzyme of pyrimidine *de novo* synthesis. TS catalyses the reductive methylation of deoxyuridine monophosphate (dUMP) to deoxythymidine monophosphate (dTMP), using folate 5,10-methylenetetrahydrofolate (CH₂THF) as the methyl donor (Avendaño and Menendez 2015) (Figure 2.10). Although this seems to be a subtle structural

change, this step is crucial for correct discrimination of thymine from the other three bases present in DNA chains by transcription factors, repressors, enhancers and other DNA-binding proteins. As a result of this reaction, *de novo* thymidylate synthesis occurs, which is necessary for DNA replication and repair (Longley *et al.* 2003).

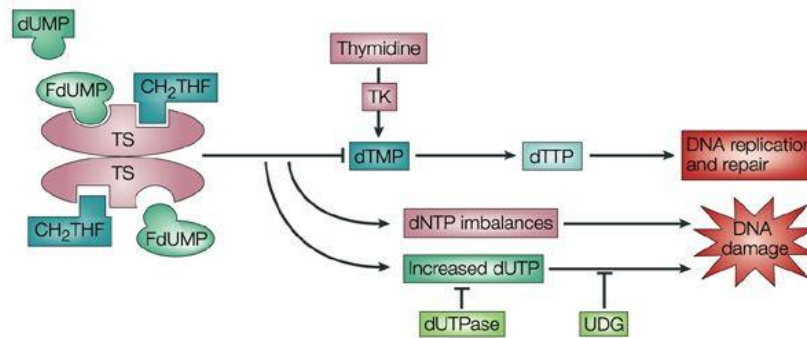


Figure 2.10. Mechanism of thymidylate synthase inhibition by 5-fluorouracil (Longley *et al.* 2003).

FdUMP, binds to the nucleotide-binding site of TS, forming a stable ternary complex with the enzyme and CH₂THF, preventing the binding of the normal substrate (dUMP) and consequently inhibiting dTMP synthesis (Zhang *et al.* 2008). This blocking step leads to depletion of dTMP and ultimately of dTTP (which is required for DNA synthesis) inducing variations in the levels of other deoxynucleotides (dATP, dGTP and dCTP) through several feedback mechanisms (Longley *et al.* 2003). Thymidine starvation and consequent deoxynucleotide imbalances lead to S-phase cell cycle arrest, disrupting DNA synthesis and repair and finally causing lethal DNA damage (the so-called thymineless death) (Focaccetti *et al.* 2015).

DNA and RNA misincorporation

Because of TS inhibition, dUMP naturally accumulates and it can be subsequently converted to dUTP. Both dUTP and 5-FdUTP (one of the previously mentioned active metabolites of 5-FU) can act as a false substrate and be misincorporated by DNA polymerase into DNA (Parker and Stivers 2011). The incorporation of these nucleotides during 5-FU treatment becomes even more avid because of dTTP level reduction. The action of base excision repair enzymes becomes worthless in the presence of high levels of FdUTP and dUTP because polymerases continue to erratically

reincorporate these nucleotides in a futile repair cycle, eventually culminating in toxic DNA fragmentation and finally cell death (Diasio and Harris 1989).

In addition to these DNA associated cytotoxicity mechanisms, several studies have suggested that transformation of 5-FU metabolite, 5-FUDP, into the corresponding triphosphate (5-FUTP) allows its misincorporation into different RNA molecules by RNA polymerase, disturbing several processes related with RNA metabolism, such as processing of pre-rRNA into mature rRNA, post-transcriptional modification of tRNAs and the assembly and activity of snRNA/protein complexes which interferes with pre-mRNA splicing and leads to impaired mRNA synthesis (Noordhuis *et al.* 2004; Zhang *et al.* 2008) (Figure 2.11).

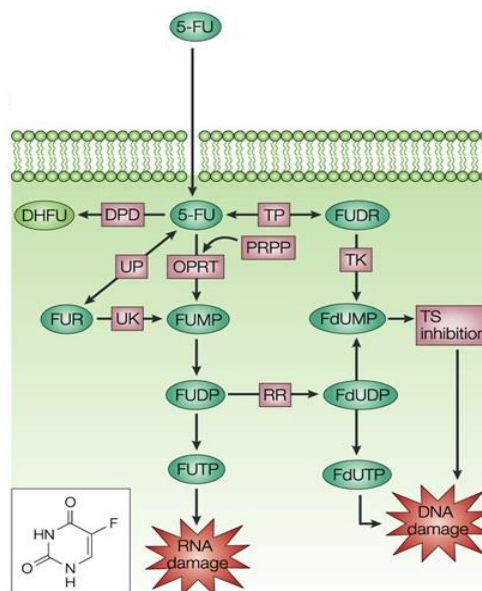


Figure 2.11. 5-Fluorouracil cytotoxic mechanisms following cellular uptake. 5-FU is converted to three main active metabolites: fluorodeoxyuridine monophosphate (FdUMP), fluorodeoxyuridine triphosphate (FdUTP) and fluorouridine triphosphate (FUTP), which cause DNA and RNA damage (Longley *et al.* 2003).

CHAPTER 3

EXPERIMENTAL PROCEDURE

In this chapter, the experimental procedure developed in this work will be described in more detail, namely the preparation of the DDS and the theoretical principles and instrumental/experimental conditions of the techniques used.

The laboratorial work was subdivided in three major parts, each taking place in distinct facilities of University of Minho: the preparation and characterization of the DDS nanomaterials were carried out in the Chemistry Department; the evaluation of the antimicrobial effects of DDS was performed in the Biology Department and finally, the third component of the experimental work, consisting on the evaluation of cellular viability of a human skin cancer cell line in the presence of the DDS, was developed in the Life and Health Sciences Research Institute (ICVS).

3.1. Zeolite host structure and compounds

As previously mentioned, the zeolite NaY (CBV100; Si/Al ratio = 2.83) in the form of white powder, purchased from Zeolyst International, was selected as host nanostructure to prepare the proposed DDS (Table 3.1).

Table 3.1. Characteristics of the zeolite NaY.

Zeolite	Structural Family	Si/Al ratio	Unit cell formula	Provider
NaY	Faujasite	2.83	$\text{Na}_{53}\text{Al}_{53}\text{Si}_{139}\text{O}_{384}$	Zeolyst International

The chosen antineoplastic drug to be introduced into the host, 5-fluoro-1H, 3H-pyrimidine-2,4-dione (5-FU), was purchased from Sigma Aldrich appearing in the form of a fine white powder. Silver (I) nitrate, provided by Fisher Scientific, was used to introduce the silver ions into the zeolite structure via ion exchange method (Table 3.2).

Table 3.2. Characteristics of the compounds to be incorporated into the host.

Compound	Molecular Formula	Molecular Weight (g/mol)	R-phrases	S-phrases	Purity (%)	Provider
5-Fluorouracil	$\text{C}_4\text{H}_3\text{FN}_2\text{O}_2$	130.078 g/mol	25-52	45	99	Sigma-Aldrich
Silver Nitrate	AgNO_3	169.87 g/mol	8-34-50/53	26-45-60-61	-	Fisher Scientific

3.2. Preparation of the DDS

Two samples were prepared from the parental zeolite, NaY: one with silver ions exchanged in the structure (AgY) and the second one with the introduction of the compound 5-FU into the structure of AgY, resulting in a hybrid zeolite system named (Ag/5-FU)Y.

3.2.1. Preparation of AgY by ion exchange method

The ion exchange method was used to prepare the nanomaterials with antimicrobial properties, introducing the desired cation (in this case, Ag^+) in the zeolitic framework. For that purpose, NaY was used as starting material. The sample was prepared by adding 3 g of NaY zeolite (without previous treatment) to 60 mL of an aqueous solution (0.01 M) of silver nitrate in a volumetric flask which was posteriorly coated with aluminum foil to prevent undesired Ag^+ reduction reactions due to silver sensibility to light exposure. The mixture was then maintained under constant stirring at 300 rpm for 24 h at room temperature. After that period, the suspension was filtered using Duran® sintered disc filter funnel, washed with deionized water and dried overnight at 60 °C to obtain the Ag-zeolite, designated AgY. Finally, the resulting powder was calcined at 350 °C for 4 h to obtain a white powder (Figure 3.1). The calcination process helps to fix the silver cations within the zeolite structure and ensures that all impurities are removed, thus avoiding subsequent contamination.

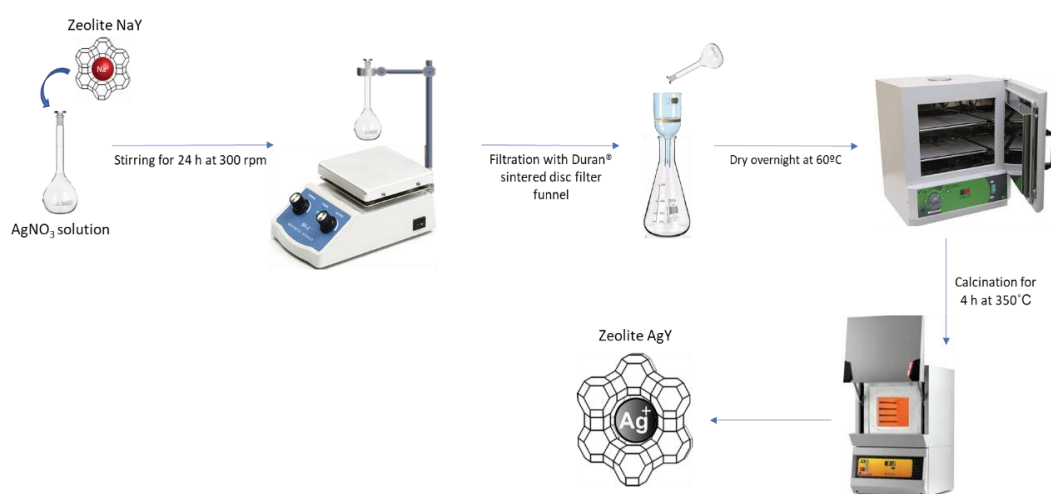


Figure 3.1. AgY preparation process. NaY is used as starting material and immersed in an AgNO_3 solution that contains the cation of interest, Ag^+ .

3.2.2. Preparation of Ag(5-FU)Y

The encapsulation of 5-Fluorouracil into AgY was performed by liquid adsorption, based on a previously followed procedure (Vilaça *et al.* 2013). Before the 5-FU loading, the AgY powder was pretreated at 150 °C for 4 h, to avoid the presence of water molecules inside the pores. The loading of the drug into the zeolite structure was achieved by adding 200 mg of AgY zeolite powder to 25 mL of a solution of 5-FU (0.023 mM) in 80 % acetone/20 % water, as solvent. The mixture was kept under constant stirring at room temperature for 48 h (to promote the drug diffusion towards the inner space of zeolite framework) and sealed to prevent the evaporation of the solvent. After this period, the resulting mixture was filtered and dried at 60 °C for 12 h to evaporate the solvent. Another sample was prepared in the same conditions but, during the filtration step, it was washed once with solvent to remove the non-encapsulated 5-FU, for comparison purposes. For simplicity, the prepared DDS will be referred to as (Ag/5-FU)Y throughout this work.

It is important to mention that the choice of acetone as solvent was due to preliminary studies, where different solvents in which 5-FU is soluble were tested (ethanol, methanol and acetone). After preparation of the DDS, ethanol and methanol, remained adsorbed in the zeolite structures and exhibited toxicity to the cell lines studied, unlike acetone, justifying its choice as most suitable solvent (Vilaça *et al.* 2013).

3.3. *In vitro* release studies

In vitro release studies were performed to evaluate the release behaviour of silver and 5-FU towards the exterior of the zeolite framework. Quantification of 5-FU released from (Ag/5-FU)Y was carried out by UV/vis spectrophotometry, while the release of silver from AgY was monitored by ICP-OES analysis.

3.3.1. 5-Fluorouracil *in vitro* release – UV/vis spectrophotometry

UV/visible spectrophotometry is one of the most commonly used analytic techniques, mainly because of its simplicity, low cost and wide range of applications. It represents a very useful tool for qualitative and quantitative analysis in various fields such as chemistry, biochemistry, material and chemical engineering and physics (Rocha and Teixeira 2004).

The technique consists on measuring the absorbance of UV or visible light by a sample, either at single wavelength or over a certain range in the spectrum (in the case of UV/vis ranges from 200 to 800 nm).

When absorption of light by the sample matter occurs, the energy content of the molecules increases. Photons of UV and visible light have enough energy to promote transitions between the different electronic energy levels (Burgess 2017; Owen and Agilent 2000). The fundamental law of spectrophotometry establishes a relationship between the reduction of light intensity caused by an absorbing substance in solution and the concentration of that same 'substance (Tissue 2002). The mathematical expression that allows the calculation of the concentration of an analyte in solution is known as the Beer-Lambert Law (Eq. 1) (Gauglitz 2008):

$$A = \log \left(\frac{I_0}{I} \right) = \epsilon \cdot b \cdot c \quad \text{Eq. 1}$$

where A refers to absorbance, I_0 to the intensity of incident monochromatic radiation and I to the intensity of radiation that emerges from the sample (transmitted radiation). The difference between these last two parameters represents the amount of light absorbed. Molar absorptivity, ϵ , is characteristic of the absorbent species and its magnitude depends on the incident radiation wavelength. Finally, b and c correspond to the sample path length and sample concentration, respectively (Rocha and Teixeira 2004). A schematic diagram of a UV-visible spectrophotometer is shown in Figure 3.2.

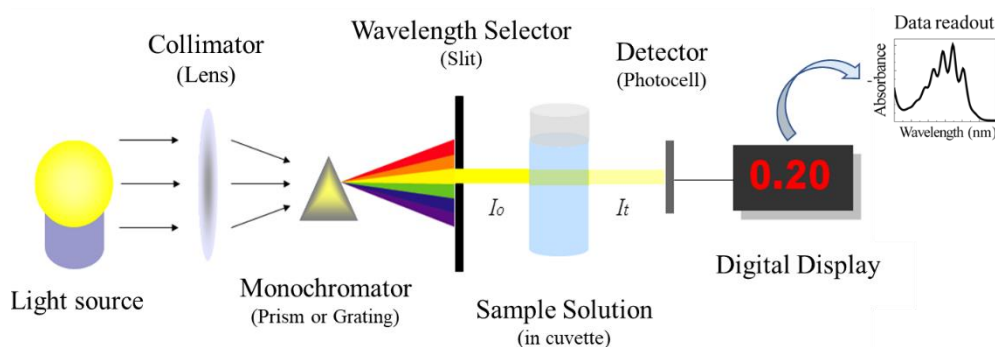


Figure 3.2. Basic structure of a spectrophotometer (retrieved from http://jacobsschool.ucsd.edu/cosmos/2016/cluster5/Lego_Spectrophotometer.html)

The light source (combination of tungsten/halogen and deuterium lamps) provides the UV/visible radiation. This light is focused onto a dispersive element that basically splits it into its component

colors of different wavelengths. Only the specific wavelength that falls directly on the monochromator exit slit passes through it and then hits the sample (l). Finally, the detector converts the incoming/transmitted light (I) into current and a chart recorder eventually plots the absorbance against wavelength in UV and visible section of the electromagnetic spectrum (Gauglitz 2008; Tissue 2002).

3.3.1.1. Instrumentation and experimental conditions

For the *in vitro* release studies, 10 mg of the drug-loaded nanoparticles ((Ag/5-FU)Y zeolite) were added to 50 mL of a buffer solution of phosphate-buffered saline (PBS), simulating body fluid, with pH = 7.4 at 37 °C. Aliquots of 5 mL of the mixture were withdrawn at predetermined intervals and replaced by the same amount of fresh buffer to maintain the volume of released medium constant. Release studies were carried out throughout 6 h. The collected aliquots were filtered with disposable filter devices (Whatman filters) consisting of a 0.20 μ m nylon membrane, purchased from GE Healthcare UK. Then, the UV-vis absorption spectrum of each withdrawn sample was recorded with a UV-2501PC spectrophotometer (Shimadzu, Japan) at 266 nm (λ_{max}) following appropriate dilution (1 mL of sample mixed with 2 mL of PBS in a quartz cuvette) and using 3 mL of PBS as blank sample for baseline correction. Measurements were conducted in triplicate and the averaged values were considered for posterior analysis. To determine the amount of 5-FU released during the 6 h experiment, a set of 10 standard solutions in the concentration range of 0.004-0.270 mM was prepared and the concentration of 5-FU was calculated according to the resulting standard curve ($r = 0.999$) (Eq. 2):

$$A_{266\text{ nm}} = 6966,1 \times |5\text{-FU}| - 0,0002 \quad \text{Eq. 2}$$

To determine the corrected concentration of 5-FU released, the following equation was used (Eq. 3):

$$C_{t\text{corr}} = C_t + \frac{v}{V} \sum_0^{t-1} C_t \quad \text{Eq. 3}$$

Where, $C_{t\text{corr}}$ corresponds to the corrected concentration at time t (corrected to account for changes in volume), C_t is the apparent concentration at time t, v is the volume of sample taken and V is the total volume of the solution.

3.3.2. Silver *in vitro* release – Inductively coupled plasma-optical emission spectrometry (ICP-OES)

ICP-OES consists of a technique that can be used to obtain both qualitative (determine what elements are present) and quantitative information (determine how much of an element is present) about the elements present in aqueous solutions. The hallmarks of this technology, namely, high speed, capacity of multi-element detection, low detection limits and reliability make it attractive for a wide range of analytical applications (Moore 1989; Zurera and López 2003). A schematic representation of the ICP spectrometer work-flow is shown in Figure 3.3.

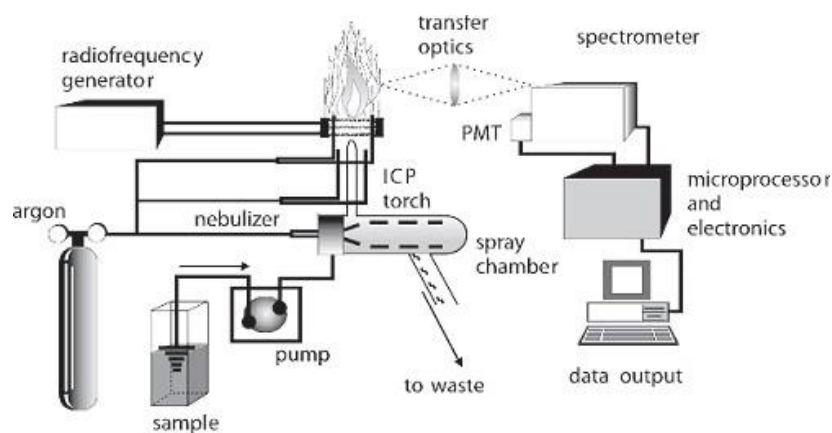


Figure 3.3. Schematic diagram of an inductively coupled plasma (ICP) spectrometer (retrieved from <https://www.azom.com>).

Argon gas is directed through a torch. The top end of that torch is surrounded by a copper coil where electric and magnetic fields are set up. With argon gas being swirled through the torch, a spark is applied to the gas causing some electrons to be stripped from their argon atoms. These electrons are then caught up in the magnetic field and accelerated by them. Adding energy to the electrons using a coil in this manner is known as inductive coupling. These high-energy electrons in turn collide with other argon atoms, stripping off still more electrons. This collisional ionization continues in a chain reaction, breaking down the gas into a very hot plasma (temperatures can reach between 6000-8000 K) consisting of argon atoms, electrons, and argon ions, forming what is known as an inductively coupled plasma (ICP) discharge. The ICP discharge appears as a very intense, brilliant white, teardrop-shaped light (Boss and Fredeen 1989; Hou *et al.* 2016).

The sample (typically a liquid) is initially nebulized into an aerosol, a very fine mist of sample droplets. This aerosol is then carried into the center of the plasma by the inner (or nebulizer) argon

flow. The high temperature of the plasma causes the removal of the solvent from the aerosol, leaving the sample as microscopic salt particles which are vaporized and then dissociated into atoms (atomization) (Moore 1989). Since many elements have their strongest emission lines emitted from the ICP as excited ions, ionization process may also be necessary for some elements. As the valence electrons of those atoms or ions take up the thermic energy, they reach a higher "excited" state. When they drop back to ground state, emission of energy occurs in the form of light (photons) in the form of discrete lines at specific wavelengths that are characteristic of each element and so allow to confirm its presence in the sample being analyzed. The emitted light intensity by the excited atoms/ions is proportional to the concentration of the analyte of interest, so it can be detected and quantified with an optical emission spectrometer (OES) and then converted to concentration by comparison with suitable calibration curves to quantify the element(s) of interest (Hou *et al.* 2016; Koons 2003).

3.3.2.1 Instrumentation and experimental conditions

The silver release behavior was also studied *in vitro*. For that purpose, 25 mg of AgY were added to 50 mL of a buffer solution of PBS, simulating body fluid, at pH = 7.4 at 37 °C. Aliquots of 5 mL of the mixture were withdrawn at predetermined intervals and replaced by the same amount of fresh buffer to maintain the volume of released medium constant. Release studies were carried out throughout 72 h. The collected aliquots were filtered with disposable filter devices (Whatman filters) consisting of a 0.20 µm nylon membrane, purchased from GE Healthcare UK. After filtration, samples were acidified with a drop of concentrated nitric acid 60 % (v/v) in order to keep metals in solution. Chemical analysis of all the collected samples was performed in the Biologic Engineering Department (DEB) facilities, using an Optima 8000 inductively coupled plasma-optical emission spectrometer (Perkin-Elmer) to quantify the released amount silver. The S10 Autosampler (Perkin-Elmer) was used for high throughput and automated analysis of the standard and sample solutions.

A series of 6 standard solutions of silver nitrate was prepared in nitric acid 5 % v/v, in the concentration range of 0.001-0.025 ppm and the silver concentration in each sample was calculated according to the resulting calibration curve ($r = 0.999$), using the WinLab ICP continuous software (PerkinElmer).

3.4. Characterization techniques

The functionalized nanomaterials were characterized by several analytical techniques whose general theoretical concepts and experimental conditions used will be presented in the following section, namely: X-ray photoelectron spectroscopy (XPS), thermogravimetric analysis (TGA), nitrogen gas adsorption isotherms and scanning electron microscopy with energy dispersive X-ray spectroscopy (SEM/EDX).

3.4.1. X-ray photoelectron spectroscopy (XPS)

XPS (X-ray photoelectron spectroscopy) is one of the most widely used techniques to characterize surfaces of solid materials. It is useful to study aspects such as the elemental composition and quantification of the surface (with a typical “sampling depth” up to 10-50 nm approximately), the chemical or electronic state of each element and the presence of contaminant elements on the surface (Seah 1980). It is based on the well-known photoelectric effect, meaning it works by irradiating the sample surface with a beam of monochromatic soft X-rays, normally from an aluminium or magnesium source ($\text{Mg-K}\alpha$ or $\text{Al-K}\alpha$ at 1253.6 and 1486.6 eV, respectively) causing the excitation and consequent ejection of electrons from the core level electron shells. Basically, the interaction between a X-ray photon and the core-level electron (K electron shell) from a superficial atom results in the complete energy transfer from the photon to the electron (Stöcker 1996). Thus, the electron (referred to as photoelectron) has enough kinetic energy to escape from atoms that are present on the surface region of the sample (Figure 3.4).

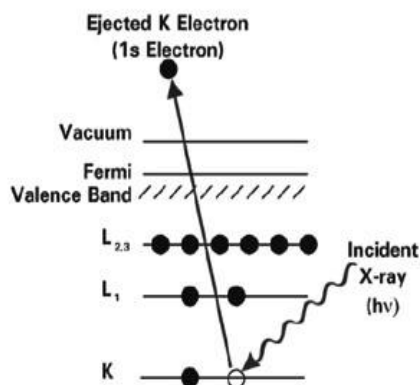


Figure 3.4. Photoemission process that occurs during XPS analysis. An electron from the K-shell is ejected from an atom as a 1s photoelectron after ionization by incident X-rays (Zaidi 2011).

The energy spectrum of the released photoelectrons is determined by means of a high-resolution electron spectrometer. Specimen analysis is carried out in a high vacuum chamber to facilitate the transmission of the photoelectrons to the analyzer and to minimize the re-contamination of a freshly cleaned sample as well. After the electron spectrometer measures the kinetic energy of the ejected photoelectrons, it is translated into binding energy for the specific atomic orbital of the electron, according to the following equation (Eq. 4) (Zaidi 2011):

$$BE = h\nu - KE - \varphi \quad \text{Eq. 4}$$

Where BE corresponds to the electron binding energy, $h\nu$ to the energy of the incident X-ray, KE to the kinetic energy of the emergent electron and φ to the spectrometer work function.

Since each element has a characteristic set of binding energies for electrons present in these core levels, as a 'fingerprint', XPS analysis allows the identification of almost all the existing elements on the sample (except hydrogen and helium) by measuring the binding energy values. Furthermore, the binding energy of core electrons can suffer changes due to the chemical environment of the element (the atoms bound to the irradiated element) and to its oxidation state in compounds. This variation results in the shift of the corresponding XPS peak, an effect known as "chemical shift", one of the most important aspects of XPS. It can be corrected through tabled values for each atom in standard compounds and provide information about the chemical status of the element in the sample under analysis. Since the number of detected photoelectrons of an element is dependent on the atomic concentration of that element in the sample, XPS is useful not only to identify the elements but also to determine their relative concentrations (Seah 1980).

3.4.1.1. Instrumentation and experimental conditions

In the current study, the chemical composition of NaY, AgY and (Ag/5-FU)Y zeolite samples was examined by XPS surface measurements, using a Kratos Axis-Supra instrument. Measurements were carried out using Al-K α radiation as monochromatic X-ray source ($h\nu = 1486.6$ eV). Photoelectrons were collected from a take-off angle of 90° (defined as the angle between the sample surface and the axis of the XPS analyzer lens). The measurement was done in a Constant Analyzer Energy mode (CAE) with a 15 mA of emission current and 160 eV and 40 eV pass energy for respectively, survey spectra and high-resolution spectra. Samples were fixed to the sample holder with double sided carbon tape. A wide scan survey spectrum was used to identify and

quantify the elements in the sample and high resolution narrow scans to build the chemical state assessment, as well as to quantify the presence of the reference elements in the sample. Data analysis and atomic quantification were determined from the XPS peak areas using the ESCApe software supplied by the manufacturer Kratos Analytical.

The binding energy values of O 1s, Na 1s, F 1s, Al 2s, Si 2p and Ag 3d were determined by setting the C 1s peak of aliphatic carbon at 285.0 eV as internal reference (charge referencing). Since a positive charge develops as the sample is irradiated with X-rays, a low energy flood gun electron source was employed to prevent net sample charging (charge compensation) otherwise it would distort the position and shape of the XPS peaks.

3.4.2. Thermogravimetric analysis (TGA)

Thermal analysis comprises several different techniques and methods, each one monitoring the variation of a specific property of a sample (optical properties, pressure, gas exchange, mass, magnetic properties, chemical composition, among others) as a function of temperature (heating or cooling), T , or as a function of time, t , at a constant temperature (isothermal mode). Thermogravimetry analysis (TGA) is one of them and it is defined as a continuous process that measures the mass change of a substance (Hatakeyama and Quinn 2018). The sample can be heated or cooled, at a specific speed (dynamic measurement), or it can be kept at a fixed temperature (isothermal measurement). An example of a common procedure is the heating programme of polymeric systems at a temperature range of 50-500 °C, at a heating rate of 5-10 °C/min until complete degradation of the sample occurs (Brown 1988). Analysis results are presented as a plot of mass (commonly exhibited as mass percentage) against temperature or time. A representative result of TGA is exhibited in Figure 3.5 A).

Upon thermal degradation, mass loss is only detected if a process occurs where a volatile component is lost. In that way, the sensor registers that loss, appearing as a step, illustrated by the curve. Instruments equipped with software for data acquisition can also provide the derivative of the TG curve as complementary information (Heal 2002). The derivative represents the rate at which the mass changes as a function of time (dm/dt) or temperature (dm/dT) and is known as DTG (derivative thermogravimetry) curve (Figure 3.5. B)).

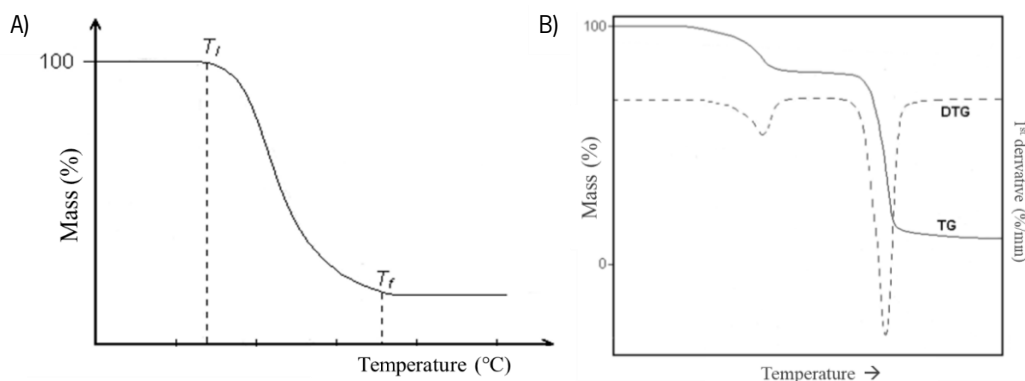


Figure 3.5. A) Thermal decomposition curve of a material. T_i indicates the temperature at which starts the mass variation and T_f refers to the temperature at which the process responsible for mass variation ends; B) Representative TGA and DTG curves. The continuous line represents the thermal decomposition that results in mass loss and the dotted line represents the 1st derivative curve, where the peaks indicate the temperatures at which the rate of that decomposition is maximum (Heal, 2002).

The analysis of these curves and their features (peaks, discontinuities and changes of slope) allow the study of several thermal events in the sample: loss or uptake of water, desorption and adsorption of gases, thermal stability, oxidative stability, pyrolysis reactions or phase transition, among others.

The experimental process of thermal decomposition itself can be explained in a very simplified way: measurements of variations in sample mass are made by placing the substance in an appropriate sample holder, typically a small inert crucible, which is attached to an electronic microbalance and has a furnace (normally an electrical resistive heater) located around the sample. The combination of the electronic microbalance with a furnace, a temperature programmer and a computer for control, is known as thermobalance (also referred to as thermogravimetric analyser), which allows the sample to be weighed and heated (or cooled) concurrently in a controlled manner, and the mass, time and temperature data to be recorded (Prime *et al.* 2008).

In the specific case of zeolites, this technique can be used to elucidate temperature-induced reactions such as dehydration, dehydroxylation and decarbonisation. Moreover, if organic molecules are used during the synthesis of these porous materials, the quantity occluded in its cavities and pores can be determined (Amrhein *et al.* 1996).

3.4.2.1 Instrumentation and experimental conditions

The loading and the thermal stability of the samples were determined by thermogravimetric analysis in a STA 409 PC Luxx® Netzsch thermal analyser. The atmosphere used was high purity air (99.99 % minimum purity) with a constant flow rate of 50 cm³/min. Crucibles of alumina oxide, supplied by Netzsch, were used as sample holders where a certain amount of the samples was placed and heated throughout 65 min, between 50 and 700 °C at a heating speed of 10 °C/min.

3.4.3. Nitrogen (N₂) gas adsorption isotherms

Gas adsorption is the process by which atoms, ions or molecules of a gas, referred as adsorbate, are attracted to and spontaneously adhere and concentrate at the surface of a solid, the adsorbent, without undergoing chemical reaction, thereby forming a surface or interfacial layer (Figure 3.6). This phenomenon is of major importance for the characterization of a wide range of porous materials such as zeolites, which are excellent adsorbents. Monitoring physical adsorption of gases and vapours by a given material allows the determination of adsorption isotherms (which correspond to the plot of adsorbed gas volume at a constant temperature as a function of gas pressure) that provide information about several parameters related to the pore structure of that solid material, such as the surface area, pore volume and pore size distribution (Miyata *et al.* 2003).

There are several available gases and vapours that can be used as adsorptive (Ar, O₂, CO₂, CO, CH₄, among others), but nitrogen gas (N₂) is generally selected (at its ebullition temperature, -196 °C) over other gases to be manipulated in the laboratory since it is relatively easy to obtain this gas with a high degree of purity and to work at its ebullition temperature using a cryogenic bath.

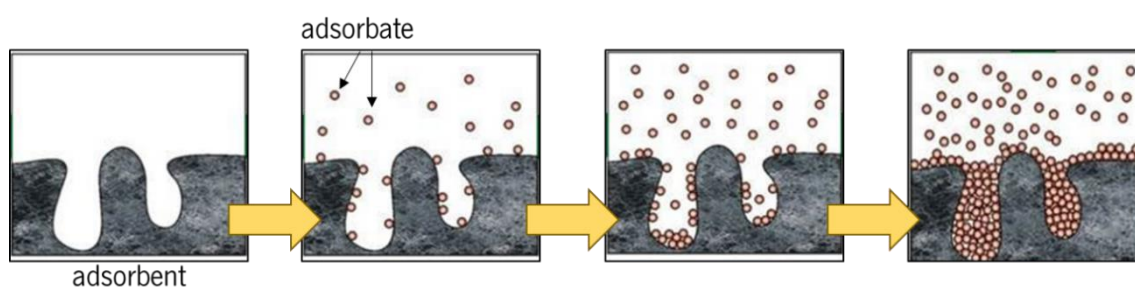


Figure 3.6. Gas adsorption process.

3.4.3.1 Instrumentation and experimental conditions

The textural characterization of the zeolites was based on the N₂ adsorption isotherms, determined at -196 °C with a Quantachrome NOVA 4200e apparatus. All samples were previously outgassed at 150 °C under vacuum. The micropore volumes (V_{micro}) and mesopore surface areas (S_{meso}) were calculated by the t-method. BET equation was used to calculate the surface areas. The desorption branch of the isotherm was utilized to obtain the mesoporous size distributions, using the Barrett, Joyner and Halenda (BJH) method.

3.4.4. Scanning Electron Microscopy with Energy Dispersive X-ray Spectroscopy (SEM/EDX)

SEM is a popular and powerful analytic tool, used in a breadth of scientific and industrial applications that involve characterization of solid materials, such as microstructure analysis of crystalline materials, providing useful information on external morphology, crystalline structure and chemical composition of the specimen (Zaefferer and Wu 2011). The basic principle of this technique consists on scanning the surface of a sample with a high-energy beam of electrons (typically 10 keV). The impact of these energetic electrons results in the generation of signals which are collected by detectors to produce real time magnified 3D images. Since the wavelength of the electron beam is much lower than the wavelength of the visible light, SEM techniques provide a magnification much higher than optical microscopes (ranging from 3x to 500,000x depending on the instrument) and an image resolution as great as 0.1 nm (Inkson, 2016).

In SEM, electrons are produced at the top of a column, by an electron gun. There are three different types of electron guns but the most common is the tungsten hairpin filament, which is heated to over 2500°C (by passing a current through it), producing thermal emission of electrons from its tip. As it moves from the source down the column, the resulting electron beam is accelerated by the anode and pass through a combination of condenser lenses and apertures to produce a tightly focused beam of electrons that is scanned across a selected area of the specimen surface in a raster pattern by scan coils (Vernon-Parry 2000) (Figure 3.7).

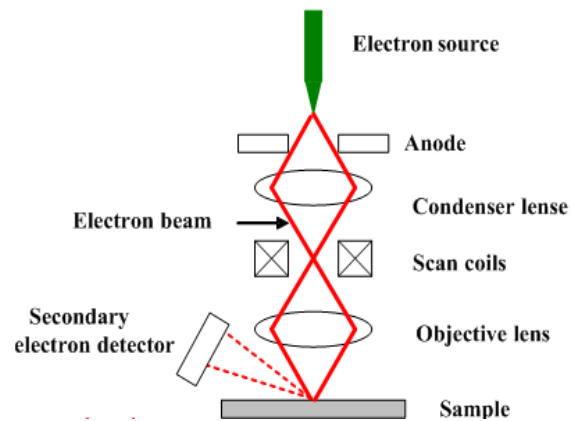


Figure 3.7. Main components of a scanning electron microscope (Inkson, 2016).

As mentioned before, these accelerated electrons carry significant amounts of kinetic energy (typically energies between 2 and 100 keV) and, as they bombard the surface of the solid sample, this energy is dissipated as a variety of signals produced by electron-sample interactions. The electron beam penetrates the specimen to a depth of a few microns and, as a result, secondary, backscattered and Auger electrons, as well as x-rays and light are emitted (Figure 3.8). The analysis of these different forms of emission reveals complementary information about the sample and the collection of these signals by various detectors in the sample chamber results in the formation of images which are then displayed on a monitor (Leonard *et al.* 2012).

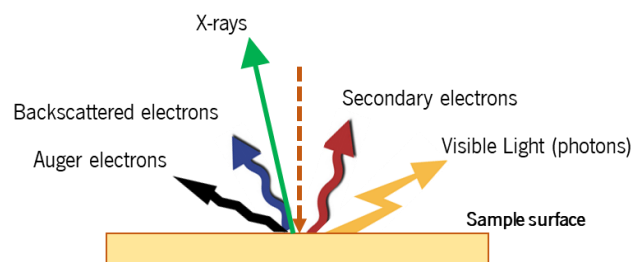


Figure 3.8. Interaction between the incident electron beam (dotted arrow) and the sample surface. Electrons penetrate the specimen resulting in the emission of secondary, backscattered and Auger electrons, as well as x-rays and light.

The diversity of signals produced by the electron beam-matter interaction provides different useful information about the sample. For example, photon emission can give information on the electronic structure and the chemical composition of materials; collection of secondary electrons provides information concerning the surface topography of the sample; backscattered electrons are mainly responsible for producing images with different contrast and the intensity of backscattered electrons reaching the detector can be correlated to the atomic number (Z) of the element within

the sample. Additionally, another useful type of signal that is commonly used in SEM is X-rays. Analysis of the energies of the emitted X-rays provides quantitative information regarding the elemental distribution and concentration, since they are characteristic of the elements involved (Scimeca *et al.* 2018). This is known as energy dispersive X-ray analysis (EDX), which reveals information about the composition of the top few microns of the sample. SEM coupled with EDX spectroscopy has the advantage of being a relatively fast and non-destructive approach that requires little or no sample preparation to perform surface characterization.

3.4.4.1 Instrumentation and experimental conditions

To study the morphology of the zeolite systems and see if there was any considerable modification upon 5-FU encapsulation, all samples were characterized by SEM. Scanning electron micrographs were collected on a LEICA Cambridge S360 scanning microscope equipped with an EDX system. Samples were coated with a thin layer of gold under vacuum (to prevent deflection of electrons caused by particles in the air) prior to analysis, using a Fisons Instruments SC502 sputter coater. This last procedure of coating is important since it prevents surface charging, which would cause image distortion.

3.5. Evaluation of the antimicrobial activity of the DDS

3.5.1. Microorganisms used as indicator strains

As previously referred, the antimicrobial properties of functionalized nanomaterials with metal ions, such as silver, have been receiving increasing attention and they can be explored as delivery systems to prevent and/or treat microbial infections, in the skin for example. So, we intended to evaluate the potential of the previously prepared zeolite samples (AgY and (Ag/5-FU)Y) and see whether they did in fact exhibit capacity to inhibit microbial growth. For that, several bacterial strains which are known to be capable of triggering several infections (including skin infections) and therefore compromise human health, were selected as predictive models, namely: the Gram-negative bacteria *Escherichia coli* and *Pseudomonas aeruginosa* and the Gram-positive bacteria *Staphylococcus aureus*, Methicillin resistant *Staphylococcus aureus* (MRSA) and

Propionibacterium acnes (Table 3.3), obtained from the culture collection of the Biology Department at the University of Minho, where these studies were performed.

Table 3.3. Characteristics of the tested bacterial strains.

Bacterial Strains	Type	Strain Code	Origin
<i>Staphylococcus aureus</i>	Gram-positive	ATCC 6538	Clinical Isolate (Human lesion)
Methicillin resistant <i>staphylococcus aureus</i>	Gram-positive	MRSA U800746	Clinical Isolate
<i>Escherichia coli</i>	Gram-negative	CECT 423	-
<i>Propionibacterium acnes</i>	Gram-positive	H60803(2961351)	Clinical Isolate
<i>Pseudomonas aeruginosa</i>	Gram-negative	7697099	Urin

3.5.2. Culture media and growth conditions

Throughout this work, all the bacterial strains were cultured and kept under aseptic conditions, using appropriate culture media. They were cultured in agar plates containing Lysogeny Broth (LB) medium supplemented with agar 2 % (w/v) (LBA) (Table 3.4) and then incubated for 24 h at 37 °C, to promote growth and obtain fresh cultures. Every culture medium was previously sterilized in the autoclave at 120 °C and 1 atm.

Table 3.4. Formulation of LBA medium per liter of H₂O

Constituent	Quantity (g)	Provider
Tryptone	10	Becton, Dickinson and Company
Yeast Extract	5	ACROS Organics
Sodium Chloride	5	Panreac
Agar	20	OXOID

3.5.3. Tested samples

The antimicrobial action of the functionalized nanomaterials, AgY and (Ag/5-FU)Y as well as of NaY zeolite, the starting material from which both nanomaterials were posteriorly synthesized, was

evaluated. Additionally, an 5-FU solution was also prepared to be tested. to investigate if the compound itself exhibited any inhibitory effect on the growth and viability of the selected microorganisms.

3.5.4. Antimicrobial assays

The main objective of this task was to verify if the prepared nanomaterials exhibited the intended antimicrobial effects due to the silver ions microbicide action, which has already been reported in several published works concerning the microbial growth inhibition caused by Ag-Y zeolite materials. In the present study, besides analysing the AgY samples, we tested the hybrid system, (Ag/5-FU)Y to determine if the zeolite still maintains its antimicrobial capacity when both silver and 5-FU are present or if, somehow, the presence of 5-FU interferes with the silver release and action or, alternatively, if the combination of silver ions and 5-FU could synergistically inhibit bacterial growth.

Before adding the culture medium to the plates, sample powders were added to the Falcon tubes containing sterilized LBA and kept under heating (approximately 45-50 °C to avoid solidification) and subtle stirring (to avoid the formation of bubbles) so that we could achieve a homogenous suspension of the nanomaterial in the medium. Meanwhile, for each bacterial strain, we prepared a pre-inoculum in Falcon tubes containing 5 mL of LB followed by overnight incubation at 37 °C and 200 rpm. An inoculum of each strain was then prepared in 5 mL of fresh culture medium, for an initial OD of 0.1 and he cultures were re-incubated at 37 °C and 200 rpm until a mid-log growth phase was reached ($OD_{600} \approx 0.4 - 0.6$) (Figure 3.9). Then, a 5 μ L drop of each inoculum was added to the microplate (in triplicate) containing the culture medium with the zeolite nanomaterials already incorporated.

The assays were performed in the presence of increasing concentrations (0.2, 0.5, 1 and 2 mg/mL) of each zeolite sample. Each assay was performed at least three times. The minimum inhibitory concentration (MIC) value, defined as the lowest concentration of zeolite that prevented bacterial growth, was determined for each pair sample/bacterial strain tested.

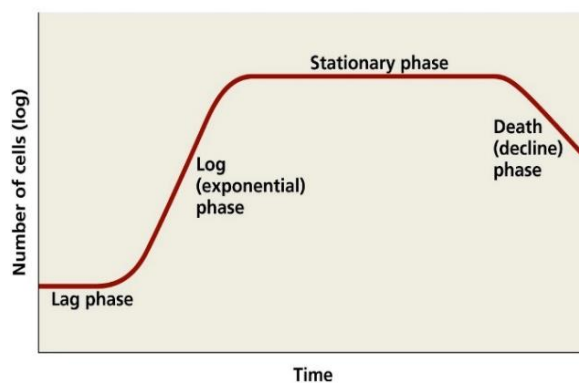


Figure 3.9. Curve of bacterial growth. The graph represents the four-phase pattern of population growth when bacteria are raised in closed culture such as a petri dish or test tube where no additional nutrients are added, no waste or dead cells are removed and where there is no additional space (Wang *et al.* 2015).

3.6. Cell viability assays

3.6.1. Cell culture conditions

Cell viability studies were performed at the Life and Health Sciences Research Institute (ICVS) facilities, using a malignant skin cancer cell line, A375 (Figure 3.10), as a model of human skin cancer to test the efficacy of the prepared functionalized nanomaterials.

The cell line, obtained from ATCC (American Type Culture Collection) was routinely cultured in Dulbecco's Modified Eagle's Medium (DMEM), supplemented with 10 % (v/v) Fetal Bovine Serum and 1 % (v/v) penicillin–streptomycin (Pen/Strep) (Table 3.5) and maintained at 37 °C in a 5 % CO₂ humidified atmosphere. Cells were subcultured every 2 to 3 days (approximately when they reached 80% confluence) to ensure their proper growth and viability.

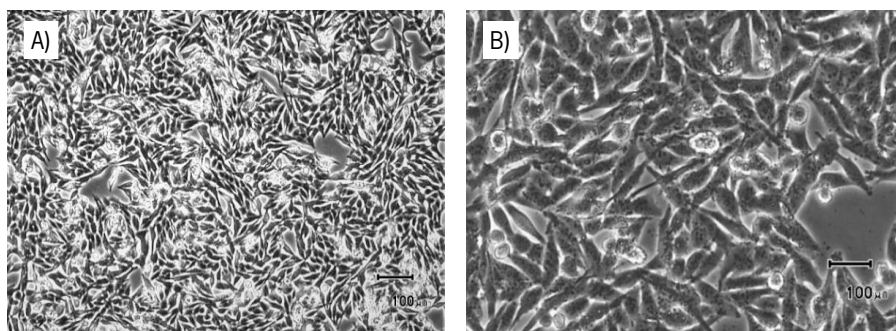


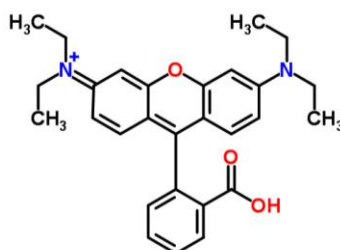
Figure 3.10. Morphological appearance of A375 cells: A) 40x magnification B) 100x magnification. Images obtained with Olympus IX81 microscope.

Table 3.5. Cell culture medium composition.

Constituent	Composition	Supplier
DMEM	[+] Glucose, [+] L-glutamina, [-] Piruvato	Gibco, Invitrogen, USA
FBS	Fetal Bovine Serum	Gibco, Invitrogen, USA
Pen Strep	1 % (v/v) penicillin/streptomycin	Gibco, Invitrogen, USA

3.6.2. Cell proliferation assay (Sulforhodamine B)

To evaluate the effect of zeolite-mediated cytotoxicity and cell proliferation *in vitro*, the Sulforhodamine B (SRB) colorimetric assay was performed. It relies on the ability of the SRB dye (Figure 3.11) to bind cellular protein components and measures the total biomass. Essentially, SRB can form an electrostatic complex with basic amino acid residues of cellular proteins under slightly acidic conditions and then it can be dissociated under basic conditions and solubilized so that the optical density (OD) can be measured. Since the binding of SRB is stoichiometric, the incorporated dye released from stained cells after washing is directly proportional to the cell biomass, which can be extrapolated to measure cell proliferation.

**Figure 3.11.** Molecular structure of Sulforhodamine B.

For this experiment, A375 cells were seeded into 96-well culture plates in triplicate at a density of 10×10^3 cells per well. Trypan blue staining method was used for cell counting using a Neubauer counting chamber (Marienfeld, Germany). Live cells with intact cell membranes are not coloured, while trypan blue traverses the damaged membrane in the case of a dead cell. Therefore, dead cells are shown in a distinctive blue colour under the microscope. So, we mixed the cell suspension with trypan blue (1:2), inserted 10 μ L of that mixture in the Neubauer chamber (Figure 3.12), counted the living cells (without blue staining) by microscopic observation (Olympus IX81) and then we calculated the appropriate volume of cell suspension required to achieve a density of 10×10^3

cells per well. After that, culture plates were incubated overnight at 37 °C in 5 % CO₂ atmosphere to allow the adhesion of the cells to the bottom of each well. Then, the medium was removed and replaced with sequential zeolite dilutions prepared in DMEM without FBS (0.010, 0.025, 0.050, 0.075 and 0.1 mg/mL), from a stock sample suspension (0.5 mg/mL). Cells were then incubated and the alterations in the cell biomass were monitored 24, 48 and 72 h after exposure.

Four different samples were tested: the parental zeolite NaY, silver-ion exchanged zeolite AgY, drug-loaded zeolite Na(5-FU)Y and the hybrid nanosystem with both species encapsulated (Ag/5-FU)Y. To ensure a better homogenization, every stock suspension (0.5 mg/mL) was sonicated (ultrasonic bath for 3 min prior to use. The first row of each plate was kept as blank, containing only culture medium, to determine the nonspecific background.

After 24 h incubation, the medium containing functionalized nanomaterials was removed from all the wells and the cells were fixed with 50 µL of 10 % (w/v) trichloroacetic acid (TCA) and stored for 1 h at 4 °C. After this period, TCA was discarded, the wells were washed four times with deionized water and left to dry at room temperature. Posteriorly, cells were stained with 50 µL of SRB solution for a 30 min period at room temperature and after that, SRB was removed and cells were washed four times with 1 % (v/v) of acetic acid and air-dried. The protein-bound dye was then solubilized with 100 µL of 10 mM Tris base solution per well.

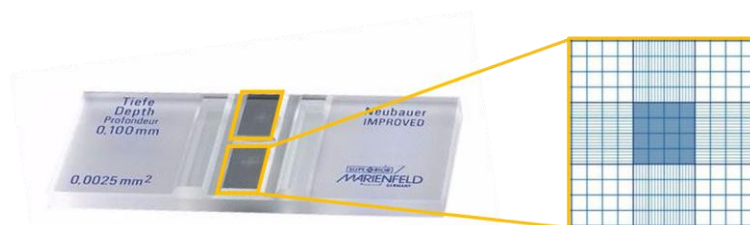


Figure 3.12. Neubauer chamber and the respective counting grid (corner squares) used for trypan blue staining and cell counting. Neubauer (Marienfiel, Germany) Tiefe 0,100 mm; 0,0025 mm². The number of viable cells/mL was calculated by taking the average cell count from the corner squares, multiplying that averaged value by 10⁴ and then by 2 (dilution factor) to correct for the 1:2 dilution from the Trypan Blue addition.

This procedure was repeated after 48 and 72 h of incubation to monitor sample effect. Finally, OD values were measured at 530 nm using a microplate reader coupled with the SkanIt™ Software and the cell viability was calculated according to the following equation (Eq. 5):

$$\text{Cell viability (\%)} = \frac{\text{OD sample}}{\text{OD control}} \times 100 \quad \text{Eq. 5}$$

Results were presented as the mean percentage \pm standard deviation (SD) of three independent assays (each of them in triplicate) of viable cells comparatively to the control condition (assumed as 100% of cell viability). Statistical analysis of the results was carried out with GraphPad Prism 5® software. Values were considered statistically significant when $p < 0.05$.

CHAPTER 4



RESULTS AND DISCUSSION

In this chapter, all the results obtained throughout the development of the experimental work will be presented and discussed. It will be divided in 4 distinct parts: the first one corresponds to the characterization of the prepared DDS based on zeolites by XPS, SEM/EDX, TGA and N₂ adsorption; the second part will focus on the *in vitro* release studies, which were performed to evaluate the release profile of silver ions and 5-FU from the DDS; then we will have a section where the antimicrobial assays and the respective results will be approached; finally, the last part will be dedicated to the discussion of the cell viability tests in the presence of the DDS, performed on a human skin cancer cell line.

4.1. Characterization of samples

4.1.1. XPS analysis

To investigate the chemical states of surface atoms, as well as composition and related distribution of the surface elements, XPS analysis was performed for NaY, the parent zeolite; AgY, the modified zeolite by ion exchange and finally the prepared DDS (Ag/5-FU)Y, the hybrid system obtained by subsequent liquid phase adsorption. The resulting “wide scan” spectra (Figure 4.1), which were obtained at low resolution and covered the entire useful range of binding energies accessible with the X-Ray source employed, were used to identify all the existing elements on the surface of our samples.

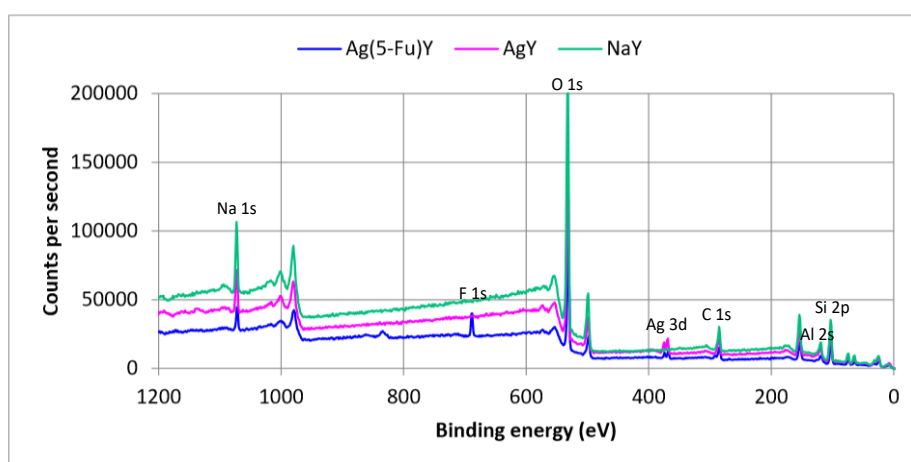


Figure 4.1. XPS spectra (0-1200 eV) of NaY, AgY and (Ag/5-FU)Y.

In each of the analysed samples, the characteristic elements of zeolite nanostructures were identified, namely: Silicon (Si 2p peak at 102-104 eV region), Aluminium (Al 2s peak at 117-118 eV region) and Oxygen (O 1s very intense peak at 532-535 eV region), which correspond to the typical three-dimensional arrangement of tetrahedral units $[\text{SiO}_4]$ and $[\text{AlO}_4]$, linked to each other through bridging oxygen ions. The peak at 1072-1075 eV in the Na 1s region corresponds to the sodium located within the zeolite framework. The surface atomic content of all the elements detected by XPS is displayed in Table 4.1 in the form of atomic percentage. In the case of these structural elements, characteristic of zeolite framework, we observe that the respective values are comparatively similar in all three samples, with a subtle, yet non-significant variation.

Table 4.1. Surface composition of each sample. Results are presented in atomic percentage.

Sample	XPS atomic (%)					
	O 1s	Na 1s	F 1s	Al 2s	Si 2p	Ag 3d
NaY	57.46±0.36	7.82±0.19	-	4.82±0.27	16.64±0.24	-
AgY	59.20±0.42	6.14±0.13	-	5.34±0.16	15.46±0.29	0.61±0.03
(Ag/5FU)Y	48.92±0.51	6.25±0.16	7.57±0.49	4.84±0.21	16.26±0.29	0.58±0.03

Silver was successfully incorporated in the zeolite nanostructure as can be observed in Ag 3d region of XPS spectrum (figure 4.2). In this high-resolution XPS spectrum, we clearly see that in the case of NaY zeolite there is no Ag 3d electron signal but then, a closely spaced doublet with 2 main peaks referring to Ag $3d_{5/2}$ and Ag $3d_{3/2}$ region is detected in the AgY and Ag(5-FU)Y spectra, which correspond to emitted photoelectrons of the 3d orbitals.

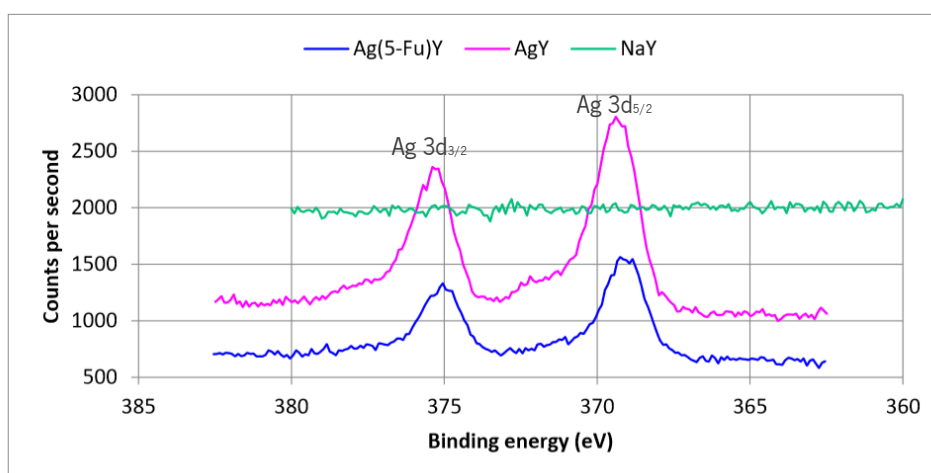


Figure 4.2. High resolution spectra of Ag 3d region for NaY, AgY and (Ag/5-FU)Y.

This split between two peaks arises from spin-orbit coupling effects in the final state. Naturally, the increase in silver content observed after NaY zeolite modification contrasts with the decrease of sodium content (Table 4.2). Sodium cations (Na^+), that are present in the interstice of the NaY zeolite framework to maintain the electroneutrality of the structure, were progressively exchanged for Ag^+ cations during the ion exchange process.

Besides allowing the identification of the elements present in the sample and their quantification, this type of analysis also provides valuable information regarding the oxidation state of silver. Peak deconvolution, a term often applied to the process of decomposing overlapping peaks, was performed on the high-resolution spectra of Ag 3d region and allowed the identification of distinct peaks and the determination of the corresponding values of binding energies. As can be observed in Figure 4.3 A), the two main peaks corresponding to Ag $3d_{5/2}$ and Ag $3d_{3/2}$ region are detected at 368.8 eV and 374.6 eV respectively. According to the NIST XPS database and other published works, these experimental binding energies values appear to correspond to Ag (I) (Ferraria *et al.* 2012; Ferreira *et al.* 2012), confirming the presence of silver in its ionic form. Furthermore, in the case of Ag(5-FU)Y (Figure 4.3 B) these values remained unaltered, which indicates that, within the hybrid system, silver remains in the ionic form. The binding energies (BE) of all the detected elements by XPS are summarized in Table 4.2.

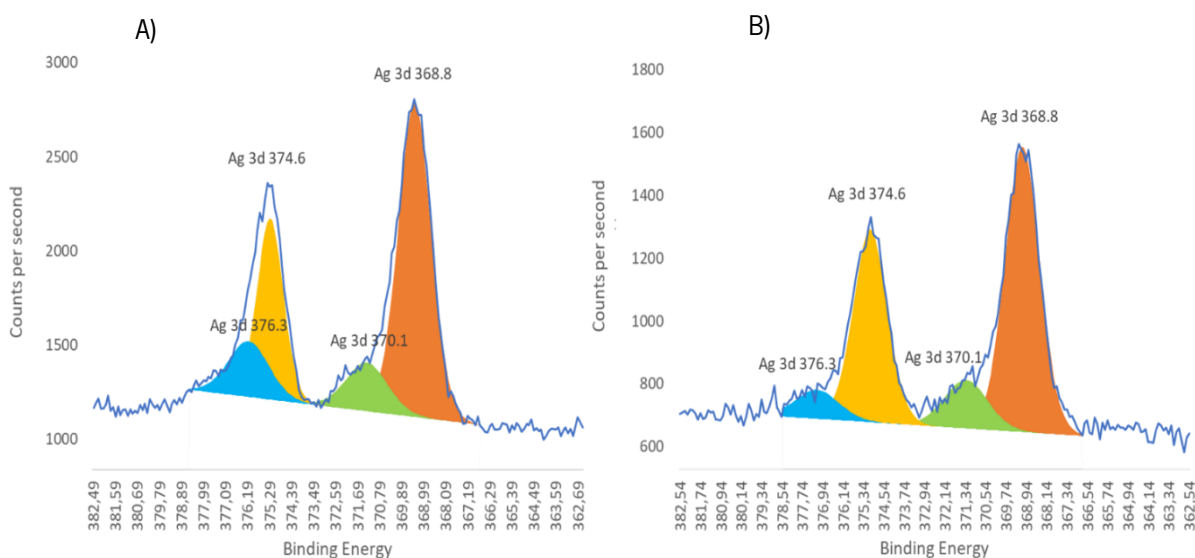
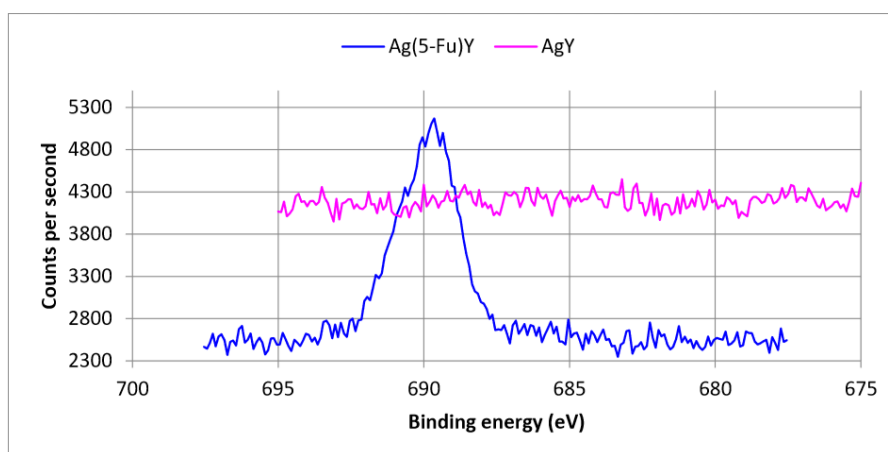


Figure 4.3. Peak deconvolution of: a) high resolution spectrum of Ag 3d region of AgY and b) high resolution spectrum of Ag 3d region of Ag(5-FU)Y.

Table 4.2. Binding energies (BE) obtained from the XPS spectrum in the O 1s, Na 1s, F 1s, Al 2s, Si 2p and Ag 3d region of each sample.

Sample	Binding Energy (eV)						
	O 1s	Na 1s	F 1s	Al 2s	Si 2p	Ag 3d _{5/2}	Ag 3d _{3/2}
NaY	534.0	1074.9	-	118.8	103.8	-	-
AgY	536.6	1072.5	-	117.7	102.1	368.8	374.6
(Ag/5FU)Y	531.5	1072.5	689.0	117.7	103.6	368.8	374.6

In the case of the third analysed sample (hybrid zeolite Ag(5-FU)Y), which resulted from the modification of the AgY zeolite, there was a natural increase of the fluorine content as observed in the XPS spectrum for the F 1s (Figure 4.4). It was detected a single peak with a symmetrical shape (typical of F 1s) centered at the binding energy value of 689.0 eV, which is attributed to organic fluorine according to the literature (Hantsche 1993), confirming the presence of 5-FU within the system.

**Figure 4.4.** High resolution spectra of F 1s region for AgY and (Ag/5-FU)Y.

4.1.2. SEM-EDX analysis

The morphology of the DDS, Ag(5-FU)Y, was observed by scanning electron microscopy and compared with the starting materials to find out possible differences between them. Figure 4.5 shows the parent zeolite NaY with 5000x magnification (Figure 4.5 A), AgY with 5000x magnification (Figure 4.5 B) and the DDS obtained after 5-FU encapsulation, with 5000x and 15000x magnification (Figure 4.5 C). The SEM micrographs showed that the particles were similar in size and appearance, suggesting that the loading of silver ions into the zeolite framework as well

as the subsequent incorporation of 5-fluorouracil had small effect on the size and shape of the zeolite particles as they kept their typical morphology and faujasite structure. The micrographs of NaY and the DDS are typical of a microporous crystalline aluminosilicate structure with relatively regular small particles and well-defined geometrical shape. The average particle diameter of the DDS varied approximately between 0.3 and 1.0 μm , similarly to AgY and the starting material NaY, which is in accordance with previous documented studies regarding the morphology of these type of materials (Amorim *et al.* 2012).

Although it is not very extensive, we can observe that some aggregation of zeolite particles occurred after NaY modification (Figure 4.5 B) and more evident in Ag(5-FU)Y (Figure 4.5 C), which is not unexpected, since this type of structure has the tendency to form these aggregates.

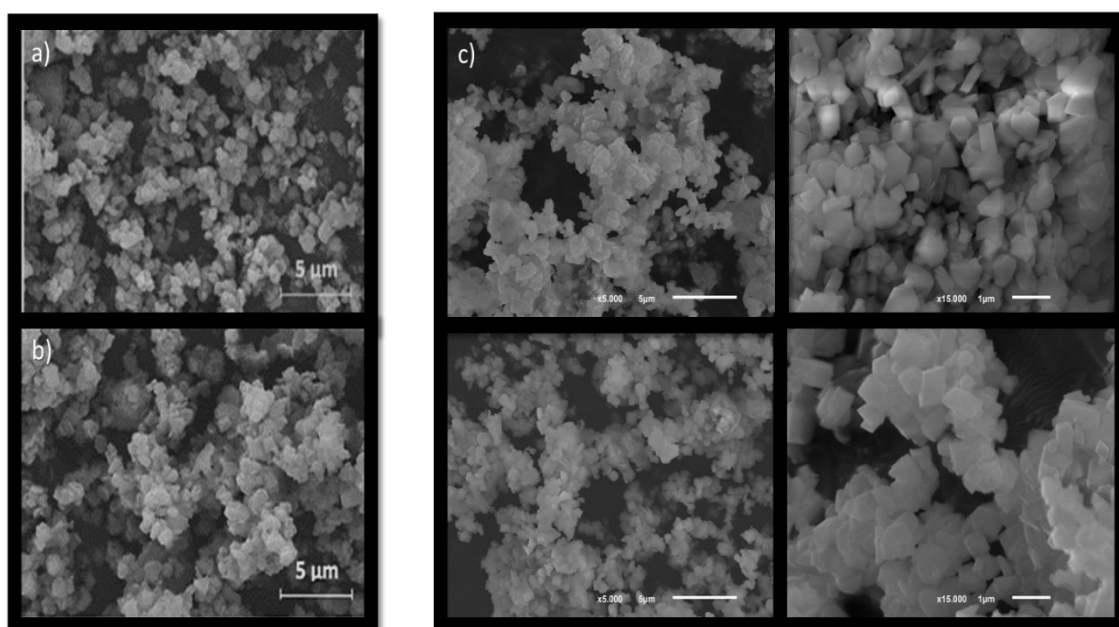


Figure 4.5. Scanning electron microscopy images of zeolites (with different magnifications): a) NaY (5000x magnification), b) AgY (5000x magnification) and c) (Ag/5-FU)Y (5000x magnification and 15000x magnification).

Since SEM is coupled with detectors of energy dispersive X-Ray (EDX), this type of analysis was also carried out to examine the elemental distribution on the surface of the samples. It must be born in mind that the results of EDX are not representative of the entire sample, because the electron beam is only focused on a specific spot of the specimen, so usually, several different spots are analysed and then the average values are considered for element quantification purposes. The resulting EDX spectra of AgY is exhibited in Figure 4.6.: both images refer to AgY spectra but

correspond to different analysed spots within sample (four different spots were analysed and we selected two of those as representative examples). The determined weight percentage of silver was 7.5 wt % (A) and 7.3 wt % (B), indicating that silver ions appear to be homogeneously distributed throughout the sample.

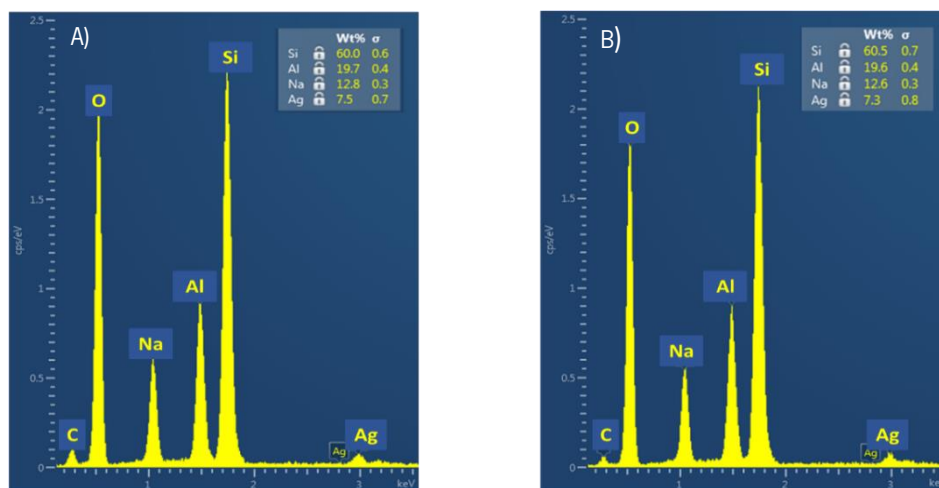


Figure 4.6. EDX spectrum of AgY; A) and B) correspond to the analysis of different spots within the same sample.

Regarding the DDS, (Ag/5-FU)Y, the EDX spectra is represented in Figure 4.7. Again, the same sample was analysed on several different spots and two of those were selected as representative examples. As observed, the compositional results in terms of weight percentage (wt %) values are relatively similar in both A) and B), with exception of one element, fluorine: 22.8 wt % in the case of spot A) and 2.2 wt % in spot B), which is a significant difference. This means that, contrary to what happened in the case of silver, the distribution of 5-FU throughout the sample is not homogeneous.

The weight percentage of silicon and aluminium detected by EDX (Figure 4.6. and 4.7.) revealed that the Si/Al ratios of AgY and Ag(5-FU)Y were relatively constant, 2.94 and 2.95, respectively. These values are similar to the theoretical value of the starting material, 2.83, which means that the framework Si/Al ratio did not suffer significant changes during the ion exchange and subsequent process of 5-FU encapsulation, in agreement with XPS analysis.

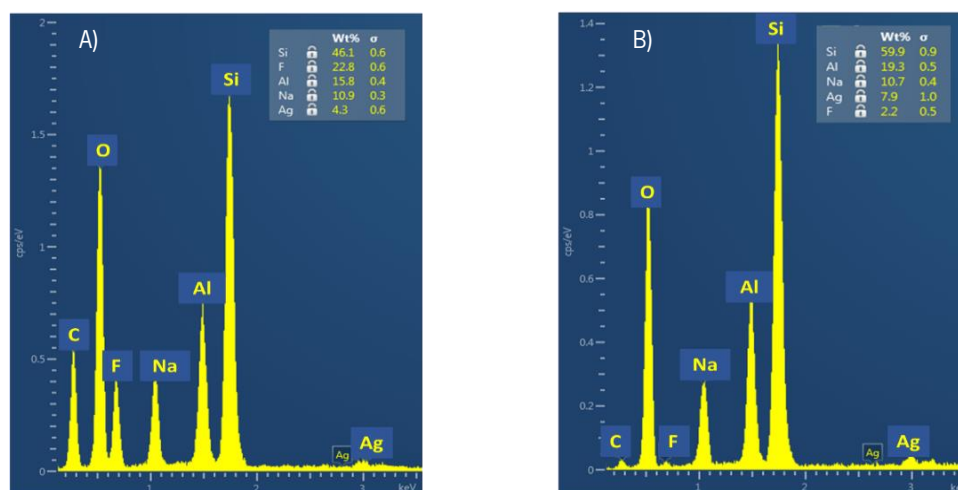


Figure 4.7. EDX spectrum of Ag(5-FU)Y; A) and B) correspond to the analysis of different spots within the same sample.

4.1.3. TGA analysis

The loading of 5-fluorouracil into the AgY was evaluated by thermogravimetric analysis (TGA) within the temperature range 50-700 °C, under oxygen. Figure X shows the thermograms of the different zeolite samples, the parental zeolite NaY, AgY and the hybrid system, (Ag/5FU)Y. As soon as the heating temperature started to increase, all the three nanomaterials exhibited a similar behaviour up to approximately 150 °C, a weight loss that can be attributed to the removal of physisorbed water in the zeolite structure. In the case of the DDS, an additional extended weight loss is visible. This loss corresponds to the melting process of the compound (until approximately 430 °C), followed by the degradation of 5-fluorouracil that extends until near the end of the analysis, approximately at 600 °C.

Thermograms of the pure drug available in the literature, suggested that 5-FU molecule remained thermally stable up to 275 °C and then underwent a rapid decomposition within a narrow temperature range, starting approximately at 285 °C (Singh et al. 2009), which was confirmed by the significant changes observed in the spectrum of 5-FU after exposure to that temperature (the characteristic absorption bands of intact 5-FU diminish significantly, revealing that the drug is no longer stable). In the case of 5-FU loaded zeolite sample, we observe a different decomposition behaviour of the molecule, as the process seems to occur throughout a wider temperature range. This extended decomposition range is probably due to the encapsulation of the drug into the zeolite framework.

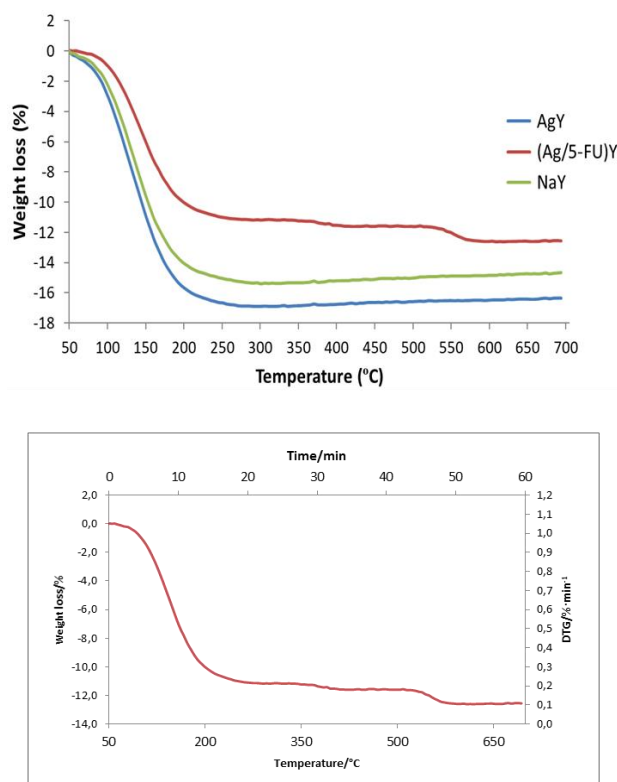


Figure 4.8. Thermogravimetric thermograms of NaY, AgY and (Ag/5-FU)Y samples. Samples were heated between 50 and 700 °C at 10 °C/min. The (Ag/5-FU)Y thermogram is shown in more detail in the below image.

Table 4.2 shows the 5-FU loading results obtained for DDS Ag(5-FU)Y. The ‘unwashed’ sample corresponds to the initial hybrid DDS that was prepared and characterized. The SEM/EDX analysis results revealed that the distribution of 5-FU throughout the sample was not homogeneous due to the presence of non-encapsulated compound coating some surface areas of the zeolite (which will be shown in more detail in the section of the *in vitro* release studies). Because of that, it was decided to prepare another sample, following the same experimental procedure but adding a washing step with solvent to remove that surplus amount of 5-FU. This last sample was used for the antimicrobial assays and skin cancer cell viability assays.

The TGA loading result of Na(5-FU)Y (a sample prepared in the context of a previously project, under the same experimental conditions, that we used in the present work) is also exhibited in Table 4.2 and it is observed that it exhibited a very high encapsulation capacity, unlike the hybrid DDS prepared in the current work whose encapsulation efficiency was considerably low.

Tabela 4.3. Loading of 5-FU into zeolite structures.

DDS	5-FU (mmoles) ^a	5-FU (mmoles) ^b
Unwashed Ag(5-FU)Y	0.58	0.17
Washed Ag(5-FU)Y	0.58	< 0.10*
Na(5-FU)Y	0.58	0.54

^a initial amount of 5-FU in solution

^b amount of 5-FU loaded into the zeolite structure determined by TGA

*since we did not have the TGA results of this sample, the exhibited value was estimated considering the results of the *in vitro* release studies which will be presented in the next section

4.1.4. N₂ adsorption analysis

Isotherm adsorption analysis is of major importance for the characterisation of a wide range of porous materials, including zeolites. In this case, we evaluated the physical adsorption behaviour (also called physisorption, which results from the relatively weak van der Waals attractive forces between the adsorbate and adsorbent surface) of a gas onto the surface of the zeolite. Since these forces of attraction are very weak, this type of adsorption can be easily reversed (desorption process) by decreasing the pressure.

The evaluation of the textural characteristics of zeolites after sample preparation was carried out based on the nitrogen adsorption isotherms (although there are other gases and vapours that can be employed as adsorbate, N₂ is considered the most suitable alternative for the characterization of porous solids), determined at its boiling point: -196 °C (\approx 77 K). All samples were previously outgassed at 150 °C under vacuum to remove adsorbed moisture and other volatile species that could block zeolite pores and interfere with the analysis. The equilibrium isotherms of AgY and Ag(5-FU)Y are illustrated in Figure 4.9.

The micropore volumes (V_{micro}) and mesopore surface areas (S_{meso}) were calculated by the t-method. Brunauer-Emmett-Teller (BET) method (Brunauer *et al.* 1938) was used to calculate the total surface area of the zeolite (S_{BET}). The mathematical theories behind this method, aim to explain the process of physical adsorption of gas molecules onto a particle surface. Briefly, the volume of N₂ adsorbed is measured at its boiling point (77 K) and at this temperature the gas is below the critical temperature, condensing on the surface of the zeolite particles. Assuming that the gas condenses onto the surface in a monolayer, and as we know the size of the gas atom/molecule, the amount of adsorbed gas can be correlated to the total surface area of the particles. So, BET theory basically

establishes a correlation between the volume absorbed and the total surface area. The pore size distribution analysis was carried out using the Barrett, Joyner and Halenda (BJH) method, which relates the amount of adsorbate removed from the pores of the material (as the relative pressure, p/p_0 , is progressively decreased) to the size of the pores, so ultimately, the desorption branch of the isotherm is utilized to perform this calculation. The resulting values of these parameters are summarized in Table 4.3.

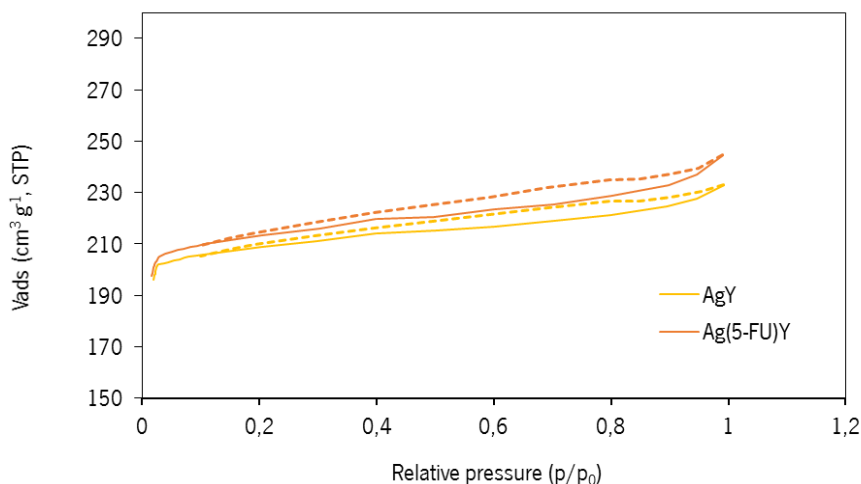


Figure 4.9. Nitrogen adsorption-desorption isotherms of AgY and DDS (Ag/5-FU)Y. Dotted line represents the desorption process and the solid line represents the adsorption process.

The adsorption-desorption isotherms of AgY and Ag(5-FU)Y show that in the relative pressure (p/p_0) range from 0.0 to 1.0, the volume of adsorbed gas increased gradually due to monolayer adsorption of N_2 onto the microporous channels of the zeolite. The desorption curve is very close to the adsorption curve in the whole range of p/p_0 .

According to the International Union of Pure and Applied Chemistry (IUPAC) classification scheme (Figure 4.10), which considers the existence of six distinct types of gas adsorption isotherms, AgY and Ag(5-FU)Y zeolites appear to correspond to Type-I isotherms, similar to isotherm of NaY (Vilaça *et al.* 2013). These type of isotherm, known as Langmuir adsorption, is the typical pattern used to describe adsorption on microporous solid materials (Donohue and Aranovich 1998). The amount of adsorbed gas approaches a limiting value as $P/P_0 \rightarrow 1$.

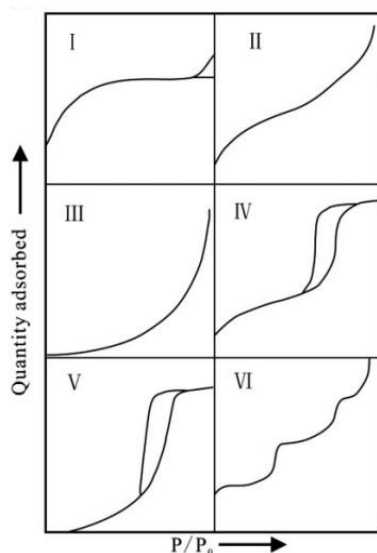


Figure 4.10. The IUPAC classification of adsorption isotherms (Yang *et al.* 2017).

Table 4.4. Structural properties of the zeolites calculated from the N₂ gas adsorption isotherms.

Sample	S_{BET} (m ² /g) ^a	S_{meso} (m ² /g) ^b	V_{micro} (cm ³ /g) ^c	$V_{PP/P_0=0.95}$ (cm ³ /g) ^d	d_{BJH} (nm) ^e	V_{BJH} (cm ³ /g) ^f
NaY (Si/Al=2.83)	786	50	0.311	0.361	3.57	0.039
AgY (Si/Al=2.83)	772	41	0.306	0.352	3.58	0.037
Ag(5FU)Y	782	51	0.309	0.367	3.58	0.048

a Total surface area

b External surface area (mesopore surface area)

c Micropore volume

d Total pore volume at $P/P_0 = 0.95$

e Pore size distribution

f Pore volume

Comparing total surface area (S_{BET}) and the micropore volume (V_{micro}) of the parental zeolite with AgY and Ag(5-FU)Y, it is observed that a decrease in both parameters occurred, as a result of the incorporation of the active agents. Regarding the values of the pore size distribution (d_{BJH}), it was found they were similar for both NaY, AgY and Ag(5-FU)Y. In general, the similarity exhibited between the experimental values of these parameters among the three samples indicates that the introduction of silver ions and 5-FU within the starting material, NaY, during the DDS preparation, only slightly affects the structural properties of the zeolite, meaning that the porous material maintained its structural integrity throughout all the process of modification.

4.2. *In vitro* release studies

4.2.1. 5-Fluorouracil *in vitro* release from DDS

As previously mentioned, the quantification of sample elements performed with EDX revealed that 5-FU was not homogeneously distributed and we observed the presence of a sort of amorphous mass coating the surface of the zeolite in one of the images obtained with scanning electron microscopy, which corresponds to non-encapsulated 5-FU (Figure 4.11). Probably, part of 5-FU was not able to diffuse into the pores and channels of the zeolite due to the presence of silver ions previously introduced into the framework by ion exchange (which exhibit a higher ionic radius compared with Na⁺). So, we decided to evaluate the release profile of two different samples of the hybrid DDS (Ag/5-FU)Y: an unwashed DDS (which was simply filtrated after the liquid adsorption process as previously explained in the methodology section), which SEM micrographs and EDX quantification results revealed the presence of some 5-FU adhered to the surface; and an washed sample of DDS, washed once with solvent (80 % acetone/ 20 % water) after the filtration process in order to remove the amount of 5-FU dispersed on the zeolite surface that did not incorporate the nanostructure.

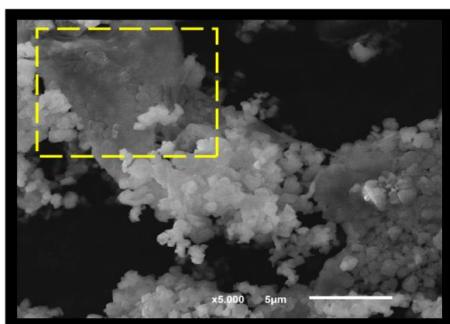


Figure 4.11. Scanning electron microscopy image of the DDS (Ag/5-FU)Y (5000x magnification). The yellow dashed square points out a zone with an amorphous appearance which corresponds to the 5-FU dispersed on the sample's surface.

The *in vitro* cumulative release behaviour of 5-FU from both samples of Ag(5-FU)Y was monitored with UV/vis spectrophotometry. The concentration of 5-Fluorouracil released in PBS solution with pH = 7.4 (release medium simulating physiological conditions for release of dermatological

formulations) was determined as a function of time at the characteristic wavelength of maximum absorption of 5-FU, 266 nm.

The results from the UV/visible absorption spectrum of each withdrawn aliquot throughout the monitoring period (360 min) (Figure 4.12) show that, after release from the zeolite nanostructure, the compound maintains its characteristic wavelength of maximum absorption ($\lambda=266$ nm), which confirms the molecular integrity of 5-FU after the encapsulation.

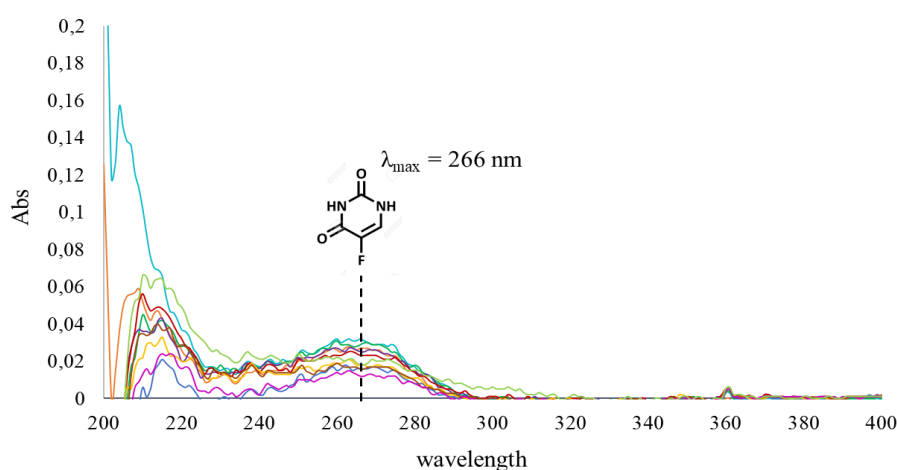


Figure 4.12. UV/vis absorption spectra of the withdrawn aliquots (each one represented in a different colour).

The resulting release profile of 5-FU from the hybrid zeolite, (Ag/5-FU)Y is exhibited in figure 4.13.

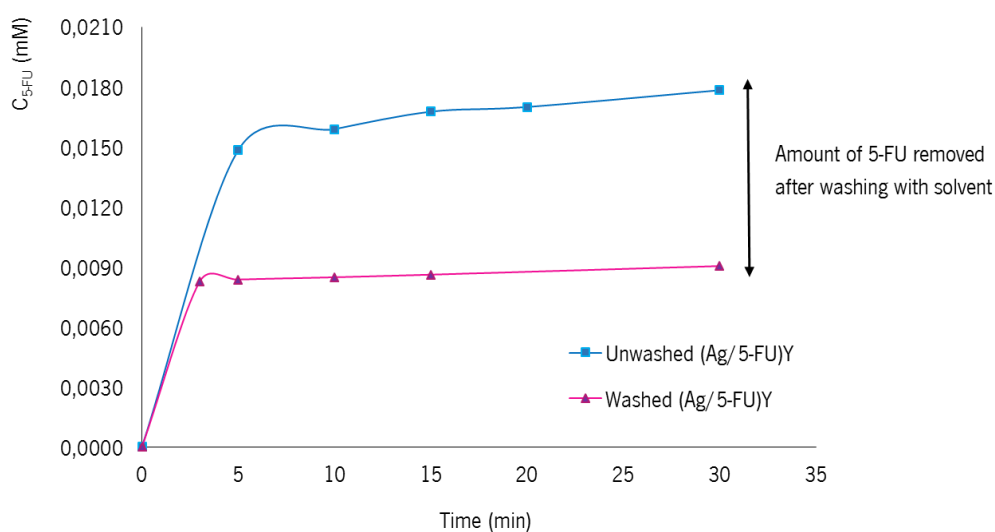


Figure 4.13. Release profiles of 5-FU from the hybrid zeolite system, (Ag/5-FU)Y. Measurements were conducted in simulated physiological conditions, using a phosphate buffer solution (PBS) at pH = 7.4 and 37 °C.

Although the release process was monitored throughout 360 min, the cumulative concentration of 5-FU (C_{cum}) stabilized after 30 min and its values remained approximately the same until the end of the assay (steady phase). Nearly the whole amount of the compound (80-85%) was released in the first 5-10 minutes. Both samples (washed and unwashed) presented a similar release profile, with an initial burst release of 5-FU, in an exponential way. In the end of this study, the amount of 5-FU released was 0.0224 mM and 0.0100 mM for unwashed and washed DDS, respectively. The difference between the amount of drug released in both cases corresponds to 5-FU that was present on the surface of the zeolite and was washed off with the solvent.

Release of drug molecules from zeolites is controlled by a number of factors such as the pore size, the existence of any attached functional groups or exchangeable cations and the nature of intermolecular interactions. In this case, the quick desorption of the compound from the zeolite framework is in accordance with previously reported results where 5-FU exhibited the same release behaviour (Vilaça et al. 2013). Since 5-FU is a small organic molecule (molecular dimensions of 4.9 Å x 5.3 Å x 5.0 Å) (Figure 4.14), it can be easily released from the micropores of the zeolite. There are no significant interactions between the drug and the zeolite structure, otherwise the stabilization of the compound within the structure would not allow such a rapid diffusion of the molecule to the exterior of its framework. Additional research would be useful to understand fundamental zeolite and drug molecule interactions so that the loading and release of the compound could be better controlled.

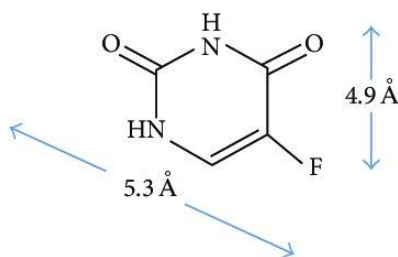


Figure 4.14. Molecular dimensions of 5-FU (Al-Thawabeia and Hodali 2015).

4.2.2. Silver *in vitro* release

To evaluate the Ag^+ release behavior, we used the same procedure as for the 5-FU release studies in PBS solution pH = 7.4, using inductively coupled plasma-optical emission spectrometry (ICP-OES) to quantify the released amount of silver throughout a 72 h period (aliquots withdrawn after 30 min, 1 h, 3 h, 6 h, 19 h, 24 h, 48 h and 72 h) from AgY. This sample exhibited an Ag^+ content

of 7.40 wt % and 3.43 wt%, determined by EDX and XPS analyses, respectively. The DDS showed similar amounts of silver, with 6.70 wt % and 3.62 wt% from EDX and XPS analyses, respectively. The resulting release profile of silver from AgY is shown in figure 4.15.

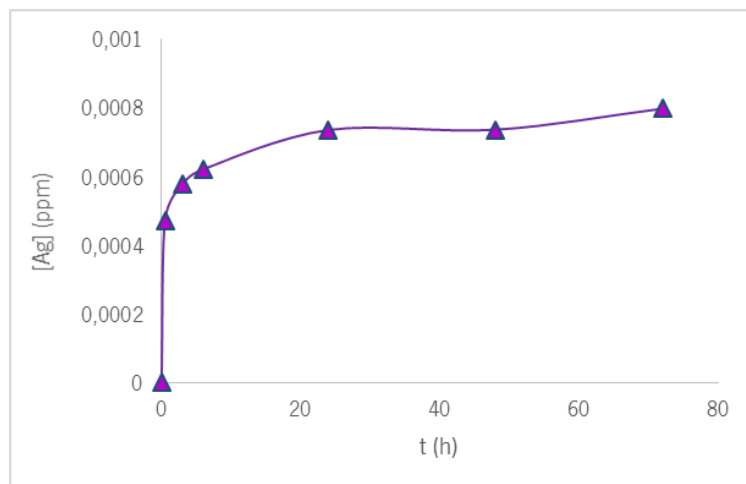


Figure 4.15. Release profile of silver ions determined by ICP-OES. Measurements were conducted in simulated physiological conditions, using a phosphate buffer solution (PBS) at pH = 7.4 and 37 °C.

Small amount of silver ions (Ag^+) are released from AgY to the PBS solution and a continuous amount of the antimicrobial agent is released within the first 6 h, which was subsequently followed by a relatively slow and sustained release throughout the remained monitored period. Unlike 5-FU, whose release stabilized shortly after 10 min, in the case of silver, a constant ion release could still be observed at the end day 3, suggesting that the zeolite system had a prolonged and steady antibacterial activity. The amount of silver released at the end of this assay was 8.28×10^{-4} ppm, which represents less than 1% of the initial amount of silver (7.4 wt %). It would be interesting to extend the test time for a few days more and see if this release pattern continues to occur.

4.3. Antimicrobial assays

4.3.1. Antimicrobial effects of NaY, AgY and (Ag/5-FU)Y

The Gram-negative bacteria *Escherichia coli* and *Pseudomonas aeruginosa*, and the Gram-positive bacteria *Staphylococcus aureus*, Methicillin Resistant *Staphylococcus aureus* (MRSA) and

Propionibacterium acnes were used as sensitive indicator strains to evaluate the antimicrobial potential of the prepared samples. The selection of this panel of microorganisms was due to the fact that these strains represent common causative agents of skin pathologies.

In these assays, every sample prepared was evaluated: the parent zeolite, NaY, the zeolite doped with silver, AgY, and the hybrid zeolite containing both silver and 5-Fluorouracil, (Ag/5-FU)Y. Growing concentrations of zeolites were tested: 0.2, 0.5, 1.0 and 2.0 mg/mL and the resulting MIC values were determined for each pair bacterial strain tested/zeolite.

We observed that bacterial growth was unaffected by the presence of parent zeolite, NaY, regardless of the concentration tested, meaning that the zeolite itself has no antibacterial effects. This is an expected result since zeolites have been described as inert and do not interact with microorganisms (Saengmee-Anupharb *et al.* 2013). As seen in Figure 4.16 every strain grew up equally in the absence of zeolite (control) as well in the presence of the parent zeolite, NaY. On the other hand, NaY modified with silver exhibited antibacterial activity against all the strains tested and no viable bacterial cells were detected in the presence of 1 mg/mL of AgY (Figure 4.17), proving that the introduction of silver in its ionic state into the zeolite framework is the active agent that gives the material its antibacterial properties. Moreover, the results from the antimicrobial assays, revealed that DDS, (Ag/5-FU)Y, also exhibits inhibitory effects on bacterial growth (Figure 4.17), which demonstrates that antibacterial capacity is maintained even in the presence of both agents within the zeolite framework. Thus, the presence of the compound 5-FU does not interfere with the release of silver ions through the pores of the zeolite and subsequent uptake and action within the microbial cells.

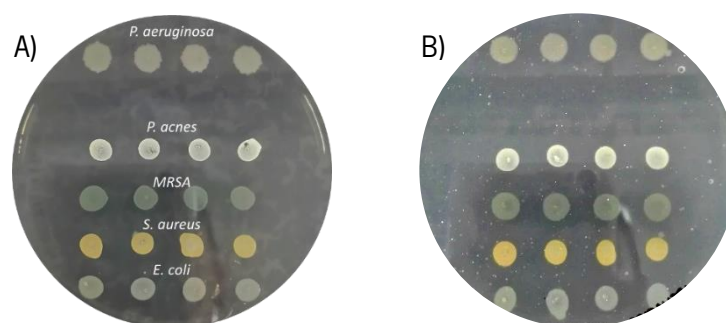


Figure 4.16. Photographs of the agar plates; Antimicrobial activity assay in the presence of the parent zeolite, NaY 1.0 mg/mL (B) as compared to the control (A), where bacteria were cultured in the absence of zeolite material. This concentration was selected merely as representative. Bacterial growth was not affected by the presence of the zeolite (regardless of the concentration tested: 0.2, 0.5, 1.0 and 2.0 mg/mL) as we can see when comparing with the control.

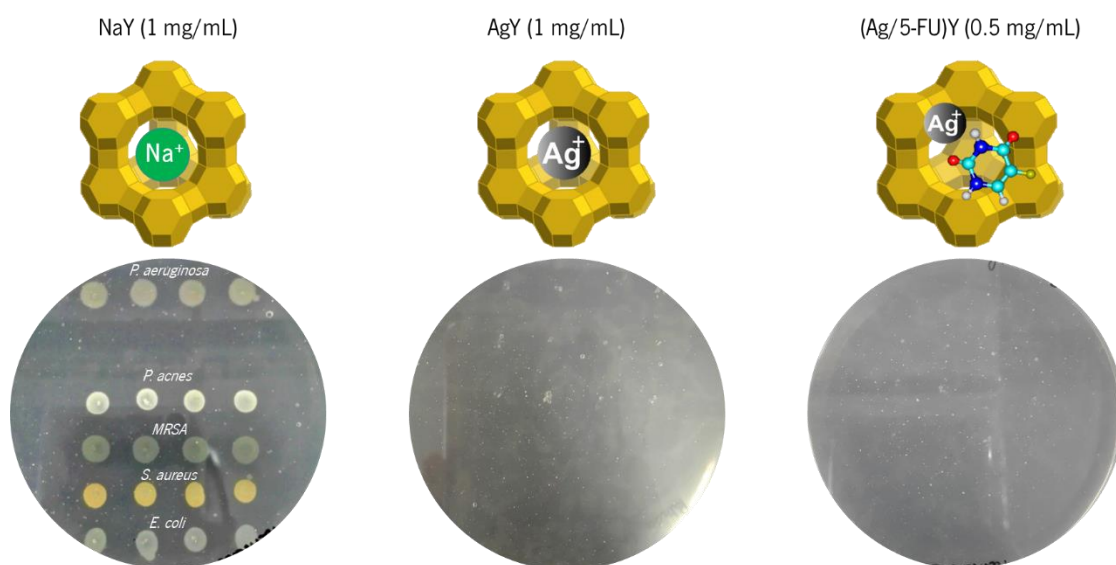


Figure 4.17. Antimicrobial activity assays against the bacteria indicator strains in the presence of NaY, AgY and (Ag/5-FU)Y. In the presence of both AgY and (Ag/5-FU)Y bacterial growth was successfully inhibited, with more pronounced effects in the case of (Ag/5-FU)Y (lower MIC values).

The resulting MIC values (which correspond to the lowest concentration that inhibited development of visible growth of colonies on the agar plates) obtained for each pair sample/indicator strain are summarized in Table 4.4.

Table 4.5. MIC values of NaY, AgY and (Ag/5-FU)Y against each of the sensitive indicator strains tested.

Microorganism	MIC (mg/mL)		
	NaY	AgY	(Ag/5-FU)Y
<i>P. acnes</i>	>2	0.5	0.5
<i>MRSA</i>	>2	1	0.5
<i>S. aureus</i>	>2	1	0.2
<i>E. coli</i>	>2	1	0.5
<i>P. aeruginosa</i>	>2	1	0.5

Interestingly, the MIC values obtained for the DDS, (Ag/5-FU)Y, were lower than the values for AgY, meaning that the hybrid system exhibited enhanced antibacterial properties, suggesting that 5-FU might be exerting an antimicrobial effect by itself, resulting in a combined action of 5-FU and silver ions. In fact, although being widely known as cytotoxic agent for cancer cells, 5-FU also exhibits inhibitory effects on the growth and viability of several microorganisms. According to the literature,

the first study of the antimicrobial action of 5-FU was performed in *Escherichia coli* and revealed that its inhibitory effects resulted from the intracellular conversion of 5-FU to the metabolite fluorodeoxyuridylate (FdUMP), which binds to the nucleotide-binding site of the enzyme thymidylate synthase, preventing the binding of the normal substrate and consequently inhibiting dTMP synthesis, resulting in depletion of dTTP. Thymidine starvation causes the cessation of DNA synthesis and repair and finally ends in the so-called 'thymineless death' (Cohen *et al.* 1958). Another study suggested the perturbation of cell wall biosynthesis as a mechanism of 5-FU toxicity towards *E. coli* and Roger and Perkins (1960) also demonstrated that 5-FU partially inhibited the synthesis of cell-wall mucopeptide in *Staphylococcus aureus*. Some years later, another investigation was carried out to evaluate the antibacterial activity of antineoplastic agents, including 5-FU, against several bacterial isolates (Bodet *et al.* 1985). It was found that 5-FU was one of the few antineoplastic agents that presented appreciable inhibitory effects, showing activity against > 80% of the bacterial isolates tested, including *Pseudomonas aeruginosa*, *Staphylococcus aureus* and MRSA.

Considering the obtained results with (Ag/5-FU)Y, which evidence an improved efficacy of the hybrid system (compared with AgY) in inhibiting the bacterial growth due to the contribution of 5-FU, we decided to prepare an aqueous solution of 5-FU to evaluate the effects of the compound itself on microbial growth. For that purpose, we had in consideration the concentrations of 5-FU in (Ag/5-FU)Y system previously tested (0.2, 0.5, 1.0 and 2.0 mg/mL) and calculated the corresponding quantity of 5-FU present in each of them. Then, from a stock solution of 5-FU we prepared the suitable dilutions in order to be in agreement with those quantities. After 24 h of incubation, we observed that the effect of 5-FU was not homogeneous in all strains. For example, the viability of *Pseudomonas aeruginosa* and Methicillin Resistant *Staphylococcus aureus* (MRSA) was not affected, as both strains grew equally in the absence (control) and in the presence of 5-FU in the culture medium (Figure 4.18), which might lead us to think that in these cases 5-FU has no effect, contrary to what literature suggests. However, as we previously mentioned, the results indicated in Table 4.4 show lower values for (Ag/5-FU)Y, indicating that, although 5-FU alone (at least in the tested range of concentrations) does not prevent the growth of *Pseudomonas aeruginosa* and MRSA, it still has an action on microbial cells that combined with the strong microbicidal capacity of silver ions totally inhibits the bacterial growth. In the case of *Escherichia coli*, even though it has grown at all 5-FU concentrations, it is clear that growth is less pronounced in the presence of the compound than in the control situation (Figure 4.18), suggesting that even

though these concentrations are still not sufficient to completely inhibit bacterial growth, 5-FU interferes with microbial cell viability (and once again the MIC value of (Ag/5-FU)Y against this species is lower than the MIC value of AgY). Results were different in the case of *Staphylococcus aureus*, no bacterial growth was observed regardless of the tested concentrations of 5-FU, meaning that 5-FU alone was effective in preventing bacterial growth which is in accordance with the respective MIC values: 1.0 mg/mL for AgY and then a significant decrease to 0.2 mg/mL for (Ag/5-FU)Y.

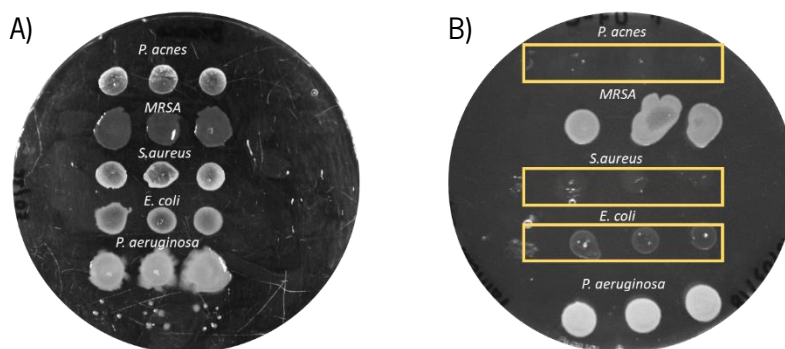


Figure 4.18. Antimicrobial activity assay in the absence (A) and in the presence of an aqueous 5-FU solution (B).

As discussed earlier, the overall inhibitory effect of silver on microbial growth is probably the sum of several distinct mechanisms of action. Silver has been reported to affect so many different functions of microbial cells, such as nucleic acids synthesis and translation, protein folding and function and cell membrane integrity (Kędziora et al., 2018). Furthermore, the fact of being non-selective explains silver antimicrobial activity against a broad spectrum of microorganisms.

Although we did not investigate the precise mechanisms behind the bactericidal action of silver zeolite, Matsumura et. al (2003) previously examined its bactericidal activity against *Escherichia coli* cells and they proposed two processes that may be involved in its mechanism of action. First, once they come in contact with the zeolite, bacterial cells take in the released silver ions, which inhibit several functions in the cell and consequently damage them. The second proposed mechanism is the generation of reactive oxygen species, possibly produced through the inhibition of a respiratory enzyme(s) (such as NADH dehydrogenase II) by silver ions and attack the cell itself. In another study, they observed that silver ion accumulates within the interior of *E. coli*, instead of residing in the cell membrane area. Results from the 2-DE and MALDI-TOF MS analysis demonstrated that a ribosomal subunit protein and some proteins were affected by silver ions. Based on these results, the interaction of silver ions with the ribosome and consequent suppression

of the expression of essential proteins for ATP production was proposed as one of the main bactericidal induced processes by silver (Yamanaka *et al.* 2005). Moreover, in a study regarding the kinetics of the release profile of silver ions from zeolite X framework and its effect on fatty acid composition of *Escherichia coli*, *Pseudomonas aeruginosa* and *Staphylococcus aureus*, it was reported that their fatty acid composition suffered significant alterations when exposed to silver loaded zeolite X. It was suggested that the interaction of silver ions with fatty acids of bacterial cells is likely to interfere with the survival of the cell (Kwakye-Awuah *et al.* 2007).

Even though our main interest regarding these antimicrobial assays was simply to test the efficiency of the prepared nanomaterials in inhibiting microbial growth, it would be interesting to examine and clarify the mechanistic basis of the antimicrobial activity of silver ions released from the zeolite framework and perform that study on several different strains to ascertain eventual patterns of resemblance or differences that might exist between them. Furthermore, in the case of the prepared DDS, which not only contains silver ions within its structure but also 5-FU, interfering both with the viability of microbial cells, it would also be interesting to verify the mechanisms that actually occur once the cells come in contact with the zeolite loaded with both active agents and the morphological and physiological changes they suffer as a consequence of that exposure.

4.4. Cell viability assays

The drug bioactivity studies were carried out in a skin cancer cell line, A375. This cell line was selected as a predictive model to evaluate the cytotoxic effects of the previously prepared DDS, (Ag/5-FU)Y. We tested a wide range of sample concentrations and observed that at a concentration of 0.5 mg/mL cells became completely coated by the zeolite, compromising the nutrient exchange with the culture medium. So, in our assays, we selected: 0.010, 0.025, 0.050, 0.075 and 0.100 mg/mL as working DDS concentrations, which were obtained by diluting a stock suspension (0.5 mg/mL) in culture medium (DMEM without FBS). As we mentioned earlier, all suspensions were submitted to an ultrasonic bath for 3 min prior to use to ensure homogenization.

The cytotoxicity of NaY sample was tested by the SRB assay to evaluate the suitability of the delivery system. To be considered an appropriate DDS, the zeolite itself should present small or no effect on cell viability. The results presented on Figure 4.19 clearly show that, compared to the control (cells cultured in the absence of NaY), the zeolite does not interfere with cell viability in the tested

range of NaY concentrations and throughout the entire period of cell exposure to the zeolite (up to 72 h), showing that it is not toxic to the cells.

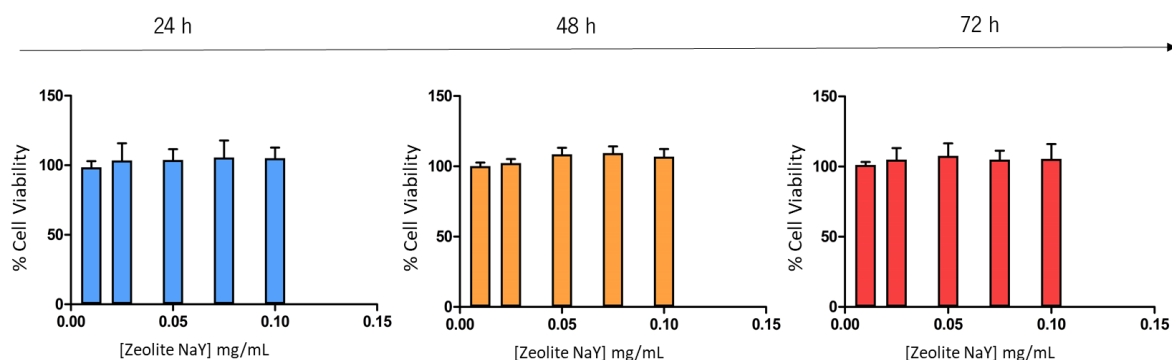


Figure 4.19. Cell viability of A375 cells measured by SRB assay after cell incubation with increasing concentrations of NaY throughout 72h. The resulting percentages (calculated as the mean percentage \pm SD of viability) were calculated in relation to the control, meaning that cells cultured in the presence of 0 mg/mL of NaY were considered as 100% of viability.

Besides testing the parental zeolite, we also carried out the cell viability assays in the presence of the silver-loaded zeolite (AgY), 5-FU-loaded zeolite, Na(5-FU)Y (this sample was already prepared, in the context of a previous work and it is used here for comparison with our samples) and the DDS, Ag(5-FU)Y. The effects of the tested materials on cellular viability throughout the 72 h period of exposure are exhibited in Figure 4.20. In the case of Na(5-FU)Y, we observed it had no effect on cellular viability 24 h after incubation. Only 48 h after being in contact with the cells, it is observed a noticeable decrease in cellular viability, which is probably explained by the fact that 5-fluorouracil is a pyrimidine analogue whose cytotoxic metabolites are cell-cycle specific, meaning that they attack cells at a specific phase of the cycle (S phase), interfering with DNA and RNA synthesis and consequently inducing cell cycle arrest and apoptosis, so, its effect on cellular viability is not immediately noticed, since it takes time to be metabolized inside the target cell and consequently exert its effect on active dividing cells. Na(5-FU)Y exhibited its more pronounced effect on cell viability (decline from 100 to 24%) 72 h after cell incubation.

Regarding the AgY sample, it revealed to be extremely toxic to this cell line. Unlike Na(5-FU)Y, the effect of AgY was not time dependent and we observed an accentuated decrease in cell viability right after 24 h of incubation (decline to 22%).

In the case of Ag(5-FU)Y, the observed effects were quite similar to AgY: a considerable decline of cellular viability after 24 h in contact with DDS. After 72 h, the cell viability dropped to 12 %, (the same value as AgY). Although both encapsulated agents, 5-FU and Ag⁺, are clearly cytotoxic to

A375 cell line, the effect of the hybrid system appears to be mainly driven by the action of Ag^+ ions rather by the combined action of both agents, especially if we recall the difference between the higher amounts of 5-FU loaded into Na(5-FU)Y compared to the DDS we prepared, which exhibited considerable lower loading capacity.

Even though the DDS revealed an excellent cytotoxicity in this skin cancer cell line (resulting in a drastic drop of 88% in terms of cell viability), one pertinent question arises: we chose silver because of its excellent antimicrobial properties (which would be highly beneficial in the prevention of possible skin infections in patients with skin cancer related lesions, often more prone to those clinical situations, but we must take into account that the Ag^+ cytotoxicity could affect, in an unspecific way, both healthy skin cells and cancer cells, as we demonstrated here for A375 cell line, causing adverse side effects.

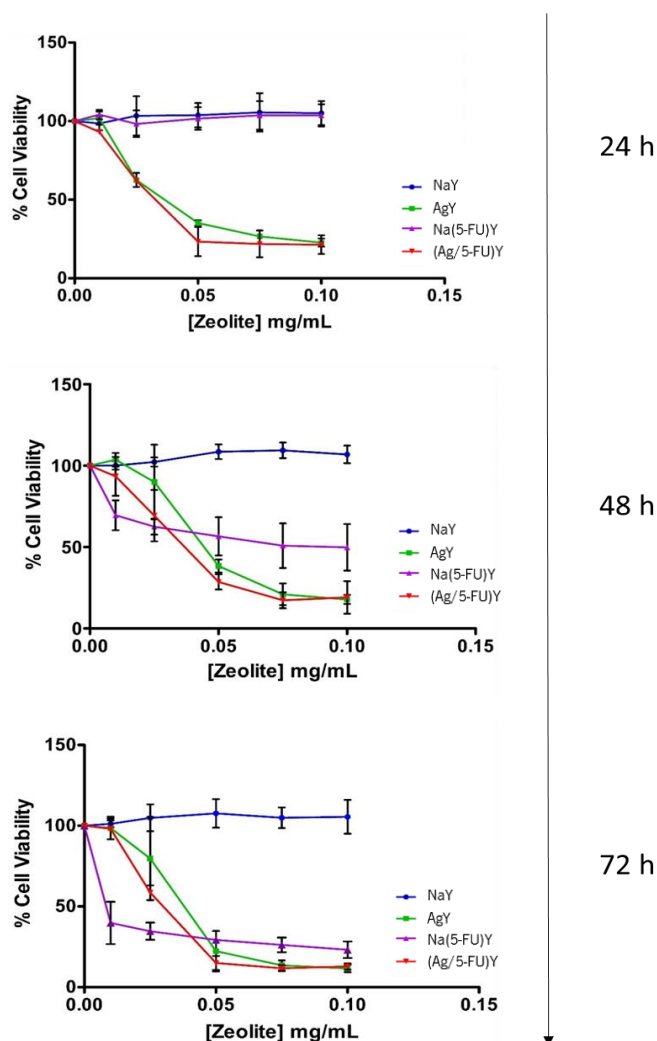


Figure 4.20. Effect of NaY (blue line), Na(5-FU)Y (purple line), AgY (green line) and the hybrid DDS Ag(5-FU)Y (red line) on A375 skin cancer cell viability. Cells were incubated in the presence of the prepared materials for 72 h. Presented values are means \pm SD of three independent experiments, each of them performed in triplicate.

The challenge here is to find a balance between the proportions of active agents, Ag⁺ and 5-fluorouracil. In the future, we should consider altering the quantities incorporated in the zeolite framework, decreasing the amount of silver and increasing the amount of encapsulated 5-FU (because, as the TGA results showed, the preparation of the hybrid system resulted in a low efficiency of 5-FU encapsulation, so it had much less amount of drug than the sample Na(5-FU)Y), in a way that the dual activity of the DDS, antineoplastic and antimicrobial, would still be preserved. Concerning the interaction between zeolite-based DDSs and cancer cells, it has already been evaluated in an earlier study, where the cytotoxicity of zeolites was tested on HCT-15 and RKO cell lines and it was suggested that NaY zeolite entered the cells by an endocytose process (Vilaça *et al.* 2013). Briefly, in this process, a portion of the plasma membrane is invaginated so that the cell engulfs some of its extracellular fluid including the material suspended in it (in this case, the zeolite particle). When this invagination detaches, a small vesicle called endosome is formed and released in the cytoplasm, subsequently fusing with a lysosome, which contains acidic hydrolases that allow the release of the vesicle content. With optical and fluorescence microscopy analysis they detected the presence of NaY zeolite within the cytoplasm (Figure 4.21), confirming the internalization of the material during the period of cellular incubation. As we used the same material in the current project as host for the DDS preparation, the same behaviour would be expected as well. However, further analysis would be required, not only to confirm that the DDS that we prepare is indeed internalized by the cells, but also to understand the mechanistic basis of that internalization process, since within endocytosis we can have distinct processes, such as clathrin-dependent endocytosis, caveolae-mediated endocytosis, clathrin- and caveolae-independent endocytosis and micropinocytosis (Sahay *et al.* 2010).

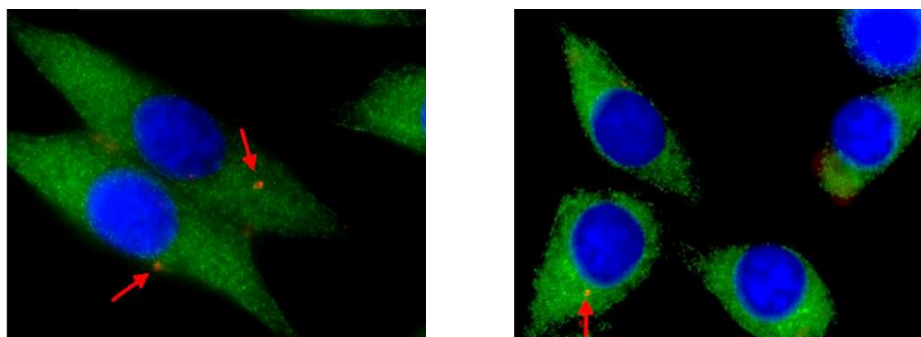


Figure 4.21. Fluorescence microscopy images (1000x magnification) showing the cellular localization of NaY zeolite marked with Rhodamine B in RKO cell line (red) (Vilaça *et al.* 2013).

CHAPTER 5

CONCLUSIONS AND FUTURE PERSPECTIVES

Concerning the morphological properties of the zeolite host, SEM/EDX, N₂ adsorption and XPS analyses revealed that there were no significant changes in the structure of the host (measured parameters such as Si/Al ratio, particle shape and size and pore distribution exhibited similar results in NaY, AgY and (Ag/5-FU)Y after Ag⁺ introduction (via ion exchange) and 5-FU (via liquid adsorption), meaning the porous material maintained its structural integrity throughout the process.

The TGA results showed that the encapsulation capacity of 5-FU in the DDS was considerably low compared to previously studies where NaY demonstrated excellent drug loading results. The introduction of Ag⁺ into the structure of the material, prior to 5-FU encapsulation, could be the cause of this lack of efficiency. The amount of Ag⁺ present (which exhibits a higher ionic ray than Na⁺) could be interfering with the entrance of 5-FU through the pores of the material. We should find a more suitable experimental strategy that would allow to improve the efficacy of the encapsulation process, perhaps opting for another method other than liquid adsorption.

Since patients with skin lesions/abnormalities such as AK, SCC or BCC are often highly susceptible to infections, combinational therapy of antineoplastic drugs and antimicrobial agents should be considered as a beneficial and viable treatment option. The main purpose of the current project was to create a hybrid drug delivery system, using NaY zeolite as host. The idea was to incorporate both 5-fluorouracil and silver (in its ionic form, Ag⁺) into the zeolite framework, combining the antineoplastic and the antimicrobial actions, respectively, in the same formulation. Considering the obtained results, the primary goal was achieved. We were able to introduce both species into the host which was confirmed by the characterization analyses. The next step would be the incorporation of the DDS into a biocompatible cream/ointment for topic delivery, to be applied as a thin coating on the affected skin areas.

From the patient's perspective, topical administration is very appealing especially because it is painless, more convenient and non-invasive. We idealized this as treatment option in cases of early and benign manifestation (at a stage where surgical intervention may not be required), as a way to prevent clinical evolution to more complicated and health threatening clinical situations, commonly accompanied by severe wounds that display an ulcerative growth and are prone to infection.

Historically, silver (Ag) has been used in several fields to inhibit microbial growth and compared to other metals (such as zinc and copper) it shows the highest antimicrobial capacity against microorganisms. However, the benefits of preventing bacterial growth using silver must be weighed against the possible side toxic effects on human epithelial cells. Considering the high cytotoxicity that the silver-loaded zeolite revealed on this cell line, further tests will be required on a human skin cell line of normal keratinocytes to assess its cytotoxicity. To overcome the possible silver-induced toxicity on epithelial cell environment, we could consider changing the quantities of 5-FU and Ag⁺ incorporated in the zeolite host, decreasing the amount of Ag⁺ and increasing the amount of 5-FU, since the antineoplastic agent also exhibited antibacterial capacity against the indicator strains tested, which resulted in a combined action of Ag⁺ and 5-FU, demonstrated by the resulting MIC values, which were lower for (Ag/5-FU)Y than for AgY. This way our hybrid system would, ideally, still prevent possible microbial infections on skin damaged areas and eliminate skin cancer cells as well, while avoiding possible unwanted side-effects of silver on normal epidermal cells around the damaged area.

CHAPTER 6



BIBLIOGRAPHY

- Al-Thawabeia, R., & Hodali, H. (2015). Use of Zeolite ZSM-5 for Loading and Release of 5-Fluorouracil. *Hindawi, Journal of Chemistry* (Vol. 2015).
- Ahuja, G., & Pathak, K. (2009). Porous Carriers for Controlled/Modulated Drug Delivery. *Indian Journal of Pharmaceutical Sciences*, 71(6), 599-607.
- Allothman, Z. A. (2012). A Review: Fundamental Aspects of Silicate Mesoporous Materials. *Materials*, 5(12), 2874-2902.
- Amorim, R., Vilaça, N., Martinho, O., Reis, R. M., Sardo, M., Rocha, J., Neves, I. C. (2012). Zeolite Structures Loading with an Anticancer Compound As Drug Delivery Systems. *The Journal of Physical Chemistry C*, 116(48), 25642-25650.
- Amrhein, C., Haghnia, G. H., Kim, T. S., Mosher, P. A., Gagajena, R. C., Amanios, T., & de la Torre, L. (1996). Synthesis and Properties of Zeolites from Coal Fly Ash. *Environmental Science & Technology*, 30(3), 735-742.
- Arruebo, M. (2011). Drug delivery from structured porous inorganic materials. *Wiley Interdisciplinary Reviews: Nanomedicine and Nanobiotechnology*, 4(1), 16-30.
- Avendaño, C., & Menéndez, J. C. (2015). Chapter 2 - Antimetabolites That Interfere with Nucleic Acid Biosynthesis. In C. Avendaño & J. C. Menéndez (Eds.), *Medicinal Chemistry of Anticancer Drugs (Second Edition)* (pp. 23-79). Boston: Elsevier.
- Bahner, J. D., & Bordeaux, J. S. (2013). Non-melanoma skin cancers: Photodynamic therapy, cryotherapy, 5-fluorouracil, imiquimod, diclofenac, Facts and controversies. *Clinics in Dermatology*, 31(6), 792-798.
- Barbé, C., Bartlett, J., Kong, L., Finnie, K., Q. Lin, H., Larkin, M., Calleja, G. (2004). *Silica Particles: A Novel Drug-Delivery System* (Vol. 16).
- Barreto, M. L., Teixeira, M. G., & Carmo, E. H. (2006). Infectious diseases epidemiology. *Journal of Epidemiology and Community Health*, 60(3), 192-195.
- Basu, A. K. (2018). DNA Damage, Mutagenesis and Cancer. *International Journal of Molecular Sciences*, 19(4), 970.
- Bertram, J. S. (2000). The molecular biology of cancer. *Molecular Aspects of Medicine*, 21(6), 167-223.
- Bodet, C. A., Jorgensen, J. H., & Drutz, D. J. (1985). Antibacterial activities of antineoplastic agents. *Antimicrobial Agents and Chemotherapy*, 28(3), 437-439.
- Boss, C., & J. Fredeen, K. (1989). *Concepts, Instrumentation and Techniques in Inductively Couple Plasma Optical Emission Spectrometry*.

- Brunauer, S., Emmett, P. H., & Teller, E. (1938). Adsorption of Gases in Multimolecular Layers. *Journal of the American Chemical Society*, 60(2), 309-319.
- Burgess, C. (2017). Chapter 1 - The Basis for Good Spectrophotometric UV–Visible Measurements. In O. Thomas & C. Burgess (Eds.), *UV-Visible Spectrophotometry of Water and Wastewater (Second Edition)* (pp. 1-35): Elsevier.
- Busch, H. (1974). CHAPTER I - Introduction. In H. Busch (Ed.), *The Molecular Biology of Cancer* (pp. 1-39): Academic Press.
- Cameron, D. A., Gabra, H., & Leonard, R. C. (1994). Continuous 5-fluorouracil in the treatment of breast cancer. *British journal of cancer*, 70(1), 120-4.
- Cao, H. (2017). *Silver Nanoparticles for Antibacterial Devices Biocompatibility and Toxicity*.
- Cohen, S. S., Flaks, J. G., Barner, H. D., Loeb, M. R., & Lichtenstein, J. (1958). The mode of action of 5-fluorouracil and its derivatives. *Proceedings of the National Academy of Sciences of the United States of America*, 44(10), 1004-1012.
- Cooper GM. The Cell: A Molecular Approach. 2nd edition. Sunderland (MA): Sinauer Associates; 2000. Available from: <https://www.ncbi.nlm.nih.gov/books/NBK9839/>
- Datt, A., Ndiege, N., & Larsen, S. C. (2012). Development of Porous Nanomaterials for Applications in Drug Delivery and Imaging .*Nanomaterials for Biomedicine* 1119, 239-258: American Chemical Society.
- De Jong, W. H., & Borm, P. J. A. (2008). Drug delivery and nanoparticles: Applications and hazards. *International Journal of Nanomedicine*, 3(2), 133-149.
- Diasio, R. B. (2002). Clinical Implications of Dihydropyrimidine Dehydrogenase on 5-Fluorouracil Pharmacology. In L. B. Saltz (Ed.), *Colorectal Cancer: Multimodality Management* 489-497. *Totowa, NJ: Humana Press*.
- Diasio, R. B., & Harris, B. E. (1989). Clinical Pharmacology of 5-Fluorouracil. *Clinical Pharmacokinetics*, 16(4), 215-237.
- Dibrov, P., Dzioba, J., Gosink, K. K., & Häse, C. C. (2002). Chemiosmotic Mechanism of Antimicrobial Activity of Ag in *Vibrio cholerae*. *Antimicrobial Agents and Chemotherapy*, 46(8), 2668.
- Didona, D., Paolino, G., Bottoni, U., & Cantisani, C. (2018). Non Melanoma Skin Cancer Pathogenesis Overview. *Biomedicines*, 6(1).
- Donohue, M. D., & Aranovich, G. L. (1998). Classification of Gibbs adsorption isotherms. *Advances in Colloid and Interface Science*, 76-77, 137-152.

- E. Brown, M. (1988). *Introduction to thermal analysis : techniques and applications* / Michael E. Brown.
- Vokes, E., Brockstein, B., Humerickhouse, R., & Haraf, D. (1998). Oral 5-FU alternatives for the treatment of head and neck cancer. *Oncology NY*, 12, 35-38.
- Feng, Q. L., Wu, J., Chen, G. Q., Cui, F. Z., Kim, T. N., & Kim, J. O. (2000). A mechanistic study of the antibacterial effect of silver ions on *Escherichia coli* and *Staphylococcus aureus*. *Journal of Biomedical Materials Research*, 52(4), 662-668.
- Ferraria, A. M., Carapeto, A. P., & Botelho do Rego, A. M. (2012). X-ray photoelectron spectroscopy: Silver salts revisited. *Vacuum*, 86(12), 1988-1991.
- Ferreira, L., Fonseca, A. M., Botelho, G., Aguiar, C. A., & Neves, I. C. (2012). Antimicrobial activity of faujasite zeolites doped with silver. *Microporous and Mesoporous Materials*, 160, 126-132.
- Focaccetti, C., Bruno, A., Magnani, E., Bartolini, D., Principi, E., Dallaglio, K., Albini, A. (2015). Effects of 5-Fluorouracil on Morphology, Cell Cycle, Proliferation, Apoptosis, Autophagy and ROS Production in Endothelial Cells and Cardiomyocytes. *PLOS ONE*, 10(2)
- Fornaguera, C., & García-Celma, J. M. (2017). Personalized Nanomedicine: A Revolution at the Nanoscale. *Journal of Personalized Medicine*, 7(4).
- Fouad, Y. A., & Aanei, C. (2017). Revisiting the hallmarks of cancer. *American Journal of Cancer Research*, 7(5), 1016-1036.
- Freitas, R. A. (2005). What is nanomedicine? *Nanomedicine: Nanotechnology, Biology and Medicine*, 1(1), 2-9.
- Gauglitz, G. (2008). Ultraviolet and Visible Spectroscopy. *Handbook of Analytical Techniques*.
- Gester, R., Bistafa, C., Georg, H., Coutinho, K., & Canuto, S. (2014). *Theoretically Describing the 170 Magnetic Shielding Constant of Biomolecular Systems: Uracil and 5-Fluorouracil in Water Environment* (Vol. 133).
- Gould, K. (2016). Antibiotics: from prehistory to the present day. *Journal of Antimicrobial Chemotherapy*, 71(3), 572-575.
- Griffin, L. L., Ali, F. R., & Lear, J. T. (2016). Non-melanoma skin cancer. *Clinical Medicine*, 16(1), 62-65.
- Guggenbichler, J. P., Böswald, M., Lugauer, S., & Krall, T. (1999). A new technology of microdispersed silver in polyurethane induces antimicrobial activity in central venous catheters. *Infection*, 27(1), 16-23.

- Gupta, A. S. (2011). Nanomedicine approaches in vascular disease: a review. *Nanomedicine: Nanotechnology, Biology and Medicine*, 7(6), 763-779.
- Gwatkin, R. (1993). Molecular cell biology, 2nd edition, by James Darnell, Harvey Lodish, and David Baltimore, Scientific American Books, distributed by W. H. Freeman, New York, *Molecular Reproduction and Development*, 34(1), 114-114.
- Hanahan, D., & Weinberg, R. (2011). *Hallmarks of Cancer: The Next Generation* (Vol. 144).
- Hanahan, D., & Weinberg, R. A. (2000). The Hallmarks of Cancer. *Cell*, 100(1), 57-70.
- Hanahan, D., & Weinberg, Robert A. (2011). Hallmarks of Cancer: The Next Generation. *Cell*, 144(5), 646-674.
- Hantsche, H. (1993). High resolution XPS of organic polymers, the scienta ESCA300 database. *Advanced Materials*, 5(10), 778-778.
- Hatakeyama, T., & Quinn, F. X. (2018). *Thermal analysis : fundamentals and applications to polymer science*
- Heal, G. R. (2002). Thermogravimetry and Derivative Thermogravimetry *Principles of Thermal Analysis and Calorimetry*, 10-54: The Royal Society of Chemistry.
- Heidelberger, C., Chaudhuri, N. K., Danneberg, P., Mooren, D., Griesbach, L., Duschinsky, R., Scheiner, J. (1957). Fluorinated pyrimidines, a new class of tumour-inhibitory compounds. *Nature*, 179(4561), 663-666.
- Hou, X., Amais, R. S., Jones, B. T., & Donati, G. L. (2016). Inductively Coupled Plasma Optical Emission Spectrometry. *Encyclopedia of Analytical Chemistry*.
- Inkson, B. J. (2016). Scanning electron microscopy (SEM) and transmission electron microscopy (TEM) for materials characterization. *Materials Characterization Using Nondestructive Evaluation (NDE) Methods* 17-43: Woodhead Publishing.
- Jain, K. K. (2008). Drug delivery systems - an overview. *Methods in molecular biology*, 437, 1-50.
- Jandrig, B. (2011). Models of Cancer Development: Genetic and Environmental Influences. *Cancer Risk Evaluation*.
- Jiang, W. G., Sanders, A. J., Katoh, M., Ungefroren, H., Gieseler, F., Prince, M., Santini, D. (2015). Tissue invasion and metastasis: Molecular, biological and clinical perspectives. *Seminars in Cancer Biology*, 35, 244-275.
- Kędziora, A., Speruda, M., Krzyżewska, E., Rybka, J., Łukowiak, A., & Bugła-Płoskońska, G. (2018). Similarities and Differences between Silver Ions and Silver in Nanoforms as Antibacterial Agents. *International Journal of Molecular Sciences*, 19(2).

- Khan, I., Saeed, K., & Khan, I. (2017). Nanoparticles: Properties, applications and toxicities. *Arabian Journal of Chemistry*.
- Khodabandehloo, H., Zahednasab, H., & Ashrafi Hafez, A. (2016). Nanocarriers Usage for Drug Delivery in Cancer Therapy. *Iranian Journal of Cancer Prevention*, 9(2),
- Koons, R. D. (2003). ICP Emission Spectrometry: A Practical Guide *Journal of the American Chemical Society*, 125(51), 16154-16154.
- Kwakye-Awuah, B., Williams, C., Kenward, M. A., & Radecka, I. (2007). Antimicrobial action and efficiency of silver-loaded zeolite X. *Journal of Applied Microbiology*, 104(5), 1516-1524.
- Schilsky, R. (1998). *Biochemical and clinical pharmacology of 5-Fluorouracil* (Vol. 12).
- Leonard, D. N., Chandler, G. W., & Seraphin, S. (2012). Scanning Electron Microscopy. *Characterization of Materials*.
- Li, X., Narayanan, S., Michaelis, V. K., Ong, T.-C., Keeler, E. G., Kim, H., Wang, E. N. (2015). Zeolite Y adsorbents with high vapor uptake capacity and robust cycling stability for potential applications in advanced adsorption heat pumps. *Microporous and Mesoporous Materials*, 201, 151-159.
- Liau, S. Y., Read, D. C., Pugh, W. J., Furr, J. R., & Russell, A. D. (2003). Interaction of silver nitrate with readily identifiable groups: relationship to the antibacterial action of silver ions. *Letters in Applied Microbiology*, 25(4), 279-283.
- Liu, D., Yang, F., Xiong, F., & Gu, N. (2016). The Smart Drug Delivery System and Its Clinical Potential. *Theranostics*, 6(9), 1306-1323.
- Lomas, A., Leonardi-Bee, J., & Bath-Hextall, F. (2012). A systematic review of worldwide incidence of nonmelanoma skin cancer. *British Journal of Dermatology*, 166(5), 1069-1080.
- Longley, D. B., Harkin, D. P., & Johnston, P. G. (2003). 5-Fluorouracil: mechanisms of action and clinical strategies. *Nature Reviews Cancer*, 3, 330.
- Martinho, O., Vilaça, N., Castro, P., Amorim, R., Fonseca, A., Baltazar, F., Reis, R. & Neves, I. (2015). In vitro and in vivo studies of temozolomide loading in zeolite structures as drug delivery systems for glioblastoma. *RSC Advances*, 5(36), 28219-28227
- Matsumura, Y., Yoshikata, K., Kunisaki, S.-i., & Tsuchido, T. (2003). Mode of Bactericidal Action of Silver Zeolite and Its Comparison with That of Silver Nitrate. *Applied and Environmental Microbiology*, 69(7), 4278-4281.

- Milenkovic, J., Hrenovic, J., Matijasevic, D., Niksic, M., & Rajic, N. (2017). Bactericidal activity of Cu-, Zn-, and Ag-containing zeolites toward *Escherichia coli* isolates. *Environmental Science and Pollution Research*, 24(25), 20273-20281.
- Miura, K., Kinouchi, M., Ishida, K., Fujibuchi, W., Naitoh, T., Ogawa, H., Sasaki, I. (2010). 5-FU Metabolism in Cancer and Orally-Administrable 5-FU Drugs. *Cancers*, 2(3), 1717-1730.
- Miyata, T., Endo, A., Ohmori, T., Akiya, T., & Nakaiwa, M. (2003). Evaluation of pore size distribution in boundary region of micropore and mesopore using gas adsorption method. *Journal of Colloid and Interface Science*, 262(1), 116-125.
- Moore, G. L. (1989a). Chapter 6 - inductively coupled plasma atomic emission spectrometry. *Introduction to Inductively Coupled Plasma Atomic Emission Spectrometry* , 119-133. Amsterdam: Elsevier.
- Moore, G. L. (1989b). Chapter 7 - Nebulization. In G. L. Moore (Ed.), *Introduction to Inductively Coupled Plasma Atomic Emission Spectrometry* 135-160. Amsterdam: Elsevier.
- Morgan, C. (1992). Essentials of medical microbiology (fourth edition) *Biochemical Education*, 20(1), 60-60.
- Murthy, S. K. (2007). Nanoparticles in modern medicine: State of the art and future challenges. *International Journal of Nanomedicine*, 2(2), 129-141.
- Nagarajan, R. (2012). *Nanomaterials for Biomedicine*, 1119: American Chemical Society.
- Noordhuis, P., Holwerda, U., Van der Wilt, C. L., Van Groeningen, C. J., Smid, K., Meijer, S., Peters, G. J. (2004). 5-Fluorouracil incorporation into RNA and DNA in relation to thymidylate synthase inhibition of human colorectal cancers. *Annals of Oncology*, 15(7), 1025-1032.
- Owen, T., & Agilent, T. (2000). Fundamentals of UV-visible spectroscopy : a primer. *Agilent Technologies*.
- Pardee, A. B., Stein, G. S., & Bronstein, E. A. (2008). What Goes Wrong in Cancer. *The Biology and Treatment of Cancer*.
- Parker, J. B., & Stivers, J. T. (2011). Dynamics of Uracil and 5-Fluorouracil in DNA. *Biochemistry*, 50(5), 612-617.
- Pavlovic, M., Mayfield, J., & Balint, B. (2013). Nanotechnology and Its Application in Medicine. *Handbook of Medical and Healthcare Technologies* 181-205. New York, NY: Springer New York.
- Percival, S. L., Bowler, P. G., & Russell, D. (2005). Bacterial resistance to silver in wound care. *Journal of Hospital Infection*, 60(1), 1-7.

- Pérez-Losada, J., Castellanos-Martín, A., & Mao, J.-H. (2011). Cancer evolution and individual susceptibility. *Integrative biology : quantitative biosciences from nano to macro*, 3(4), 316-328.
- Prime, R. B., Bair, H. E., Vyazovkin, S., Gallagher, P. K., & Riga, A. (2008). Thermogravimetric Analysis (TGA). *Thermal Analysis of Polymers*.
- Rai, M., Yadav, A., & Gade, A. (2009). Silver nanoparticles as a new generation of antimicrobials. *Biotechnology Advances*, 27(1), 76-83.
- Rajendran, V., Agarwal, R., Jagannathan, S., Pachamuthu, R. G., & R, R. (2013). *Application of Nanotechnology in Medicine: A View*.
- Rhodes, C. J. (2010). Properties and applications of zeolites. *Science Progress*, 93(3), 223-284.
- Rieger, K. A., Cho, H. J., Yeung, H. F., Fan, W., & Schiffman, J. D. (2016). Antimicrobial Activity of Silver Ions Released from Zeolites Immobilized on Cellulose Nanofiber Mats. *ACS Applied Materials & Interfaces*, 8(5), 3032-3040.
- Rimoli, M. G., Rabaioli, M. R., Melisi, D., Curcio, A., Mondello, S., Mirabelli, R., & Abignente, E. (2007). Synthetic zeolites as a new tool for drug delivery. *Journal of Biomedical Materials Research Part A*, 87A(1), 156-164.
- Rizvi, S. A. A., & Saleh, A. M. (2018). Applications of nanoparticle systems in drug delivery technology. *Saudi Pharmaceutical Journal*, 26(1), 64-70.
- Rocha, F. R. P., & Teixeira, L. S. G. (2004). Estratégias para aumento de sensibilidade em espectrofotometria UV-VIS. *Química Nova*, 27, 807-812.
- Rogers, H. J., & Perkins, H. R. (1960). 5-Fluorouracil and mucopeptide biosynthesis by *Staphylococcus aureus*. *Biochemical Journal*, 77(3), 448-459.
- Roser, M. & Ritchie, H. (2018). Cancer. *Published online at OurWorldInData.org*. Retrieved from: <https://ourworldindata.org/cancer>
- Rutman, R. J., Cantarow, A., & Paschkis, K. E. (1954). Studies in 2-Acetylaminofluorene Carcinogenesis. *Cancer Research*, 14(2), 119.
- Saengmee-Anupharb, S., Srihirin, T., Thaweboon, B., Thaweboon, S., Amornsakchai, T., Dechkunakorn, S., & Suddhasthira, T. (2013). Antimicrobial effects of silver zeolite, silver zirconium phosphate silicate and silver zirconium phosphate against oral microorganisms. *Asian Pacific journal of tropical biomedicine*, 3(1), 47-52.
- Sahay, G., Alakhova, D. Y., & Kabanov, A. V. (2010). Endocytosis of nanomedicines. *Journal of Controlled Release*, 145(3), 182-195.

- Saini, R., Saini, S., & Sharma, S. (2010). Nanotechnology: The Future Medicine. *Journal of Cutaneous and Aesthetic Surgery*, 3(1), 32-33.
- Sayed, E., Haj-Ahmad, R., Ruparelia, K., Arshad, M. S., Chang, M. W., & Ahmad, Z. (2017). Porous Inorganic Drug Delivery Systems—a Review. *AAPS PharmSciTech*, 18(5), 1507-1525.
- Scimeca, M., Bischetti, S., Lamsira, H. K., Bonfiglio, R., & Bonanno, E. (2018). Energy Dispersive X-ray (EDX) microanalysis: A powerful tool in biomedical research and diagnosis. *European journal of histochemistry* : 62(1), 2841-2841.
- Seah, M. P. (1980). The quantitative analysis of surfaces by XPS: A review. *Surface and Interface Analysis*, 2(6), 222-239.
- Sharquie, K. E., & Noaimi, A. A. (2012). Basal cell carcinoma: Topical therapy versus surgical treatment. *Journal of the Saudi Society of Dermatology & Dermatologic Surgery*, 16(2), 41-51.
- Silva, G. A. (2004). Introduction to nanotechnology and its applications to medicine. *Surgical Neurology*, 61(3), 216-220.
- Singh, P., Tyagi, G., Mehrotra, R., & Bakhshi, A. K. (2009). Thermal stability studies of 5-fluorouracil using diffuse reflectance infrared spectroscopy. *Drug Testing and Analysis*, 1(5), 240-244.
- Singh, R., & Lillard, J. W. (2009). Nanoparticle-based targeted drug delivery. *Experimental and molecular pathology*, 86(3), 215-223.
- Stöcker, M. (1996). X-Ray photoelectron spectroscopy on zeolites and related materials. *Microporous Materials*, 6(5), 235-257.
- Tissue, B. M. (2002). Ultraviolet and Visible Absorption Spectroscopy. *Characterization of Materials*.
- Tiwari, G., Tiwari, R., Sriwastawa, B., Bhati, L., Pandey, S., Pandey, P., & Bannerjee, S. K. (2012). Drug delivery systems: An updated review. *International Journal of Pharmaceutical Investigation*, 2(1), 2-11
- Uzman, A. (2006). Molecular biology of the cell (4th ed.) *Biochemistry and Molecular Biology Education*, 31(4), 212-214.
- van Ruth, S., Jansman, F. G. A., & Sanders, C. J. (2006). Total body topical 5-fluorouracil for extensive non-melanoma skin cancer. *Pharmacy World & Science*, 28(3), 159-162.
- Ventola, C. L. (2015). The Antibiotic Resistance Crisis: Part 1: Causes and Threats. *Pharmacy and Therapeutics*, 40(4), 277-283.

- Vernon-Parry, K. D. (2000). Scanning electron microscopy: an introduction. *III-Vs Review*, 13(4), 40-44.
- Vilaça, N., Amorim, R., Machado, A., Parpot, P., Pereira, M., Sardo, M., Baltazar, F. (2013). *Potential of 5-fluorouracil encapsulated in zeolites as drug delivery systems for in vitro models of colorectal carcinoma*. *Colloids Surf B Biointerfaces* 112:237-244
- Wang, L., Fan, D., Chen, W., & Terentjev, E. M. (2015). Bacterial growth, detachment and cell size control on polyethylene terephthalate surfaces. *Scientific Reports*, 5: 151-159.
- Wang, S. (2009). Ordered mesoporous materials for drug delivery. *Microporous and Mesoporous Materials*, 117(1), 1-9.
- Wang, Y. F., Liu, L., Xue, X., & Liang, X. J. Nanoparticle-based drug delivery systems. *F1000 Research*, 6:681
- Wennersten, R., Fidler, J., & Spitsyna, A. (2008). Nanotechnology: A New Technological Revolution in the 21st Century. *Handbook of Performability Engineering*, 943-952. London: Springer London.
- Wilczewska, A. Z., Niemirowicz, K., Markiewicz, K. H., & Car, H. (2012). Nanoparticles as drug delivery systems. *Pharmacological Reports*, 64(5), 1020-1037.
- Yamanaka, M., Hara, K., & Kudo, J. (2005). Bactericidal Actions of a Silver Ion Solution on Escherichia coli Studied by Energy-Filtering Transmission Electron Microscopy and Proteomic Analysis. *Applied and Environmental Microbiology*, 71(11), 7589.
- Yang, S., Chen, G., Lv, C., Li, C., Yin, N., Yang, F., & Xue, L. (2017). Evolution of nanopore structure in lacustrine organic-rich shales during thermal maturation from hydrous pyrolysis. *Minhe Basin, Northwest China*, 36.
- Young, V. B. (2017). The role of the microbiome in human health and disease: an introduction for clinicians. *BMJ*, 356.
- Zaefferer, S., & Wu, G. (2011). A critical review of orientation microscopy in SEM and TEM (Vol. 46).
- Zaidi, E. (2011). XPS, AES and laser raman spectroscopy: A fingerprint for a materials surface characterisation. *Jurnal Sains Nuklear Malaysia*, 23(2), 26-45.
- Zhang, N., Yin, Y., Xu, S.-J., & Chen, W.-S. (2008). 5-Fluorouracil: Mechanisms of Resistance and Reversal Strategies. *Molecules*, 13(8).

- Zhu, X., Radovic-Moreno, A. F., Wu, J., Langer, R., & Shi, J. (2014). Nanomedicine in the Management of Microbial Infection – Overview and Perspectives. *Nano today*, 9(4), 478-498.
- Zurera Cosano, G., & Amaro López, M. A. (2003). CADMIUM | Properties and Determination. *Encyclopedia of Food Sciences and Nutrition (Second Edition)* 733-739. Oxford: Academic Press.

